Mechanisms of decay and interspecific interactions of white and brown rot fungi

A DISSERTATION

SUBMITTED TO THE FACULTY OF

UNIVERSITY OF MINNESOTA

BY

Gerald Presley

IN PARTIAL FULFILLMENT OF THE REQUIREMENTS

FOR THE DEGREE OF

DOCTOR OF PHILOSOPHY

Advisor: Dr. Jonathan Schilling

April 2018

Acknowledgements

I am very grateful for the help and support of my research advisor, Jonathan Schilling. He has played a critical role in fostering my development as a scientist and has provided an invaluable creative space for me to learn, make mistakes, and succeed. I feel very fortunate to have had the opportunity to do what I have done during my time at the University of Minnesota and my educational experience would be a shadow of what it is without Jonathan.

I would also like to thank all my colleagues I have worked with in the Schilling laboratory over the vast expanse of my 6-year PhD. I have been mentored by several post docs and have helped train several undergraduate students, all of whom have played an integral role in my learning experience. I would like to thank Dr. Jiwei Zhang for his help teaching me molecular biology techniques over the years. Jiwei has helped me greatly with laboratory techniques with a care and dedication that can only come from a kind soul.

I would also like to thank my student peers from around the University of Minnesota that have participated in the University of Minnesota (UMN) Mycology Club and put in the work to make it a lasting student organization. The hard, unpaid work of these students has made the UMN Mycology Club a fantastic campus resource for undergraduate and graduate student education, personal development, and networking.

Funding for this research was provided by US Department of Energy (DOE) grants GO18088 from the Biomass Research and Development Initiative (BRDI), DE SC0004012 Early Career grant and Grant DE-SC0012742 from the Biological and Ecological Research (BER) program. This work was also funded by the National Science Foundation Graduate Research Fellowship Program Grant No. 00039202, an international travel allowance through the Graduate Research Opportunities Worldwide (GROW) Program, and a Research and Innovations Fellowship through the U.S. Global Development Lab (Grant number AID-LAB-T-15-00002). Any opinions, findings, and conclusions or recommendations expressed in this material are those of the authors and do not necessarily reflect the views of the DOE, NSF, or USAID.

This work was also supported by a University of Minnesota Doctoral Dissertation Fellowship awarded for the 2017-2018 academic year.

Abstract

Wood is the largest source of biotic carbon on earth and the principle drivers of its decay are basidiomycete fungi. The biochemical mechanisms of wood decay by basidiomycete fungi are fundamental processes in forest ecosystems that dictate carbon evolution rates, soil organic matter deposition, and overall ecosystem function. These decay mechanisms are also unique in their ability to efficiently convert recalcitrant woody biomass to fermentable sugars and can serve as a biological template for industrial lignocellulose conversion to make renewable biofuels more economical. However, basidiomycete wood decay mechanisms are not fully understood and therefore not replicable in vitro, due in part to a lack of understanding of how decay mechanisms change throughout the progression of decay. In addition, gene transcripts and proteins used to facilitate decay are produced in concert with other biomolecules with non-degradative functions which makes resolution of degradative genes difficult.

This dissertation contributes to resolving these problems by describing the temporal progression of decay among several species of wood-degrading basidiomycetes and functionally categorizing genes and secreted proteins involved in mediating interspecific interactions. This was done by first spatially resolving decay into a temporal sequence by growing model brown-rot fungi directionally on thin wood wafers. This system was used to co-localize changes in fungal physiology with chemical changes in wood substrates and the production of fungal metabolites to identify the functional

significance of those physiological changes. The same wafer culture design was then used to resolve changes in fungal secretomes between two phylogenetically disparate brown-rot species over the course of decay using proteomics co-localized with lignocellulose-degrading enzyme assays. Interspecific differences were further investigated by comparing decay performance of the same two fungi on a Poales substrate, sorghum bagasse. Sorghum decay rates along with component removal and enzyme assays were monitored during decay to determine the genetic and biochemical basis of substrate preferences of the two species. Temporal alterations to fungal secretomes were compared among several model white and brown-rot fungi as well. Comparative proteomics concurrent with lignocellulose-degrading enzyme assays were used to identify common patterns among both rot types, as well as interspecific variability of decay mechanisms within species. Finally, changes in gene expression, protein secretion, and enzyme activity profiles in response to fungal competitors were described by modifying the thin wood wafer microcosms to incorporate two brown-rot species grown in opposition to one another.

Resolution of decay into a sequence revealed a biphasic decay mechanism in brown-rot fungi delineated by early stage, non-hydrolytic pretreatment followed by later stage glycoside hydrolase-mediated saccharification. Proteomic investigation confirmed this pattern by showing later stage secretomes contain a greater proportion of glycoside hydrolases and their activities than earlier stages of decay. Brown-rot secretomes varied considerably by species as did their ability to degrade sorghum bagasse, likely due to a difference in the ability to hydrolyze ferulic acid esters present in sorghum biomass.

Comparison of white and brown-rot secretomes identified a common segregation of decay into a biphasic decay mechanism characterized by high lignolysis, in white-rot fungi, upon wood colonization followed by later stage glycoside hydrolase secretion in both decay types. Considerable interspecific variability in decay mechanism within decay types was also detected, with the white-rot species producing different suites of ligninolytic enzymes and brown-rot species diverging in the types of glycoside hydrolases produced. Investigation of interspecific interactions identified several proteins exclusively produced during the interaction of two brown-rot species as well as identifying the general downregulation of lignocellulose-degrading genes during the interaction. In addition, comparative transcriptomics identified two different interaction strategies employed by species and implicates several secondary metabolite-synthesizing genes in facilitating interspecific interactions. Overall, this work contributes toward functional categorization of a wide range of basidiomycete proteins and provides a better understanding of decay mechanisms and interspecific interactions in these understudied organisms.

Table of Contents

List of Tables

List of Figures

Chapter 1 Introduction

1.1 Problem Statement

Wood-degrading basidiomycetes are the principle degraders of woody biomass in the environment and as such mediate the recycling of the world's largest biotic sink of carbon (DIXON *et al.* 1994). Decay and interspecific competition among basidiomycetes are two of major drivers of carbon cycles (HISCOX *et al.* 2015b; PASTORELLI *et al.* 2017), ecosystem function (SNAJDR *et al.* 2011), and ecological outcomes (RAJALA *et al.* 2012). However, the biochemical mechanisms by which these processes occur are not fully understood and are in some cases not well resolved from one another, even in axenic single species cultures. Better resolution of these fundamental ecological processes is necessary to both utilize decay mechanisms as a bio-based template for lignocellulose biorefining and to identify the biological mechanisms at the root of forest carbon cycles.

Currently, most liquid fuels are derived from non-renewable fossil resources whose consumption results in a net addition of greenhouse gasses to the atmosphere (GUPTA and VERMA 2015). Petroleum is also a primary source of chemicals used to produce plastics. Continued primary reliance on fossil resources for energy and materials is untenable because the predicted greenhouse gas-induced global temperature increases are predicted to have catastrophic ecological and human impacts (WEED *et al.* 2013). Increased reliance on renewable sources of liquid fuels and high-value biodegradable chemicals is one avenue to mitigate the ongoing environmental catastrophes caused by the consumption of non-renewable fuels and materials. Liquid fossil fuels can be partially

replaced with bioethanol derived from renewable plant sources of simple sugars, primarily glucose. Starchy substrates such as corn grain are the most commonly used sources of sugar for renewable fuels, primarily bioethanol (KIM and DALE 2004). However, first-generation biofuels such as corn ethanol may result in greater negative environmental impacts than gasoline, including nutrient pollution and greater water usage (YANG *et al.* 2012). More recent efforts to reduce the environmental impact of bioethanol production have focused on utilizing the inedible portions of plant biomass, known as lignocellulose, as a bioethanol feedstock (KIM and DALE 2004).

However, the complex nature of lignocellulose makes it difficult to break into fermentable sugars. Cellulose is the primary target for bioethanol production, but it is poorly accessible due to several factors including its crystalline nature, the presence of hemicellulose, and the presence of the randomly-linked aromatic polymer, lignin (ZHAO *et al.* 2012). The inaccessibility of cellulose in plant biomass necessitates the use of harsh chemical pretreatments to liberate glucose from cellulose, but these also produce fermentation inhibitors (JONSSON and MARTIN 2016) that cause yield reductions. Harsh chemical treatments are also incompatible with enzyme mediated saccharification, and the pretreated substrate must be cooled and neutralized to enzyme-friendly conditions, further increasing processing costs (STEPHEN *et al.* 2012). Milder pretreatment techniques that are compatible with enzymatic saccharification and fermentation would make second generation biofuel production much more efficient and economically viable by allowing consolidation of all relevant processing steps into a single bio-based treatment (OLSON *et al.* 2012).

Wood-degrading basidiomycetes efficiently derive sugars from complex lignocellulose at low temperatures and conditions amenable for life, characteristics that are attractive for more cost effective lignocellulosic ethanol production. Decay mechanism components may prove useful in the production of renewable fuels from plant biomass and understanding these biological processes have the potential to help promote a sustainable bio economy (GOODELL *et al.* 2017). Two major groupings of these fungi, white rot and brown rot, access carbohydrates using different techniques to negate the lignin and other carbohydrate barriers in wood. White-rot fungi mineralize lignin using a suite of lignin-degrading enzymes that allow them to access to wood polysaccharides (HAMMEL and CULLEN 2008). Brown-rot fungi selectively degrade wood polysaccharides using a combination of chemical pretreatments followed by enzymatic saccharification in discrete space (ZHANG *et al.* 2016). Both approaches provide time-tested biological methods for lignocellulose conversion that can serve as templates for biomimetic pretreatments. Biological pretreatments of plant biomass by growing decay fungi on it has been done with some success, but the process is too slow for industrial use and results in yield loss due to metabolism (SCHILLING *et al.* 2012). For fungal decay mechanisms to be of any industrial use, biochemical and chemical facilitators of decay must be identified and recreated in vitro on a large scale. However, there are still significant gaps in the understanding of white-rot and brown-rot decay mechanisms that have inhibited their application in lignocellulose biorefineries. Modern biological research techniques have accelerated the study of wood decay mechanisms enabling rapid identification of genes and proteins that mediate decay.

Recent advances in genome sequencing have led to an explosion in the study of microbial genomes, including an increasing number of wood-degrading basidiomycetes (GRIGORIEV *et al.* 2014). Publicly available sequences make genomics, transcriptomics, and proteomics techniques available to study these fungi and have resulted in the resolution of fungal wood decay mechanism among a growing diversity of model species (FLOUDAS *et al.* 2012; ALFARO *et al.* 2014). Studies using omics techniques have provided unprecedented amounts of knowledge of wood-degrading basidiomycete decay mechanisms. However, these studies have also identified more gaps in our understanding of the biology of these fungi including the following:

1) Many of the early -omics studies of basidiomycete wood decay mechanisms do not use intact substrates and natural growth conditions, precluding the observation of any physiological adaptations fungi use to deal with intact wood substrates.
2) Many of these studies do not adequately resolve temporal changes in decay mechanisms, especially in early stages of wood decay, when changes are occurring very rapidly.
3) Expansion of these studies beyond a few model organisms shows significant interspecific variability in decay mechanisms and generalized decay mechanism models offer an incomplete understanding of wood decay in nature.
4) While many genes/proteins are expressed/produced during decay, their biological function, decay-related or not, often remains unknown.

The use of in-tact wood in studying basidiomycete wood decay mechanisms is necessary to produce an accurate recreation of the process of wood decay because of its

spatial heterogeneity. Wood-degrading basidiomycetes colonize wood through the cell lumens and degrade wood from the secondary cell walls outward, contacting layers with differing chemical composition throughout the progression of decay (BLANCHETTE 1995). Many of the early -omics studies of basidiomycete wood decay mechanisms used milled wood substrates in liquid culture to identify decay mechanisms which disrupt the spatially heterogenous structure of wood (MARTINEZ *et al.* 2009; WYMELENBERG *et al.* 2010; WYMELENBERG *et al.* 2011; HORI *et al.* 2014). Milling alters the physical arrangement of wood cells and increases the accessibility of wood polymers to fungal enzymes (FUKAZAWA *et al.* 1982), undoubtedly producing unnatural physiological responses in fungi. Growth in liquid medium also introduces stressors not found in solid-state cultures, potentially confounding findings by introducing non-substrate variables affecting fungal physiology (IMANAKA *et al.* 2010).

In-tact wood has been used in several studies of white-rot and brown-rot wood decay mechanisms (RYU *et al.* 2011). However, most of these studies do not resolve crucial changes in fungal physiology that occur in the very earliest stages of decay. Incipient decay may consist an early pretreatment in white-rot (HORI *et al.* 2014; KUUSKERI *et al.* 2016) and brown-rot (ZHANG *et al.* 2016) fungi that may serve to negate the lignin barrier and allows access to wood polysaccharides. Resolving and understanding these steps is crucial to recreating bio-based wood saccharification *in vitro*, and can pair secreted proteins with their effect on wood substrates, inferring their biological function.

Comparative genomics studies have also shown that there is considerable diversity in the suite of decay enzymes available to different species of white and brown-rot fungi and that the distinction between these two categories of organisms is a continuum (RILEY *et al.* 2014). In addition, brown rot has evolved several times independently in several phylogenetically disparate white-rot species (FLOUDAS *et al.* 2012). These studies suggest that decay mechanisms may vary by species, and recent studies have found major differences in the decay proteins secreted on lignocellulose among species (ZHU *et al.* 2016). These differences are only just being investigated and further work is needed to identify the diversity of decay enzymes produced among basidiomycete species. To complicate things further, degradative enzymes are produced in concert with other proteins that perform other biological processes necessary for survival in wood (BODDY and HISCOX 2016). These non-degradative proteins must be resolved from decay-associated proteins to identify the basal decomposition machinery needed to break apart wood in addition to functionally categorizing non-degradative proteins.

In nature, wood-degrading basidiomycota fungi exist in complex communities of thousands of different microorganisms (RAJALA *et al.* 2012) and have evolved mechanisms to compete and otherwise interact with them to ensure their survival (BODDY 2000). Interspecific interactions are fundamental ecological processes that help determine carbon evolution rates (HISCOX *et al.* 2015b), community successional dynamics (HISCOX *et al.* 2015a), and the ecological niches of fungal species. However, the mechanisms of wood-degrading basidiomycota interactions are yet poorly described with most of the

prior literature for this group of fungi describing successional patterns (CHAPELA and BODDY 1988; BODDY and HEILMANN-CLAUSEN 2008; HISCOX *et al.* 2015a), morphological responses (BODDY 2000), and interaction enzymology (BALDRIAN 2004; HISCOX *et al.* 2010; MALI *et al.* 2017). Few attempts have been made to describe the response of specific genes (EYRE *et al.* 2010; ARFI *et al.* 2013) and proteins during interspecific interactions of wood-degrading basidiomycetes. Omics tools are now available to study more complex, multi-species systems involving a wide variety of wood-degrading basidiomycetes. These techniques will identify specific gene/protein actors responsible for interspecific interactions and help separate them from decay-related genes/proteins.

1.2 Objectives

This dissertation refines the understanding of the mechanisms of decay and interspecific interactions of wood-degrading basidiomycota through a set of experiments aimed at accomplishing the following objectives:

Objective 1: Spatially resolve brown-rot decay mechanisms into a sequence and identify changes and their role in wood decay. This objective is accomplished through a series of experiments described in chapter 3. Two model brown-rot fungi were grown directionally on thin wood wafers so that their degraded substrate could be used to view a progression of decay stages in a single piece of wood. This decay system was used to overlay several enzymatic, gene expression, and chemical analyses of the wood substrate to resolve differences in early and late stages of wood decay also described in later chapters.

Objective 2: Identify temporal changes in the secretomes of two phylogenetically disparate brown-rot fungi and identify interspecific differences in decay mechanisms by investigating the decay of a non-native substrate. Chapter 4 details specific protein secretion patterns of two brown-rot fungi over the course of spruce decay, highlighting disparities in the decay mechanism among species. These differences are again shown in their differing ability to degrade *Sorghum bicolor* (Poales) biomass, described in chapter 5.

Objective 3: Determine the temporal differences in white-rot and brown-rot secretomes and identify interspecific variability in decay mechanisms of each decay type. This work, described in chapter 6, identifies universal secretome characteristics among white-rot and brown-rot fungi at varying decay stages, and describes interspecific diversity in decay mechanism among species of each decay type.

Objective 4: Identify genes and proteins that are important in mediating interspecific interactions to parse secreted proteins into decay and non-decay-related proteins. Chapter 7 describes experiments that recreate antagonistic interactions between two model brown-rot fungi to identify genes and proteins that are specifically used to mediate interactions. This work narrows current mechanistic models to fewer decay-mediating genes and identifies distinct interaction strategies between the competitor species.

Chapter 2 Literature Review

2.1 Plant cell wall micromorphology

Most of the dry mass of plant cells consist of cell wall material and they are the main source of carbon for lignocellulose-degrading fungi. The anatomy and ultrastructure of wood cells help determine the accessibility of these nutrients. Wood cell walls are organized into three main layers: a middle lamella, a primary cell wall, and a secondary cell wall that differ in the timing of their synthesis and their chemical composition (Figure 2.1).

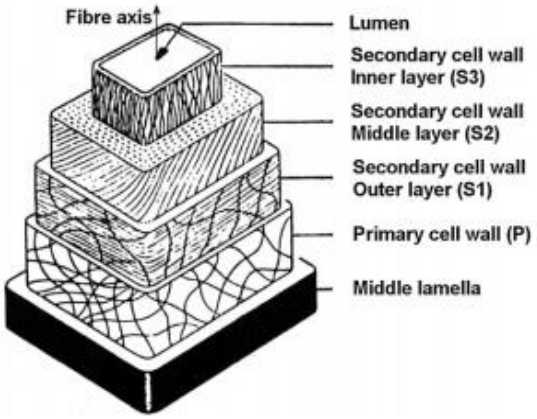

Figure 2.1: Depiction of cell wall layers in wood cells (NIEMINEN *et al.* 2013).

The middle lamella serves as an adhesive layer between neighboring cell walls and is the pectin and lignin-rich outermost point of content with neighboring plant cell walls (ROWELL 2005; DICK-PEREZ *et al.* 2011). Primary cell walls are the thin outermost cell wall layer with respect to the cell lumen and they are in direct contact with the middle lamella (Figure 2.1) (ROWELL 2005). The primary cell walls are composed of

cellulose, hemicelluloses, and pectin, but in most cases, are not lignified (SJORSTROM 1981). Secondary cell walls border the primary cell wall and the cell lumen (Figure 2.1). The secondary cell wall is the thickest cell wall layer and constitutes most of the mass of wood cell walls. Secondary cell walls are lignified (HIMMEL 2008) and the cells of wood-degrading fungi directly contact the secondary cell walls during decay. In wood, conductive xylem cells are connected by perforations in the cell walls called pits that allow the conductance of water and dissolved nutrients in plants (Figure 2.2) (CHOAT *et al.* 2008). The morphology and chemical constitution of these perforations varies between angiosperms (hardwoods) and gymnosperms, but pits in both groups of organisms are covered by a membrane composed of cellulose fibrils embedded in a matrix of pectin polysaccharides (CHOAT *et al.* 2008).

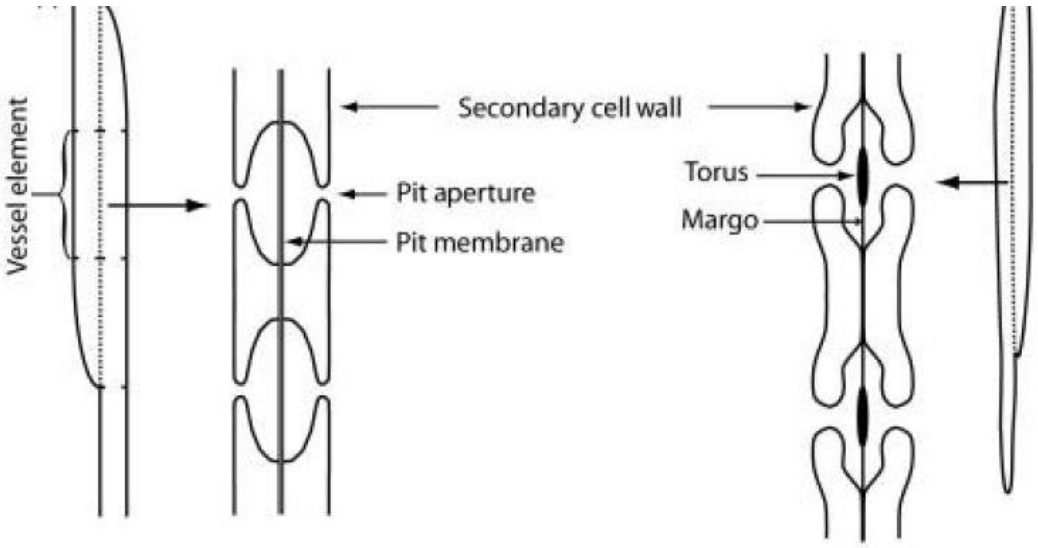

Figure 2.2: Diagram of intercellular pits in angiosperms (left) and gymnosperms (right) (CHOAT *et al.* 2008)

Cellular arrangement of grass (Poales) biomass is fundamentally different than wood and fewer cells in the stem produce thickened secondary cell walls. Conductive

cells are clustered in vascular bundles embedded in a matrix of thin-walled pith cells. The lower abundance of thick, secondary cells walls make grass biomass lower in lignin than wood.

2.2 Plant cell wall chemical composition

Plant cell walls are a complex matrix of polysaccharides and the aromatic polymer lignin collectively referred to as lignocellulose (Figure 2.3). The complex chemical nature of plant cell walls make it recalcitrant and difficult to deconstruct due to the large number of enzyme specificities needed to depolymerize it (ZHAO *et al.* 2012). In addition, cell wall components are tightly associated, leaving structural carbohydrates such as cellulose heavily encrusted with other polymers and difficult to access (Figure 2.3).

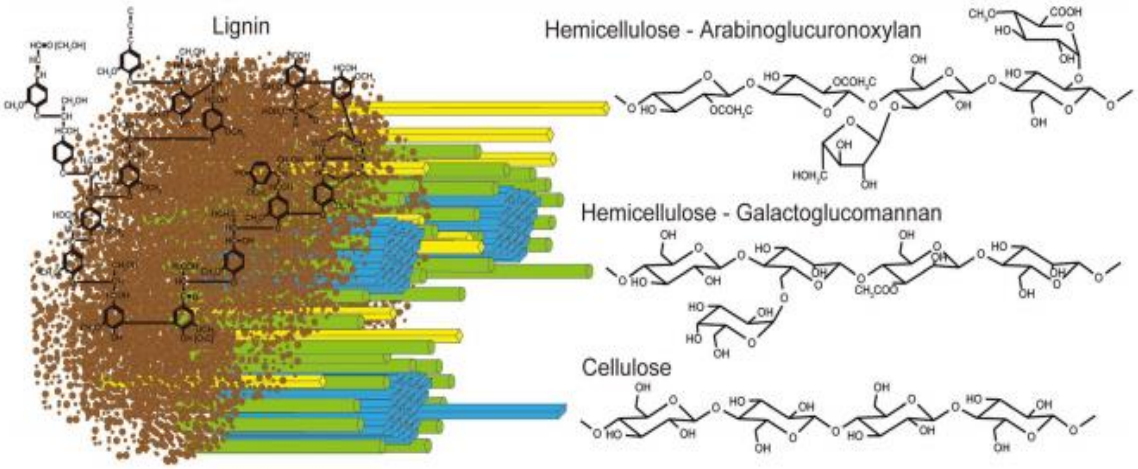

Figure 2.3: Depiction of the polysaccharide components of plant cell walls in association with one another and the aromatic polymer lignin serving as a protective encrusting material (HORI *et al.* 2014).

2.2.1 Cellulose composition and structure

Cellulose is the major polysaccharide component of plant cell walls. Cellulose constitutes 40-55% of the total dry mass in wood and 25-50% of total dry mass in grasses (ZHAO *et al.* 2012). Native cellulose is a linear polysaccharide composed of β-D-1,4-glucopyranose with a repeating unit of two ring-flipped glucose molecules attached in the beta conformation called cellobiose (SJORSTROM 1981). Each glucose molecule adopts a chair conformation with hydroxyl groups on C2, C3, and C5 arranged in the equatorial plane, leaving the axial space occupied by hydrogen atoms (SJORSTROM 1981). This arrangement makes the edges of glucose molecules hydrophilic and the axial surface of the ring hydrophobic, a property that is exploited by cellulose-binding enzymes (KIM *et al.* 2013).

Chains of β-D-1,4-glucopyranose are synthesized into bundles of 24-36 chains called microfibrils (FERNANDES *et al.* 2011), which become associated with each other and embed in a matrix of other polysaccharides to form the cell wall gel matrix (HIMMEL 2008). Inter-chain hydrogen bonds and inter-chain Van der Waals forces between the axial hexose surfaces of stacked chains allow cellulose chains to pack together tightly and form a crystalline structure that excludes water molecules (SJORSTROM 1981). This makes hydrolysis difficult and only specific fungal enzymes, namely cellobiohydrolases, with the aid of cellulose-binding modules can access crystalline cellulose for hydrolysis. Cellulose also contains amorphous regions that are less ordered than crystalline cellulose and are more accessible to water and other β-1,4-glucose-hydrolyzing enzymes (Figure 2.4) (FERNANDES *et al.* 2011). Amorphous regions are interspersed sporadically between

cellulose microfibrils where hemicellulose and lignin form an encrusting layer (OSULLIVAN 1997). These regions are typically degraded first because of their greater accessibility to hydrolases than crystalline regions (BORNSCHEUER *et al.* 2014).

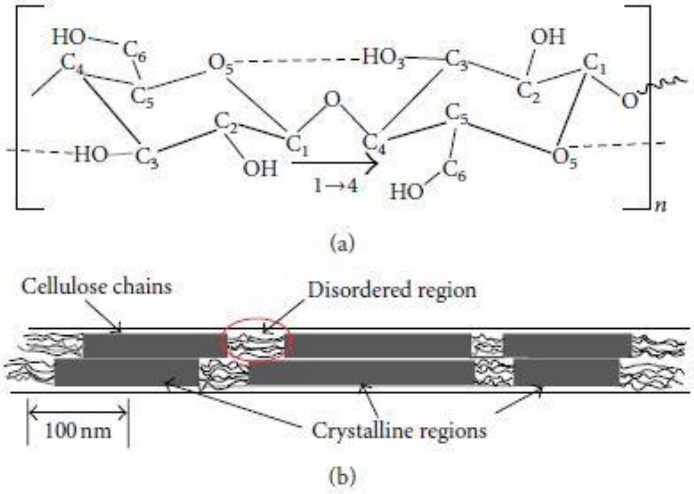

Figure 2.4: A) Diagram of the repeating unit of cellulose, β-1,4-glucopyranose. B) Diagram of amorphous cellulose interspersed in crystalline regions (KHAZRAJI and ROBERT 2013).

2.2.2 Hemicelluloses and Pectin

Hemicelluloses are heterogeneous polysaccharides composed of several pentose and hexose sugars, depending on the biomass source. Hemicelluloses are generally defined by their extractability in alkali and are generally more hydrolysable and amorphous than cellulose (ZHAO *et al.* 2012). Hardwood biomass consists of about 15-30% hemicelluloses which are composed 4-O-methyl glucuronoacetyl xylan (MGAX) a polysaccharide composed of a backbone of about 80% by mass β-D-1,4-xylopyranose, some of which are substituted with O-acetyl groups at C2 and C3 and/or α-1,2-linked 4-

O-methyl glucuronic acid at C2 (SJORSTROM 1981; SCHADEL *et al.* 2010). Hardwoods also contain 2-5% glucomannan (GM), a copolymer of β-1,4-glucopyranose and β-1,4-mannopyranose with a molar ratio of these two components of 1:1 to 1:2 (PULS 1997).

Softwood is composed of about 20% hemicellulose, consisting of mostly galactoglucomannan (GGM), a copolymer of β-1,4-glucopyranose and β-1,4-mannopyranose substituted with α-1,6-linked galactopyranose in addition to O-acetyl groups every 3-4 backbone residues (ROWELL 2005). Softwoods also contain xylans in minor quantities, but unlike hardwoods they are substituted with arabinose residues α-1,3-linked instead of O-acetyl groups (PULS 1997).

Grass (Poales) biomass contains about 20-50% hemicellulose that is primarily composed of O-acetyl-4-O-methyl glucuronoxylan (ZHAO *et al.* 2012). Grass xylans differ in that they are more highly branched, have a lower glucuronic acid content, and contain more L-arabinofuranose than hardwood xylans (PULS 1997). Grass hemicellulose also contains frequent hemicellulose-lignin linkages consisting of ferulic acid and p-coumaric acid moieties of lignin esterified to sugars such as arabinose branching off the xylan backbone (VOGEL 2008).

Pectins are another carbohydrate component of plant cell walls that are a primary component of the gel matrix that other carbohydrates are embedded in during cell wall synthesis (HIMMEL 2008; XIAO and ANDERSON 2013). Pectins are a heterogeneous group of polymers primarily composed of galacturonic acid. Homogalacturonan is the most common (about 65% of pectins) and consists of α-1,4-galacturonic acid partially

methylesterified at C-6 and O-acetylated at O-2 or O-3 (MOHNEN 2008). Substituted homogalacturonans (about 10% of pectins) are composed of a backbone of α-1,4-galacturonic acid decorated with up to 12 different sugars in various types of linkages. Rhamnogalacturonan (20-35% of pectin) is composed of a backbone of repeating units of -α-D-galacturonic acid-1,2-α-L-Rhamnose-1,4- with various sugars and oligosaccharides decorated along the backbone including α-L-arabinofuranose and β-D-galactopyranose (MOHNEN 2008). Pectin functions in cell adhesion in the middle lamellae, as well as forming a gel-like matrix for the deposition of cellulose and hemicellulose in cell wall formation. Pectin is intimately associated with other wood polymers and can reduce accessibility to other wood polysaccharides, making it a primary barrier to wood-degrading organisms (XIAO and ANDERSON 2013).

2.2.3 Lignin structure and composition

Lignin is a heterogeneous aromatic polymer present primarily in plant secondary cell walls and middle lamellae that comprises 10-35% of grass or woody biomass (SJORSTROM 1981). Lignin is composed of three different phenyl-propanoid monomers, *para*-coumaroyl alcohol, coniferyl alcohol, and sinapyl alcohol referred to as p-hydroxyphenyl (H lignin), guaiacyl lignin (G lignin) and syringyl lignin (S lignin), respectively (Figure 2.5)(LEWIS and YAMAMOTO 1990). Lignin is synthesized by coupling resonance delocalized phenoxy radicals of these monomers, generating a seemingly random arrangement of aromatic monomers cross-linked with wood carbohydrates (Figure 2.5) (BRUNOW *et al.* 1998). Radical coupling results in several types of linkages including β-O-4 ether, biphenyl, diaryl ethers, diaryl propane,

phenylcoumarane, spirodenone, and pinoresinol linkages, with β-O-4 ether typically constituting 50% or more of the bonds (BUGG *et al.* 2011). This diversity of linkage types require lignin-degrading organisms to produce a non-selective lignin-depolymerizing system to mineralize lignin (HAMMEL and CULLEN 2008). Hardwood lignins contain a mixture of S and G lignin, softwood lignin is primarily composed of G lignin, and grass lignin contains a mixture of all three monolignols, notably H-lignin which is found in greater amounts than in wood (SJORSTROM 1981). Hardwoods, softwoods, and grasses also differ in the ratios of bond types that exist in lignin, further differentiating the chemistry of the substrates (BUGG *et al.* 2011).

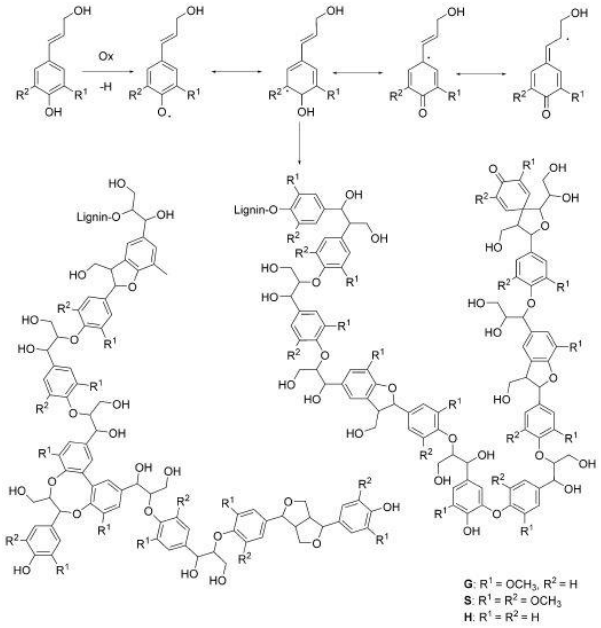

Figure 2.5: Major lignin monomers and some examples of polymerization products (BORNSCHEUER *et al.* 2014).

2.3 Characteristics of fungal wood decay

Wood-degrading basidiomycetes are traditionally broken into two major categories, white rot and brown rot, based on the differences in decay mechanisms and

the chemical and physical properties of degraded wood residues they create (COWLING 1961). White-rot fungi are characterized by their ability to degrade lignin along with all other cell wall components, leaving a cellulose-rich bleached wood residue. Brown-rot fungi selectively attack wood carbohydrates, leaving behind a brown, lignin-rich residue. Despite the common classification into these broad groups, there is a large amount of variability in decay micromorphology (BLANCHETTE 1991), genomics (RILEY *et al.* 2014), and biochemistry (MACDONALD *et al.* 2011; SALVACHUA *et al.* 2013; PRESLEY and SCHILLING 2017) within each group.

2.3.1 White rot

White-rot fungi are the most common type of wood-degrading fungi (GILBERTSON and RYVARDEN 1986) and it is the ancestral rot type for all wood-degrading basidiomycetes (HIBBETT and DONOGHUE 2001). Several major classifications of white rot exist, including simultaneous white rot and selective delignifying species. Simultaneous white-rot fungi degrade all plant cell wall components together, and decaying residues maintain relatively stable percentages of cellulose, hemicellulose, and lignin throughout decay (COWLING 1961). These fungi progressively erode into the secondary cell walls from wood cell lumens to the middle lamellae (Figure 2.6) (ERIKSSON *et al.* 1990).

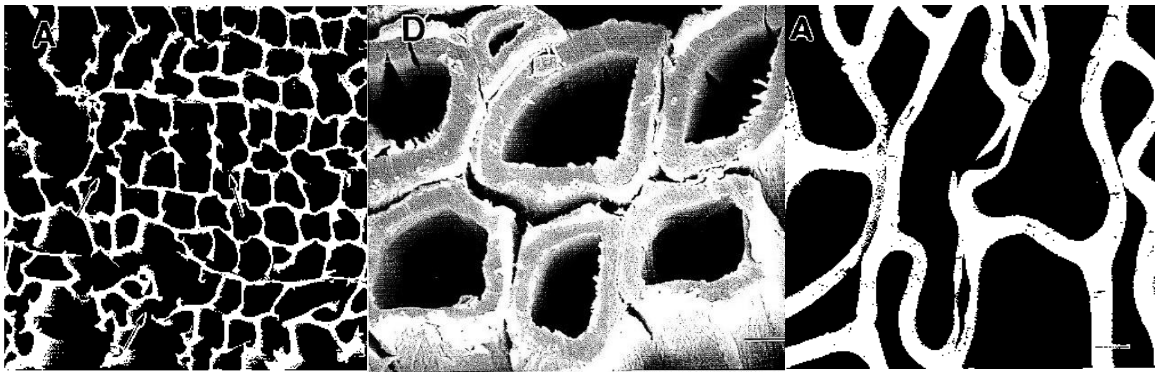

Figure 2.6: Scanning electron micrographs transverse sections of simultaneous white-rotted (left), selective white-rotted (middle), and brown-rotted (right) wood (BLANCHETTE 1995).

Selective lignin-degrading fungi leave wood heavily delignified, sometimes leaving white patches of nearly pure, crystalline cellulose distributed in pockets in the degraded wood (BLANCHETTE 1980). These fungi degrade lignin rich middle lamellae first and leave behind "unglued" wood cells with reduced electron density at the compound middle lamellae (Figure 2.6) (BLANCHETTE 1991).

2.3.2 Brown rot

Brown-rot fungi generally degrade lignin to a lesser degree than white-rot fungi, and selectively attack structural carbohydrates, leaving a residue that is high in lignin, weak, and cubically checked (COWLING 1961). Brown-rotted wood cells have little structural integrity and fracture readily when sectioned (Figure 2.6). Strength loss is due to the early loss of hemicellulose and depolymerization of cellulose (HIGHLEY 1987). Although brown-rot fungi are generally thought to degrade less lignin than white-rot fungi, recent studies show some species of brown-rot fungi can remove up to 40% of lignin from corn stover (KAFFENBERGER and SCHILLING 2013), pine, and aspen wood

(KAFFENBERGER and SCHILLING 2015). These studies indicate that the traditional view of brown-rot fungi primarily leaving lignin in place is not wholly accurate and ligninolytic ability varies among species.

2.3.3 Non-enzymatic Fenton-based decay mechanisms in brown-rot fungi

Selective carbohydrate depolymerization in brown-rot fungi begins when wood is in-tact and has a low porosity (FLOURNOY *et al.* 1991) and enzymes cannot readily penetrate the cell wall structure. Brown-rot fungi produce low molecular weight extracellular oxidants generated by Fenton's reagent (Fe^{2+} and H_2O_2) to depolymerize wood polysaccharides not accessible by large enzymes (KOENIGS 1974). Free oxalate-Fe^{3+} chelates are thought to be reduced by extracellular hydroquinones regenerated by an extracellular quinone redox cycle (JENSEN *et al.* 2001) driven by intracellular or membrane-bound quinone reductases (COHEN *et al.* 2004). Fe^{2+}-oxalate chelates can reduce O_2 in wood and produce H_2O_2 and a full Fenton system (BALDRIAN and VALASKOVA 2008). There is some disagreement as to when Fenton-based oxidative chemistry occurs during brown rot. Some authors postulate that it occurs as an early stage pretreatment (ZHANG *et al.* 2016), followed by enzymatic saccharification, while others suggest that chelator-mediated Fenton chemistry expressed throughout the decay process (GOODELL *et al.* 2017).

2.3.4 Oxalic acid secretion

Brown-rot fungi produce large amounts of oxalic acid during decay, resulting in wood residues with pH ≤ 3 (GREEN *et al.* 1991; SCHILLING and JELLISON 2005). Oxalate

is thought to play several roles in wood decay, including chelating and solubilizing Fe^{3+} to facilitate Fenton chemistry (VARELA and TIEN 2003; ARANTES *et al.* 2009) and serving as a carbon sink to drive cellular energy production (MUNIR *et al.* 2001b). Interestingly, at low concentrations, below 1 mM, oxalate facilitates Fenton-mediated polysaccharide depolymerization, but inhibits it at higher concentrations (TANAKA 1994). This property may create a Fenton reaction gradient inversely related to oxalate concentration, where the reaction is repressed at high oxalate concentrations near the hyphae and facilitated at lower concentrations near wood polymers (HYDE and WOOD 1997). Its effect on Fenton chemistry is likely one of the reasons oxalate levels are tightly controlled by brown-rot fungi (SCHILLING and JELLISON 2005). Oxalate-mediated Fenton-inhibition prevents the destruction of fungal glycoside hydrolases in vitro (PRESLEY *et al.* 2016), and can help segregate incompatible mechanism components in brown-rot fungi.

2.4 Secretomes of wood-degrading basidiomycetes

Wood decay mechanisms and other essential functions are mediated by proteins secreted into the extracellular space, collectively called the secretome. Secretomes vary greatly between the two rot types, with brown-rot fungi generally producing a reduced secretome lacking many of the characteristic enzyme classes found in white-rot fungi (WYMELENBERG *et al.* 2010; FLOUDAS *et al.* 2012). In addition, comparative genomics studies suggest that within rot types there is significant functional diversity and that rot type characteristics are lie on a spectrum rather than two rigid categories (RILEY *et al.* 2014). Recent studies have shown that secretome composition varies significantly among species of white-rot (SALVACHUA *et al.* 2013) and brown-rot fungi (PRESLEY and

SCHILLING 2017). This increased complexity makes it more difficult to qualify decay types by their secretome composition, and instead presence of absence of each relevant decay enzyme type must be considered individually within secretomes of each model species.

2.4.1 Glycoside hydrolases (GHs) and carbohydrate esterases (CE)

GHs are found in all kingdoms of life and are vital to the turnover of plant organic matter. GHs are separated into different families based on their sequence similarity, which is indicative of common folds and substrate preferences (LOMBARD *et al.* 2014). GHs cleave glycosidic bonds between sugars in poly-, oligo-, or disaccharides by adding water to the bond forming two alcohol groups at the reducing and non-reducing end of the sugar molecules (SINNOTT 1990). Carbohydrate esterases catalyze the hydrolysis of ester bonds and are similarly classified into different families based on their sequence similarity and substrate affinities (LOMBARD *et al.* 2014). CEs relevant to lignocellulose decay are primarily hemicellulose-debranching enzymes, where they hydrolyze acetyl groups esterified to hemicellulose sugars as well as ester bonds made between lignin and hemicellulose sugars (BIELY *et al.* 2016). GHs and CEs play an important role in the fungal metabolism of wood and the former are some of the most abundantly-produced proteins in wood-degrading basidiomycete secretomes (ALFARO *et al.* 2014).

Cellulose degradation requires several types of GHs that differ in white-rot and brown-rot fungi. Both groups of fungi secrete endoglucanases (EG) and β-glucosidases (BGL), but most brown-rot fungi either lack cellobiohydrolases (CBH) in their genome

sequences (RILEY *et al.* 2014), or do not produce them during wood decay (EASTWOOD *et al.* 2011). EGs primarily cleave amorphous cellulose internally and liberate reducing and non-reducing ends from the polymer (ERIKSSON *et al.* 1990), and EGs primarily belong to GH families 5,7,12, and 45 (PAYNE *et al.* 2015). GH 5 proteins produce the majority of the cellulolytic activity found in brown-rot secretomes (RYU *et al.* 2011). Fungal proteins classified as GH 5 also act on a wide range of polysaccharides, including mannan (endo-β-1,4-mannanase), branched beta glucan (exo-β-1,3-glucanase and endo-β-1,6-glucanases), and others (ASPEBORG *et al.* 2012; LOMBARD *et al.* 2014).

CBHs processively hydrolyze cellobiose units from the non-reducing or reducing ends of cellulose, found in GH families 6 and 7, respectively (PAYNE *et al.* 2015). CBHs are not found in brown-rot genomes except in the Boletales (RILEY *et al.* 2014), where they are not major components of the secretomes of these fungi (EASTWOOD *et al.* 2011). The only brown-rot fungus shown to produce significant amounts of CBH in artificial culture is *Coniophora puteana* (SCHMIDHALTER and CANEVASCINI 1993b). However, both variants of this enzyme produced by this fungus constituted only about 13% of all secreted protein by mass, indicating it is not the primary component of the cellulose-degrading cocktail of this brown-rot fungus (SCHMIDHALTER and CANEVASCINI 1993b). CBHs allow white-rot fungi to degrade crystalline cellulose, because CBHs often contain a cellulose-specific carbohydrate-binding module (CBM) that directs the catalytic domain to crystalline cellulose surfaces, leading to hydrolysis (PAYNE *et al.* 2015). These cellulose-specific CBMs are not found in brown-rot genomes (FLOUDAS *et al.* 2012). Depending on the species, CBHs can be the most abundant protein in white-rot

secretomes (SALVACHUA *et al.* 2013), a place taken by other GHs in brown-rot fungi (PRESLEY and SCHILLING 2017).

BGLs catalyze the hydrolysis of glycosidic bonds between glucose and an aglycone, and they are common constituents of white-rot and brown-rot secretomes (MARTINEZ *et al.* 2009; FERNANDEZ-FUEYO *et al.* 2016). BGLs are necessary to cleave cellobiose generated by CBHs into glucose in white-rot fungi. In brown-rot fungi they act on cellobiose and cello-oligomers produced by EGs or Fenton-mediated oxidative cellulose cleavage (BALDRIAN and VALASKOVA 2008). BGLs are mostly found in GH families 1, 2, and 3 (PAYNE *et al.* 2015), but proteins in these families also act on other sugar-aglycone combinations, including pentoses such as xylose, mannose, and other hemicellulose-derived sugars.

White-rot and brown-rot fungi both secrete GHs that degrade hemicelluloses and pectins, although the type and relative abundance of each type varies by species. In wood-degrading basidiomycetes, endo-β-1,4-xylanases (EX) belonging to GH family 10, 11, and 30 cleave the backbone of xylan polymers into smaller oligomers (BIELY *et al.* 1997). Debranching enzymes such as GH 67 and 115 α-1,2-glucuronidases and CE family 1, 4, and 16 acetyl xylan esterases remove side groups from xylan backbones (BIELY 2012). Xylose residues are cleaved from xylooligomers by secreted β-xylosidases, typically found in GH 3 and 42 in wood-degrading basidiomycetes (BIELY *et al.* 2016). Grass xylans contain α-1,2 or α-1,3-arabinofuranose residues, that are sometimes esterified to lignin via ferulic acid esters. Wood-degrading basidiomycetes hydrolyze

arabinose residues from xylan by secreting primarily GH 43 and 51 arabinofuranosidases, and ferulic acid esters are cleaved primarily by certain CE 1 enzymes (BIELY *et al.* 2016). Interestingly, not all brown-rot fungi contain CE 1 putative ferulic acid esterases in their genome sequences (RILEY *et al.* 2014), which may be the reason some species have difficulty degrading grass biomass (KAFFENBERGER and SCHILLING 2013).

Glucomannan backbones found in softwood hemicellulose are cleaved internally by members of GH 2, 5, and 26, and monosaccharides are liberated from manno-oligomers by β-mannosidases and β-glucosidases found in GH 2 and 5 (RYTIOJA *et al.* 2014). Mannan contains α-1,6-galactose branching groups on its backbone that are hydrolyzed by α-galactosidases found primarily in GH 27 in wood-degrading basidiomycetes (RILEY *et al.* 2014). O-acetyl groups found in mannan are removed by similar de-acetylating enzymes that act on xylan.

Pectin is degraded by a mixture of GHs and polysaccharide lyases. The α-1,4-galacturonic acid bonds in polygalacturonic acids hydrolyzed by GH 28 proteins possessing endo/exo-polygalacturonase activity. Rhamnogalacturonan is degraded by different GH 28 proteins that can hydrolyze α-1,2-glycosidic bonds between rhamnose and galacturonic acid (VAN DEN BRINK and DE VRIES 2011). Other pectin-specific enzymes secreted by wood-degrading basidiomycetes include GH 78 α-rhamnosidases, GH 88 rhamnogalacturonanases, GH 53 β-endogalactanases, and pectin methylesterases primarily CE 8 proteins (VAN DEN BRINK and DE VRIES 2011). Some enzymes such as α-

arabinofuranosidases employed to degrade hemicellulose are also used to debranch minor components of pectin.

2.4.2 Polysaccharide lyases (PL)

Unlike GHs, polysaccharide lyases (PLs) cleave glycosidic bonds in polysaccharides by a β-elimination mechanism, which can only occur in polysaccharides containing a carboxylic acid a C5 (uronic acids) (GARRON and CYGLER 2010). In wood, pectin is the major polyuronic acid polymer and a few types of PLs are produced by wood-degrading basidiomycetes to degrade heavily methylated (pectin lyases) and less methylated (pectate lyases) pectin (VAN DEN BRINK and DE VRIES 2011). Most fungal pectin/pectate lyases belong to PL family 1.

2.4.3 Polysaccharide monooxygenases PMOs

Originally described as GH 61 proteins with weak endoglucanase activity, polysaccharide monooxygenases (PMOs) have been shown to be copper-containing oxidoreductases that perform single electron oxidations on polysaccharide chains internally. They cleave glycosidic bonds, yielding a 4-keto aldose or aldonic acids at the non-reducing and reducing ends, respectively (QUINLAN *et al.* 2011; BEESON *et al.* 2012). PMOs require reducing agents to generate their catalytic cycle, and these can be biomass-derived phenolics such as gallic acid (QUINLAN *et al.* 2011), laccase-generated lignin breakdown products (FROMMHAGEN *et al.* 2017), or other oxidoreductases such as cellobiose dehydrogenase (PHILLIPS *et al.* 2011). PMOs are found in both white-rot and brown-rot genomes, but brown-rot fungi typically have fewer copies (RILEY *et al.* 2014).

PMOs are highly expressed by white-rot fungi (MAHAJAN and MASTER 2010; MACDONALD *et al.* 2011), but they are a much smaller component if found at all in brown-rot secretomes (EASTWOOD *et al.* 2011; RYU *et al.* 2011), indicating a reduced role in brown-rot type cellulose decay.

2.4.4 Fungal peroxidases

Fungal type II peroxidases (POD) are the primary enzymatic agents thought to be responsible for lignin decomposition wood-degrading basidiomycetes, and they are only found in white-rot secretomes (FLOUDAS *et al.* 2012). PODs are heme-containing oxidoreductases that catalyze the two-electron reduction of hydrogen peroxide to water and the concomitant single electron oxidation of two molecules of substrate (HRYCAY and BANDIERA 2015). Several types of lignin degrading peroxidases have been identified in white-rot fungi, including Lignin peroxidase (LiP), Manganese peroxidase (MnP), Versatile peroxidase (VP), and Dye-decolorizing peroxidase (DyP), each differentiated by their preferred substrate and enzyme architecture (POLLEGIONI *et al.* 2015).

LiPs are high redox potential peroxidases capable of oxidizing phenolic and nonphenolic moieties in lignin. LiPs are also thought to use small phenolic fungal metabolites such as veratryl alcohol as redox mediators that diffuse into the lignocellulose and oxidize lignin (RUIZ-DUENAS and MARTINEZ 2009). They are distinguished from other peroxidases by the presence of a surface-exposed tryptophan involved in substrate oxidation and the lack of a Mn-binding site (PIONTEK *et al.* 2001; ACEBES *et al.* 2017). LiPs were first discovered in the model white-rot fungus

Phanerochaete chrysosporium (TIEN and KIRK 1983) as the main component of its ligninolytic system. However, genomic (RILEY *et al.* 2014) and proteomic (FERNANDEZ-FUEYO *et al.* 2016; RYTIOJA *et al.* 2017) studies of a wider diversity of white-rot fungi show that many fungi lack LiPs and utilize other peroxidase types such as MnP and VP as their main ligninolytic component.

MnPs lack the surface exposed tryptophan found in LiPs and instead oxidize Mn^{2+} to Mn^{3+} by coordinating it at a triad of acidic residues located at the heme edge (SUNDARAMOORTHY *et al.* 1994). Mn^{3+} is thought to mediate lignin oxidation, but it is only able to oxidize phenolic lignin, which only constitutes a minority portion of lignin. MnPs may be able to oxidize non-phenolic lignin through a radical cascade where Mn^{3+} oxidizes extracellular fatty acids to peroxy radicals that oxidize of non-phenolic portions of lignin (KAPICH *et al.* 1999; HAMMEL and CULLEN 2008). MnPs are the ancestral form of type II peroxidases and as such are widely distributed among and produced by white-rot fungi (RUIZ-DUENAS *et al.* 2013). Some white-rot fungi secrete MnPs as the major peroxidase in their secretome, particularly in the early stages of wood decay (HORI *et al.* 2014; KUUSKERI *et al.* 2016).

VPs are hybrid peroxidases that possess an acidic Mn-binding site and a surface exposed tryptophan. This allows them to oxidize Mn^{2+} and higher redox potential aromatic substrates such as veratryl alcohol and reactive black 5 that may serve as reaction mediators that diffuse into the lignocellulose matrix to oxidize lignin (PEREZ-BOADA *et al.* 2005). VPs appear to be evolutionary intermediates between MnPs and

LiPs, and not all white-rot fungi possess these enzymes (RUIZ-DUENAS *et al.* 2013). VPs were originally isolated from *Pleurotus* species (CAMARERO *et al.* 1999), and they are the predominant peroxidases secreted by *Pleurotus ostreatus* (SALVACHUA *et al.* 2013).

DyPs were isolated from fungi based on their ability to oxidize high redox potential anthraquinone dyes not oxidizable by other peroxidases (HOFRICHTER *et al.* 2010). They are phylogenetically disparate from other fungal peroxidases, showing little sequence similarity (RUIZ-DUENAS *et al.* 2013). Like LiPs, DyPs oxidize bulky substrates by long range electron transfer from the substrate to the oxidized heme (LINDE *et al.* 2015). DyPs are widely present in a number of white-rot secretomes, but they typically are less abundant than other peroxidases (SALVACHUA *et al.* 2013; FERNANDEZ-FUEYO *et al.* 2016). They are also found in some lignin-degrading bacteria, where they are thought to further depolymerize soluble lignin oligomers into fragments small enough to take up into the cell (ROBERTS *et al.* 2011; SANTOS *et al.* 2014).

2.4.5 Multicopper oxidases (MCO)

MCOs are a diverse group of copper-containing oxidoreductases found in all kingdoms of life, particularly in plants and fungi. MCOs catalyze the 4-electron reduction of O_2 to water and the concomitant oxidation of 4 equivalents of an organic substrate, typically a phenol (KUES and RUHL 2011). Laccases are MCOs that oxidize free or lignin-associated phenolic substrates to reactive phenoxy radicals and are thought to participate in degradation of lignin, primarily in white-rot fungi (BALDRIAN 2006). In addition to degradative functions, fungi also use laccases for defensive functions such as

melanin synthesis (KUES and RUHL 2011; UPADHYAY *et al.* 2016b) and the degradation of toxic metabolites (HISCOX and BODDY 2017). However, most research on laccases of wood-degrading basidiomycetes has focused on their role in lignin degradation. Some brown-rot fungi such as *Postia placenta* also express a laccase during decay (AN *et al.* 2015), were it is thought to be involved in producing an extracellular Fenton system (WEI *et al.* 2010). However, brown-rot laccases are either minor component of the proteome or not detectable at all, and herculean efforts must be taken to produce enough of this enzyme from crude extracts for study (WEI *et al.* 2010). Not all white-rot fungi produce laccase either and it is notably absent in the genome of *Phanerochaete chrysosporium* (MARTINEZ *et al.* 2004). However most white-rot fungi do produce laccase (ALFARO *et al.* 2014), and laccases are the most abundant protein in several white-rot secretomes including *Dichomitus squalens* and *Pleurotus ostreatus*, indicating their importance in wood decay mechanisms (FERNANDEZ-FUEYO *et al.* 2016; RYTIOJA *et al.* 2017).

2.4.6 Oxidases in wood decay

Several oxidases are thought to function as a source of H_2O_2 for white-rot peroxidases or brown-rot Fenton chemistry by using wood degradation products in the extracellular medium as electron sources for O_2 reduction. While both white-rot and brown-rot fungi produce some type of oxidases, white-rot fungi have a more diverse genomic arsenal of oxidases (RILEY *et al.* 2014) and they generally are found in greater abundance in white-rot secretomes (ALFARO *et al.* 2014).

Glucose oxidases (GOX) are extracellular proteins that oxidize glucose and to a lesser extent other pyranoses to aldonic acids and simultaneously reduce O_2 to H_2O_2 (WONGNATE and CHAIYEN 2013). GOXs are members of the flavin-containing Glucose-Methanol-Choline (GMC) oxidoreductase family and GOX-like GMCs are commonly found in white-rot and brown-rot genomes (RILEY *et al.* 2014). GOXs are commonly found in white-rot secretomes and several examples of glucose oxidases from these fungi have been characterized (SHIN *et al.* 1993; DANIEL *et al.* 1994). Brown-rot fungi secrete some GMC oxidoreductases of unknown function, and it is not clear if they function as GOXs because no examples of characterized brown-rot GOXs exist. Some secreted GMCs in brown-rot fungi are not homologous to any known GOXs and are not uniformly secreted among brown-rot species (PRESLEY and SCHILLING 2017). These brown-rot GMCs likely function as other types of H_2O_2-generating oxidases known to exist in wood-decay fungal secretomes such as alcohol oxidases.

Methanol oxidases (MOX) are also GMC oxidoreductases produced by both white-rot and brown-rot fungi that utilize methanol and to a lesser degree other primary alcohols as a source of electrons to reduce O_2 to H_2O_2 (WONGNATE and CHAIYEN 2013). MOX has been implicated in producing H_2O_2 for Fenton chemistry in the brown-rot fungus *Gloeophyllum trabeum* (DANIEL *et al.* 2007), however it is not clear if this enzyme could function in the conditions present in the extracellular medium. MOX is also commonly found in white-rot secretomes (KUUSKERI *et al.* 2016) where it is likely a source of H_2O_2 to power peroxidase enzymes.

Aryl alcohol oxidases (AAO) are GMC oxidoreductases that utilize primary aromatic alcohols from wood or fungal origin as a source of electrons for H_2O_2 production (HERNANDEZ-ORTEGA *et al.* 2012). AAOs were originally isolated from the white-rot fungus *Pleurotus eryngii* (GUILLEN *et al.* 1990). AAOs typically constitute only a small portion of total protein in the secretome (FERNANDEZ-FUEYO *et al.* 2016), except in *Schizophyllum commune*, which produces a large amount of GMC oxidoreductases, including an AAO (ZHU *et al.* 2016). Wood-degrading fungi produce several aromatic compounds that are oxidized by AAO that may drive their degradative systems in addition to lignin breakdown products that serve as substrates (GUTIERREZ *et al.* 1994). Aryl alcohol dehydrogenases and aryl aldehyde dehydrogenases are also present in a number of wood-degrading basidiomycete secretomes (GUILLEN and EVANS 1994), and these may drive the regeneration of AAO substrates for H_2O_2 production (HERNANDEZ-ORTEGA *et al.* 2012).

Copper radical oxidases (CROs) are extracellular enzymes that utilize C2 and C3 organic aldehydes and alcohols as an electron donors for H_2O_2 production (WHITTAKER 2005). The most relevant CRO involved in lignocellulose decay by wood-degrading basidiomycetes is glyoxal oxidase, produced primarily by white-rot fungi (KERSTEN and CULLEN 2014). Brown-rot fungi produce CROs as well, but no examples of these enzymes have been characterized and the importance of these enzymes as a component of brown-rot secretomes varies by species (PRESLEY and SCHILLING 2017). Some brown-rot species such as *Wolfiporia cocos* secret CROs on wood substrates, one of which is highly upregulated (GASKELL *et al.* 2016), whereas CROs in *Postia placenta* are not as highly

upregulated on wood substrates (WYMELENBERG *et al.* 2010). Brown-rot secretomes also vary in their CRO content. The secretome of the brown-rot fungus *Serpula lacrymans* grown on spruce wood contains an uncharacterized CRO, whereas a homologous protein was not found in the secretome of the brown-rot fungus *Gloeophyllum trabeum* (PRESLEY and SCHILLING 2017).

Glyoxal oxidases (GLX) are the major CRO produced by white-rot fungi. GLXs oxidize C_1-C_3 aldehydes, with the concurrent reduction of O_2 to H_2O_2 (WHITTAKER *et al.* 1996), which can then be used as a substrate for ligninolytic peroxidases or to facilitate Fenton chemistry (KERSTEN and CULLEN 2014). The relative amounts of this enzyme present in white-rot secretomes and the number of copies found in white-rot genomes varies considerably (FLOUDAS *et al.* 2012; RILEY *et al.* 2014). In addition, substrate affinities among GLX variants also differ considerably, making the catalytic capabilities of different white-rot species non-uniform (VANDEN WYMELENBERG *et al.* 2006). GLX is a much smaller component of the *Phanerochaete chrysosporium* secretome than LiP, but it has a much higher kcat, illustrating that low or relatively low abundance proteins in fungal secretomes can have disproportionate roles in the decay mechanism (KERSTEN 1990).

2.4.7 Cellobiose Dehydrogenase

Cellobiose dehydrogenase (CDH) is a flavin-containing hemoprotein that carries out the 2 electron oxidation of cellobiose to cellobionic acid with the concomitant reduction of an electron acceptor such as a quinone, phenoxy radical, Fe^{3+}, or Cu^{2+}

(HENRIKSSON *et al.* 2000). CDHs have also been shown to serve as an enzymatic electron source for PMOs and regenerate the active form of those enzymes (LANGSTON *et al.* 2011). In this way, CDH may be a component of the cellulolytic system of PMO-producing fungi, including most white-rot fungi (PHILLIPS *et al.* 2011). CDHs may also function in reducing concentrations of cellobiose, a known inhibitor of CBHs produced by white-rot fungi (HENRIKSSON *et al.* 2000). CDHs are present in the genomes of most white-rot fungi, but are absent from the genomes of many brown-rot fungi outside of those found in Boletales (SCHMIDHALTER and CANEVASCINI 1993a) and Gloeophyllales (FLOUDAS *et al.* 2012). In those brown-rot fungi that do produce CDH, it may serve to reduce Fe^{3+} to create Fenton's reagent extracellularly (HYDE and WOOD 1997).

2.4.8 Non-degradative protein functions

The secretomes of wood-degrading basidiomycetes have been extensively studied for their capacity to facilitate wood decay. However, fungal secretomes contain a large proportion of proteins of unknown function that likely do not participate in decay. Identifying the complete set of proteins required for decay requires segregating out those that perform non-degradative functions. In addition, wood-degrading basidiomycete secretomes are relatively poorly characterized and as a result a large proportion of identified proteins are hypothetical proteins of unknown function, often comprising 20% or more of all proteins identified (PRESLEY and SCHILLING 2017).

Hydrophobins are small ~20 kDa, Cys-rich, amphiphilic proteins associated with fungal cell walls that help form a hydrophobic barrier around the fungal cells and are

sometimes found in fungal secretomes (LINDER *et al.* 2005). These proteins function in concert with melanins in the cell wall to prevent desiccation and increase cell wall complexity to inhibit enzymatic degradation. These proteins self-assemble into a layer within the cell wall and help allow fungal hyphae to grow aerially without desiccating, as well as mediating host invasion in plant pathogens (BAYRY *et al.* 2012).

Wood-degrading basidiomycetes also secrete several proteins that may mediate interspecific interactions. Lectins are carbohydrate-binding proteins and are found in a wide diversity of mushroom-forming and wood-degrading species (TATENO and GOLDSTEIN 2003; BOVI *et al.* 2013). Some lectins are known to possess insecticidal properties, and may function as antifeedants toward invertebrates (VARROT *et al.* 2013). There are relatively few characterized basidiomycete lectins and their biological function is not well known, but they are frequently found in basidiomycete secretomes where they may be some most abundant components of the secretome (PRESLEY and SCHILLING 2017).

Some basidiomycetes are also known to produce pore-forming toxins in vegetative hyphae and/or fruiting bodies that may be involved in mediating defense or interspecific combat. The mushroom-forming fungus *Volvariella volvacea* produces a pore-forming delta-endotoxin homologous to *Bacillus thuringiensis* toxin named volvatoxin (SCHNEPF 1995; LIN *et al.* 2004). Volvatoxin oligomerizes on the membranes of eukaryotic cells, forming pores that lead to cell lysis (WENG *et al.* 2004). Similar hemolytic protein toxins are found in fruiting bodies of the brown-rot fungus *Laetiporus*

sulphureus which produces a lectin that functions by oligomerizing within cell membranes of the cells of target species, producing a pore that causes cell lysis (TATENO and GOLDSTEIN 2003). This protein shares high homology to a mosquitocidal protein produced by *Bacillus sphaericus*, which suggests it may be an insect deterrent. Other wood-degrading basidiomycetes such as *Gloeophyllum trabeum* secrete uncharacterized proteins with high homology to volvatoxin in great abundance when grown in axenic cultures on wood (PRESLEY and SCHILLING 2017). This suggests that the production of pore-forming endotoxins is a hard-wired component of some fungal secretomes and is expressed even in the absence of fungivores or competitor species.

2.5 Interspecific interactions of wood-degrading basidiomycetes

Rotting wood is an ecologically complex environment that contains communities of hundreds to thousands of fungal and bacterial species across a variety of taxonomic groups (RAJALA *et al.* 2012). Community composition is dynamic and species are constantly being replaced by successors as the substrate becomes more degraded (BODDY and HEILMANN-CLAUSEN 2008; RAJALA *et al.* 2011). Life in wood therefore requires that wood decay fungi deploy tactics to deal with competitors and exclude other microorganisms from a volume of wood.

Wood-degrading basidiomycetes utilize several physical, chemical, and biochemical techniques to compete with other fungi (BODDY 2000). Wood-degrading basidiomycetes exclude competitors from captured wood by constructing melanized physical barriers between the hyphae of the competitors, as is seen in spalted wood

(RAYNER and BODDY 1988). Melanized tissue serves as an oxidant-resistant barrier deposited in fungal cell walls that protects fungal cells from extracellular oxidants produced by competitor species and also increases the heterogeneity of the cell wall matrix, making it more difficult to degrade (CORDERO and CASADEVALL 2017). The synthesis of melanins is mediated in part by polyphenol oxidases that polymerize phenolic metabolites (KUES and RUHL 2011). Interaction boundaries between competing fungi show increases in laccase activity, supporting their involvement in producing melanized zones between fungi, or degrading the melanins of competitors (IAKOVLEV and STENLID 2000; BALDRIAN 2004). In *Trichoderma viride*, laccase activity induced during hyphal contact with competitors, but it is not necessarily involved in melanin synthesis (LAKSHMANAN and SADASIVAN 2016). In white-rot fungi, MnP activity also increases at the interaction zone, indicating an increase in extracellular oxidant production is part of an interaction strategy (HISCOX *et al.* 2010).

Wood-degrading basidiomycetes also secrete enzymes that can degrade competitor proteins and cell wall components, such as proteases, chitinases, and β-glucanases. For example, β-N-acetyl-glucosaminidase was induced in interacting hyphae of two wood-degrading basidiomycetes, *Phanerochaete vetulina* and *Hypholoma fasciculare*, suggesting that fungal cell wall degradation was upregulated (SNAJDR *et al.* 2011). Chitinase activity was induced in the interaction of *Phanerochaete chrysosporium* and *Heterobasidion irregulare*, likely a result of the induction of a GH 18 protein in the former (KARLSSON *et al.* 2016). Some proteases were upregulated in the interaction of the white-rot fungus *Pycnoporus coccinius* with competitor fungi (ARFI *et al.* 2013), but this

class of protein appears to be more commonly upregulated in parasitic interactions of *Trichoderma harzianum* (UJOR *et al.* 2012).

Small molecules are also potent combative tools used by microbes, and secondary metabolite production is often induced by interspecific contact. Wood-degrading fungi are rich sources of secondary metabolites (SMs) as shown by the diversity of SM-synthesizing genes in their genomes (LACKNER *et al.* 2012; WAWRZYN *et al.* 2012). Some of these metabolites are produced to mediate interspecific interactions (HISCOX and BODDY 2017), and changes in fungal metabolome during interactions has been observed in many fungi, including wood-degrading basidiomycetes. Several changes to volatile metabolite profiles of wood-degrading basidiomycetes have been observed in interaction cultures, including increases in certain sesquiterpenes (EL ARIEBI *et al.* 2016), monoterpenes (EVANS *et al.* 2008), glycosides (YAO *et al.* 2016), and small aromatics (HYNES *et al.* 2007; PEIRIS *et al.* 2008). Many of these previous studies only track changes in the production of volatile SM scaffolds, during interactions, leaving the identity of the soluble, bioactive SMs and their biological activity unknown.

Central carbon metabolism pathways are also altered because of interspecific interactions, likely due to the energy-intensive nature of interspecific interactions. Metabolomics analysis of interacting hyphae of the white-rot fungi *Trametes versicolor*, *Dichomitus squalens,* and *Pleurotus ostreatus* has also identified upregulated intracellular carnitine metabolites that signified an increase in fatty and amino acid metabolism and general energy production (LUO *et al.* 2017). In a separate study, when confronted with

other wood-degrading basidiomycetes, *T. versicolor* upregulated the expression several oxidoreductases such as cytochrome p450s that may be involved in SM synthesis (EYRE *et al.* 2010). These studies show that in addition to extracellular proteins and metabolites, interactions are ultimately mediated by intracellular processes.

Individual species have varying combative abilities, often indicative of which successional stage they occupy during the process of wood decay. Primary colonizers rapidly enter freshly felled wood and exhibit rapid growth and a short reproductive cycle (RAYNER and BODDY 1988). Many primary colonizers may be latently present in living wood and begin decomposition when the host is killed (PARFITT *et al.* 2010). Secondary colonizers occupy wood by displacing primary colonizers, which requires a greater combative ability (HOLMER and STENLID 1997). Some secondary colonizers, such as *Lenzites betulina*, act as facultative parasites on primary or early secondary colonizers such as *Trametes versicolor*, a very common early secondary colonizer of angiosperm wood (RAYNER *et al.* 1987). *L. betulina* colonizes wood already infiltrated by *T. versicolor* by digesting its hyphae. Mycoparasite-host interactions have been extensively studied in *Trichoderma harzianum*, because of its potential for use as a biocontrol agent of plant pests (HARMAN *et al.* 2004). While it is not a wood-degrading basidiomycete, *T. harzianum* can provides insight into how basidiomycetes may mediate these interactions. *T. harzianum* recognizes host hyphae by binding to lectins on the surface of the host and subsequently form appressorium-like structures on their cell wall (INBAR *et al.* 1996). The parasite then secretes endo and exo-chitinases and proteases which act

synergistically with mycotoxins to kill host cells (SCHIRMBOCK *et al.* 1994). Similar mechanisms may be employed in by basidiomycete mycoparasites to overtake their hosts.

Interspecific interactions in wood-degrading basidiomycetes have been studied by recreating interactions in synthetic cultures by growing different species in opposition to one another (BODDY 2000). Performing interactions on plate cultures clearly resolves the interacting hyphae and the interaction zone can easily be separated from non-interacting hyphae for various analyses (HISCOX *et al.* 2010; YAO *et al.* 2016). However, culturing on defined medium may not recapitulate native interaction mechanisms due to unnaturally high nutrient abundance or other confounding influence on fungal physiology (CROWTHER *et al.* 2017). Several studies utilize whole-block microcosms to study fungal interspecific interactions, but these often do not have the ability to resolve interacting hyphae as easily (SONG *et al.* 2012; HISCOX and BODDY 2017). Wood-based microcosms with better spatial resolution of hyphal types must be employed to recreate interaction mechanisms under more natural physiological conditions.

Chapter 3 Spatial resolution of a temporal progression of decay and the identification of a two-step wood decay mechanism in brown-rot fungi

3.1 Introduction

Brown-rot fungi are essential components of coniferous forest ecosystems that drive the evolution of CO_2 from wood and the deposition of lignin-rich soil organic matter (SONG *et al.* 2012; BAI *et al.* 2017). Brown-rot fungi differ from white-rot fungi in that they generally degrade lignin to a lesser degree, rather than mineralizing it as in white rot (YELLE *et al.* 2008; YELLE *et al.* 2011). Brown-rot fungi are of biotechnological interest because of their ability to selectively depolymerize wood polysaccharides while circumventing lignin, an attractive strategy with potential for use in lignocellulose conversion for biofuels.

Brown-rot fungi are thought to use a two-component decay strategy to attack wood polysaccharides consisting of a low-molecular weight Fenton system and hydrolytic enzymes (ERIKSSON *et al.* 1990). The major cellulolytic enzyme activity found in brown-rot fungi is endoglucanase (EG) activity. EG activity is primarily mediated by GH 5 proteins (RYU *et al.* 2011), but these enzymes are too large to diffuse into in-tact wood and require cell wall loosening treatments to access cellulose in wood (BORNSCHEUER *et al.* 2014). Non-enzymatic pretreatment by Fenton's reagent produced by Fe^{3+}-reducing hydroquinones may loosen the cell wall matrix for hydrolytic enzymes (JENSEN *et al.* 2001). These oxidants are small enough to circumvent low cell wall

porosity (FLOURNOY *et al.* 1991), and they are highly reactive and non-specific, causing characteristic lignin modifications and polysaccharide cleavage (FILLEY *et al.* 2002). However, their non-specificity also makes them incompatible with hydrolytic enzymes in discrete space, and these reaction components must be separated during decay to preserve the function of fungal enzymes.

Previous work has suggested that brown-rot fungi may spatially separate oxidative pretreatments from hydrolytic enzyme secretion during decay (HYDE and WOOD 1997). Changes in decay mechanisms may be modulated by abiotic extracellular conditions, which are notably acidic in brown-rot fungi due to the secretion of oxalate as decay proceeds (GREEN *et al.* 1991). Lower pH values reduce the rate of hydroquinone-mediated Fe^{3+} reduction, slowing Fenton chemistry once rotted wood becomes acidified (VARELA and TIEN 2003). Oxalate concentrations also modulate Fenton chemistry and affect the rate of oxidative cleavage of cellulose through Fe-chelate speciation (TANAKA 1994). At low oxalate concentrations, Fe^{3+}-mono-oxalate complexes facilitate Fenton chemistry, but as oxalate accumulates Fe^{3+}/Fe^{2+}- $(oxalate)_{2\text{-}3}$ complexes predominate that are not readily reduced or autooxidized, respectively (VARELA and TIEN 2003). In theory, concentration gradients could provide a protective mechanism for fungal enzymes on a sub cellular scale, but the high diffusivity of H^+ and of small metal ion chelates suggests that reaction partitioning occurs on a coarser spatial scale (HUNT *et al.* 2013).

Differential expression of oxalate-regulating genes and hydrolytic enzymes during the progression of decay may effectively segregate these non-compatible reaction types

in decaying wood. Regulation of oxalate levels in brown-rot fungi has been shown in *Fomitopsis pinicola* and *Meruliporia incrassata* where these fungi achieve an equilibrium level of oxalate (SCHILLING and JELLISON 2005). Oxalate degradation is mediated by extracellular oxalate decarboxylase (ODC), likely induced by increasing extracellular concentrations of oxalate (MICALES 1997). Similar patterns of regulation have also been described in white-rot fungi (DUTTON *et al.* 1994; MAKELA *et al.* 2014), suggesting that ODC-mediated regulation is widespread among wood-degrading basidiomycetes. However, previous studies of oxalate regulation lack the temporal resolution to indicate whether they are involved in segregating an oxidative pretreatment from later stage enzymatic hydrolysis in brown-rot fungi.

We aimed to first spatially resolve wood decay into a temporal progression of decay stages so that physiological changes in the decay fungus could be co-localized with chemical modifications to the wood and wood environment. We did this by growing fungi on thin wood wafers directionally such that decay was initiated at a leading hyphal front and behind it wood became progressively more degraded. Wafers were then sectioned along the advancing hyphal front and concurrent chemical and biochemical analyses to the wood and secreted protein were done at equivalent distances along the length of the wood wafers. Initially we co-localized carbohydrate depolymerization with EG activity to test our hypothesis that brown-rot fungi spatially separate cellulolytic enzyme secretion from another non-hydrolytic decay mechanism. Next, we utilized the same wood wafer design to co-localize oxalate production in brown-rot fungi with EG activity and the expression of oxalate synthesizing and degrading genes. We

hypothesized that these fungi would upregulate oxalate synthesis ahead of GH enzymes and wood acidification, and would upregulate genes associated with oxalate degradation and GHs at a later decay stage. We also included an in vitro study of the ability of oxalate to protect cellulases from oxidants, as a complement to earlier studies showing oxalate's ability to modulate oxidant production.

3.2 Methods

3.2.1 Cultures and Microcosm Design

Cultures of *Postia placenta* MAD-698 and *Gloeophyllum trabeum* ATCC 11539 were propagated and maintained on potato dextrose agar. Decay experiments were done in modified ASTM standard soil-block microcosms consisting of pint mason jars filled 1/3rd full of a 1:1:1 mixture of peat moss, top soil, and vermiculite hydrated to about 55-60% moisture. The mixture was tamped down lightly and two thin strips of birch wood (tongue depressors) were placed flat on the medium. The jars were autoclaved for one hour with the lids inverted and allowed to cool prior to inoculation with four 1 cm diameter agar plugs taken from PDA plates colonized with either fungus. Jars were incubated at room temperature in the dark until a continuous hyphal mat was formed on the surface to the birch strips (about 2 weeks).

Sterilized spruce (60 x 23 x 7 mm) or aspen (60 x 23 x 3 mm) with the largest face in cross sections were place on the hyphal mats transverse-section down such that the long axis of each wafer was oriented vertically (Figure 3.1). Spruce wafers were only degraded by *Postia placenta* for endoglucanase colocalization experiments (3.2.2-3.2.3)

and aspen wafers were degraded by *Postia placenta* and *Gloeophyllum trabeum* for oxalate metabolism experiments (3.2.4-). Wood wafers were incubated in the dark and colonized by fungi until the advancing hyphal front had advanced about 50 mm up the wafer (2-3 weeks). Once fully colonized the distance travelled by the fungal hyphae was measured to determine average growth rate less an approximately 3-day lag before the hyphae entered the wafers.

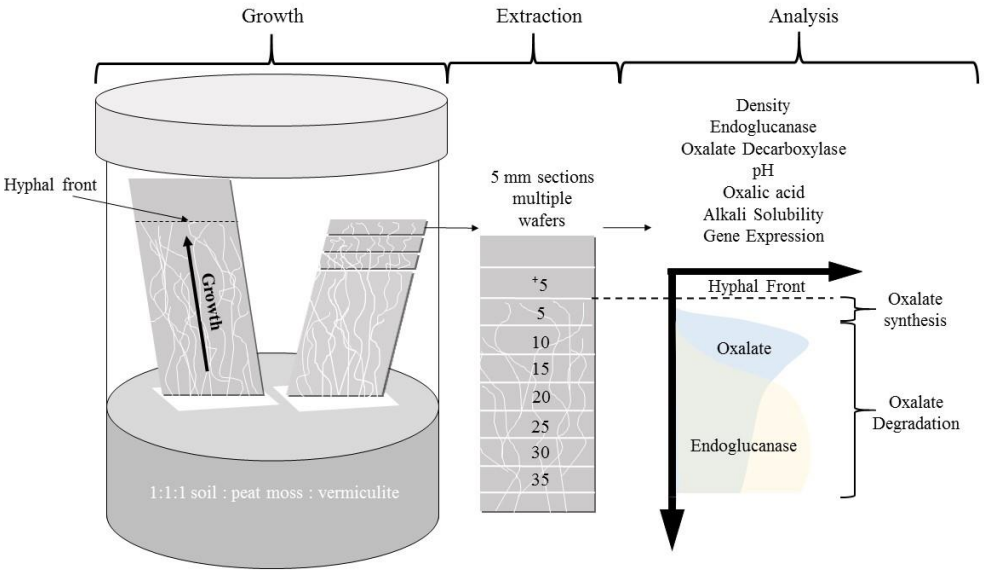

Figure 3.1: Wood wafer decay microcosms and an example of the sampling regime used to extract protein and analyze degraded wood along the advancing hyphal fronts. Analyses of equivalent pooled sections were then overlaid to view multiple aspects of decay together.

3.2.2 Spruce wafer sampling and alkali solubility

Spruce wafers colonized by *Postia placenta* were immediately processed after the completion of incubation. Wafers were divided in half along the long axis and surface hyphae was removed from the surface with gentle scraping after marking the location of

the visible hyphae. One half of the wafer was sectioned into 2 mm sections along its length using razor blade, the sections were oven dried, and reserved for alkali solubility measurements. The other half of the wafer was sectioned into 1 mm sections along the length of the wafer, each section was chopped into smaller pieces, and frozen at -20˚C for protein extraction and EG activity measurements. The 2-mm section of wood were ground in a Wiley mill using a 40-mesh screen. The sections were small, so the resulting powder did not uniformly sift through the 40-mesh screen and the smallest grind attainable was used for alkali solubility measurements. Alkali solubility was measured as previously described (SHORTLE *et al.* 2010).

3.2.3 Protein extraction and endoglucanase activity measurements

The 1 mm wood sections were thawed and suspended in 1 ml 0.1 M sodium acetate buffer pH 4.6 for 3 hours to extract extracellular enzymes. The extracts were centrifuged to remove particulates and used for the measurement of EG activity. The EG activity was measured in the protein extracts of 1 mm sections using a scaled-down Azo-carboxymethylcellulose assay (Megazyme, Bray, Ireland) according to the manufacturer's instructions. 100 µl of the extract was incubated with 100 µl of Azo-CMC substrate solution in microtiter plates for 10 min at 40˚C. The reactions were stopped, vortexed, centrifuged, and the absorbance at 590 nm of the supernatant was measured according to the manufacturer's guidelines. Units were defined as according to the manufacturer as *Trichoderma reesei* CMC unit equivalents per ml of protein extract. One unit was equivalent to the amount of *T. reesei* enzyme required to cleave1 µmol of

glucose reducing equivalents from CMC per minute. Activity was expressed CMC units per 1-mm wood section.

3.2.4 Aspen wafer sampling and density loss

Aspen wafers fully colonized by *Postia placenta* and *Gloeophyllum trabeum* were harvested and sectioned into eight 5-mm increments (5 x 25 x 3 mm sections) starting 5 mm in front of the visible hyphal front and ending 35 mm behind it. Sections from multiple wafers were pooled according to their distance relative to the advancing hyphal front for analyses that required greater amounts of wood or fungal protein. A separate pool of wafers decayed by *P. placenta* and *G. trabeum* were used to determine wood density loss per section. Wafer sections were dried at 100˚C overnight and weighed. The dimensions of the sections were measured to calculate the density as g cm^{-3}.

3.2.5 Oxalate quantification, alkali solubility, and pH

Three separate pools of dried wafer sections from *P. placenta* and *G. trabeum* cultures were ground to 40 mesh and used to assess a potentially correlated set of wood chemical characteristics. Approximately 0.2 g portions of wood were soaked in 4 ml of de-ionized water and incubated at room temperature for 2 h, after which the pH of the slurry was measured. Alkali solubility was measured in 0.1 g portions of wood extracted in 0.2 M NaOH (pH~ 13.3), following previously described methods (SHORTLE *et al.* 2010). To measure oxalate, approximately 0.3 g portions of wood was acid-hydrolyzed in 4% H_2SO_4 (pH ~ 2.3), filtered, and neutralized to a pH above that of the mobile phase used for chromatography. Oxalate concentration of the hydrolysates was determined by HPLC using an Aminex HPX87-H column (Bio-Rad, Hercules, CA) and a mobile phase

of 5 mM H_2SO_4 (pH ~ 2.3) with a flow rate of 0.4 ml min^{-1} with continuous detection of absorbance at 210 nm. All chemical analyses were done in triplicate.

3.2.6 Enzyme extraction, EG activities and oxalate decarboxylase assay

30 aspen wafers degraded by *P. placenta* and *G. trabeum* were sectioned into seven 5-mm sections along the length of the wafer and sections of equivalent distance from the hyphal front were pooled and chopped into smaller pieces prior to protein extraction. Pooled sections were suspended immediately in 50 ml of 0.5 M NaCl and soaked for 12 h at 4˚C with gentle shaking after which the extract was filtered through Miracloth (a fine cellulose mesh) and kept at 4˚C. Another 50 ml of 0.5 M NaCl was added to the wood and the extraction was continued for another 12 h. The extracts were filtered through miracloth, pooled, centrifuged at 4000g for 10 min, and the supernatants filtered through sterile 0.2 μm Polyvinylidene difluoride (PVDF) filters. Protein concentrations were determined using the Bradford method (Bio-Rad Protein assay kit, Bio-Rad, Hercules, CA). EG was determined according to IUPAC standard procedures (GHOSE 1987) using 1.5% carboxymethyl cellulose (CMC) as a substrate. Reactions were done in 50 mM sodium citrate at pH 5.0 at 50˚C for 30 min. One unit of activity is defined as the amount of enzyme required to generate one μmol of glucose reducing equivalents per minute from the above solution of CMC under the specified conditions. Each reaction was done in triplicate.

Oxalate decarboxylase activity (Units ml^{-1}) was measured on enzyme extracts generated as described above. The enzyme extract was assayed using an oxalate decarboxylase assay kit (Sigma Aldrich, St. Louis, MO) according to the manufacturer's

instructions. Units were defined as the amount of enzyme needed to form 1 μmol of formic acid per minute.

3.2.7 Target gene selection, RNA extraction, and RT-qPCR

Primers specific for gene sequences of enzymes involved in oxalate synthesis and decomposition were identified in the genomes of *P. placenta* and *G. trabeum* (Table S3.1). Homologs of *Trametes versicolor* ODC AAQ67425.1 previously identified in the *P. placenta* and *G. trabeum* genomes were targeted for expression analysis (WALZ 2003; MAKELA *et al.* 2014). Three paralogous oxalate decarboxylase (ODC) sequences from each fungus containing secretion signals (PETERSEN *et al.* 2011) that were expressed at significant levels in thin aspen wafers (unpublished data) were targeted for expression analysis. Three genes associated with oxalate synthesis, isocitrate lyase (ICL), oxaloacetase (OXA), and glyoxylate dehydrogenase (GXD), were targeted in this study (Table S3.1). ICL is a branch point between the TCA cycle and the glyoxylate cycle, and OXA and GXD both yield oxalate and make all three key control points in oxalate synthesis (MUNIR *et al.* 2001b; MUNIR *et al.* 2002).

RNA from three wafer sections decayed by *P. placenta* 0–5, 15–20, and 30–35 mm from the hyphal front and four sections decayed by *G. trabeum* 0–5, 15–20, 20–25, and 30–35 mm from the hyphal front were isolated. Individual wood sections were snap frozen in liquid nitrogen and ground with a pre-chilled mortar and pestle and RNase-free glass beads. RNA was extracted with Trizol reagent according to the manufacturer's instructions, and further purified using an RNeasy minikit (Qiagen, Valencia, CA).

Approximately 100 ng of total RNA for each wafer section was reverse transcribed into cDNA using the PrimeScript RT Reagent Kit (Clonetech Laboratories, Mountain View, CA). Quantitative PCR reactions were carried out in an Applied Biosystems 7900HT system (Thermo Fisher Scientific Inc., Foster City, CA) and were done in triplicate. Reactions totaled 15 µl and contained 7.5 µl iTaq^{TM} Universal SYBR Green Supermix (Bio-Rad, Hercules, CA) and 0.5 µM forward and reverse primers. The reaction conditions were as follows: 95˚C for 30 s followed by 40 cycles of 95˚C for 15 s and 60˚C for 60 s. Expression levels of target genes were normalized to β-actin (*P. placenta*) and *sar* (*G. trabeum*) (STEIGER *et al.* 2010) using the $2^{-\Delta\Delta Ct}$ method (SCHMITTGEN and LIVAK 2008). Five (*P. placenta*) and four (*G. trabeum*) RNA isolations from separate wafers were used as biological replicates.

3.2.8 In vitro oxalate antioxidant assessment

To assess how oxalate might offer a protective function during brown rot, via Fe^{2+} chelation, we assessed cellulase activity in the presence of Fenton reactants and various biologically-relevant oxalate concentrations (SCHILLING and JELLISON 2005). A preparation of *Trichoderma reesei* cellulases (Celluclast®, 1.5L, Sigma Aldrich) was diluted 1:1000 (~62 µg ml^{-1}) in citrate buffer pH 5.0. The Celluclast® dilution was treated with a mixture of 1 mM $FeSO_4$ and 15 mM H_2O_2 and varying concentrations of oxalate up to 2 mM in 50 mM sodium citrate buffer at pH 5.0. Reactions were initiated with the addition of H_2O_2 and the reaction was carried out for two hours at room temperature, followed by an overnight incubation at 4˚C. The EG specific activity of the dilution was measured as described above. All reactions were done in triplicate.

3.2.9 Statistics

Variation in density loss and oxalate concentration among wafer sections and among oxalate treatments in the Fenton mediator assays were determined using one-way ANOVA. Significant differences were determined post-hoc for protected ANOVA results using Tukey's HSD test, $\alpha = 0.05$, as a relatively conservative statistical assessment. Normalized RNA expression data was log transformed and analyzed with a one-way ANOVA followed by Tukey's HSD test, $\alpha = 0.05$ to determine significant differences.

3.3 Results and Discussion

3.3.1 Resolution of biphasic decay mechanism in brown-rot fungi

The brown-rot fungus *P. placenta* readily advanced up spruce wafers, forming a progression of decay from the hyphal front to the opposite end of the wafers. The distal ends of the wafers were clearly more degraded, being brown in color and having considerably higher % dilute alkali solubility (Figure 3.1 A). Alkali solubility increases after a lagging behind the advancing hyphal front. EG activity also lagged behind the progress of the mycelial front and, surprisingly, behind an advance in detectable depolymerization using DAS (Figure 3.2 A). Brown-rot fungi are known to initiate decay with hemicellulose removal (HIGHLEY 1987), and the early increases in DAS may be due to hemicellulose depolymerization. However, we cannot rule out an alternative oxidative pretreatment functioning at initial decay stages. In correlating DAS with EG in this wafer (Figure 3.2 B), DAS preceded the EG front by approximately four sections, representing 8 mm or nearly 20% of the total colonization progress of the fungus. These results show

that the process of carbohydrate depolymerization begins before cellulose hydrolysis, and clearly identifies a period in early decay that is physiologically distinct from the later decay stages.

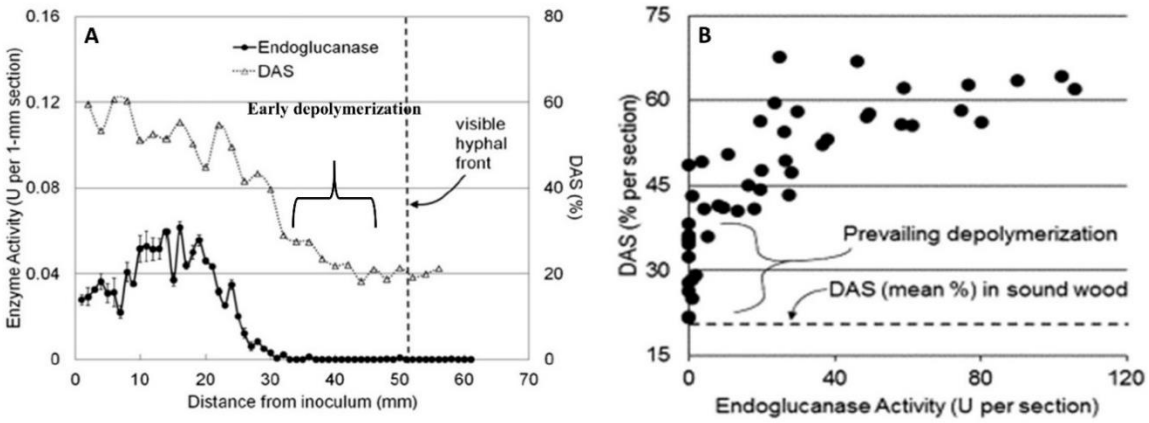

Figure 3.2: (A) Colocalization of dilute alkali solubility (DAS) and endoglucanase activity (EG) in spruce wood wafers colonized by P. placenta along the advancing hyphal front of degrading spruce wafers. EG error bars are standard deviations of three replicate assays. (B) Correlation of alkali solubility with EG activity per section of wood wafers, showing a zone of depolymerization (6-8 mm) in front of detectable EG in data pooled from three wafers. Because DAS was performed every 2 mm, while EG every 1 mm, only coincident data was used and the progression was thus at 2-mm increments.

3.3.2 Fungal growth and wood modifications on thin aspen wafers

Thin wafer microcosms used in this study proved effective for simultaneously viewing a fine-scale sequence of decay stages in a single piece of wood. *P. placenta* and *G. trabeum* colonized aspen wafers at an average rate of 2.7 ± 0.4 mm day^{-1} and 3.2 ± 0.4 mm day^{-1}, respectively (Table S2). The most degraded sections reached a density loss of 26.7% and 35.5%, respectively, a mid-decay stage for a carbohydrate-selective brown-rot

process. Alkali solubility of wafer pools increased more rapidly than density loss, in approximately 6 days (134 h) for *P. placenta* and 3 days (74 h) days for *G. trabeum*, whereas density loss did not differ from

non-degraded wood until approximately 9 days (223 h) and 7 days (178 h), respectively (Figure 3.3) (Table S2). Higher alkali solubility indicates, in part, that wood polysaccharides have a lower degree of polymerization (SHORTLE *et al.* 2010). The observed trends are in line with previous findings from a similar wafer design that an early, diffuse pretreatment depolymerizes polysaccharides in brown-rot fungi ahead of saccharification via endoglucanases (SCHILLING *et al.* 2013).

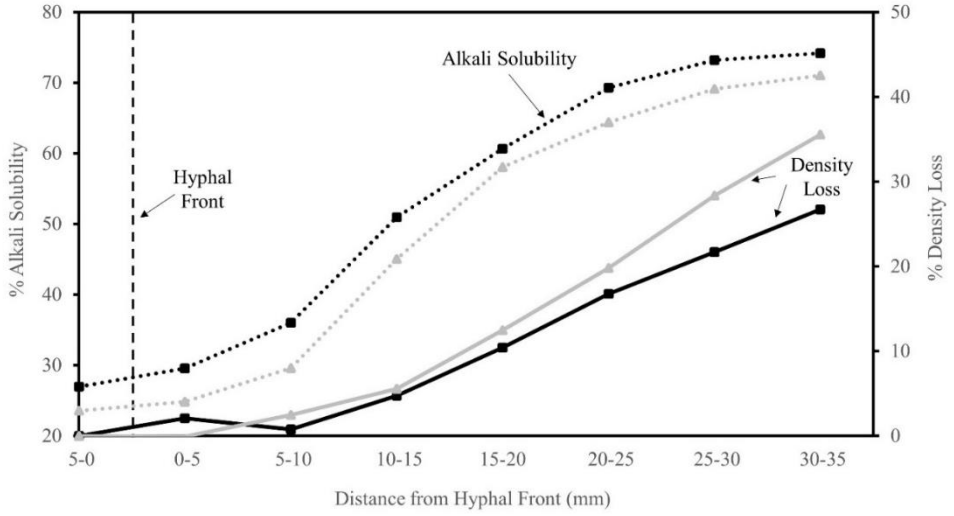

Figure 3.3: Percentage density loss (solid lines) and alkali solubility (dotted lines) measurements among pooled aspen wafer sections degraded by *Postia placenta* (black squares) and *Gloeophyllum trabeum* (grey triangles) at varying distance from the visible hyphal front. Average density loss values were determined from 6 (*P. placenta*) and 9 (*G. trabeum*) wafer sections. Error values associated with each point are listed in Table S3.2.

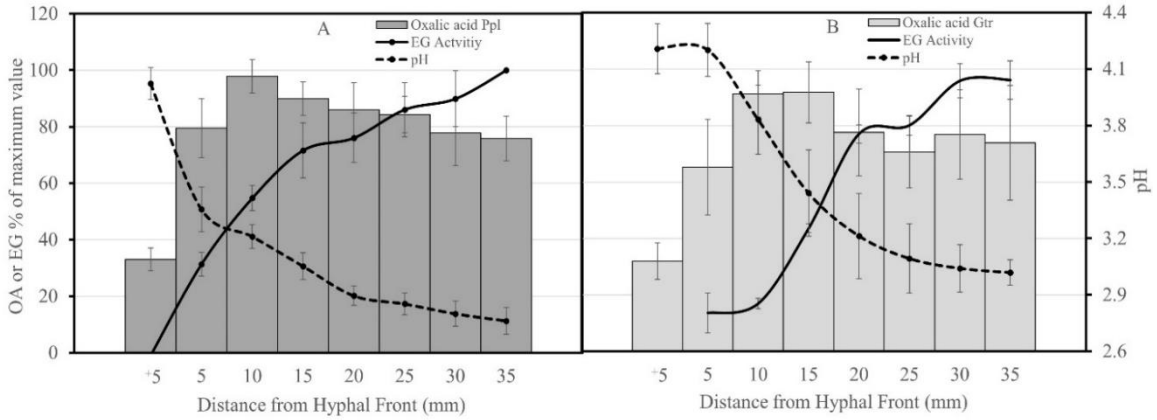

Figure 3.4: Oxalic acid (OA, grey bars) and pH (dashed line) of wood from pooled aspen wafer sections and endoglucanase activity (EG, solid line) from protein extracts of aspen wafers degraded by *Postia placenta* (A) and *Gloeophyllum trabeum* (B). Oxalic acid is represented as the average percentage of the maximum value for each parameter. The values used to calculate percentages are listed in the Table S3.3. Error bars for EG activity levels represent the standard deviation among three assays of one protein extract. Error bars for oxalate levels and pH represent the standard deviation of extracts from three separate wafers section pools.

Oxalate levels reached a peak 5–10 mm behind the hyphal front in both fungi and declined gradually thereafter, but pH continued to decrease beyond this point (Fig. 3.4). This would support an alternative acidification mechanism that predominates in the later stages of decay (SHIMADA *et al.* 1997), although oxalic acid secretion and decarboxylation of the carboxylate anion by ODC could also explain this coincident mismatch of oxalate and H^+ concentrations. Oxalate concentrations measured in wood for this study were close to levels found previously for these fungi, including for *G. trabeum*

that is often characterized in liquid culture by low oxalate accumulation (JORDAN *et al.* 1996; SCHILLING and JELLISON 2006).

Endoglucanase (EG) specific activity was low (*P. placenta*) or not above baseline (*G. trabeum*) as wood was colonized, but steadily increased to a maximum as wood become more degraded (Figure 3.4). Early studies describing the enzymatic system of brown-rot fungi have suggested that endoglucanase expression is constitutive (HIGHLEY 1973b), and more recent work has indicated that the secretome composition of *P. placenta* grown on aspen wafers does not significantly differ in composition over a 1–8 week time series (RYU *et al.* 2011). The temporal resolution of EG activity here suggests differential rather than constitutive expression, and collectively suggests that a more comprehensive overlay of genes, transcripts, metabolites, and wood modifications would be useful for these fungi.

3.3.3 Regulation of oxalate

Brown-rot fungi are known to reduce oxalate levels if it is present in excess (SCHILLING and JELLISON 2005), likely via ODC. One ODC, Gt130556, was up-regulated further behind the hyphal front (Figure 3.5), but no differential expression was seen among *P. placenta* ODCs. In our system, *P. placenta* grew more slowly than *G. trabeum*, leading to coarser temporal resolution per section in the former (~46 and ~36 h, respectively). ODC expression in *P. placenta* was likely already induced by this time, as was previously shown within two days of exposure to oxalate (MICALES 1997). Our expression analysis included three of four ODC genes for each fungus identified in their genome sequences, leaving one ODC from each fungus, Pp106821 and Gt129186, that

are poorly expressed under our conditions (unpublished data) out of the analysis. Enzyme extracts from *P. placenta* and *G. trabeum* both showed higher, albeit variable ODC activity in more degraded wood (Figure 3.6), but total lack of ODC activity near the hyphal front may be due to a lag between transcription and translation/secretion.

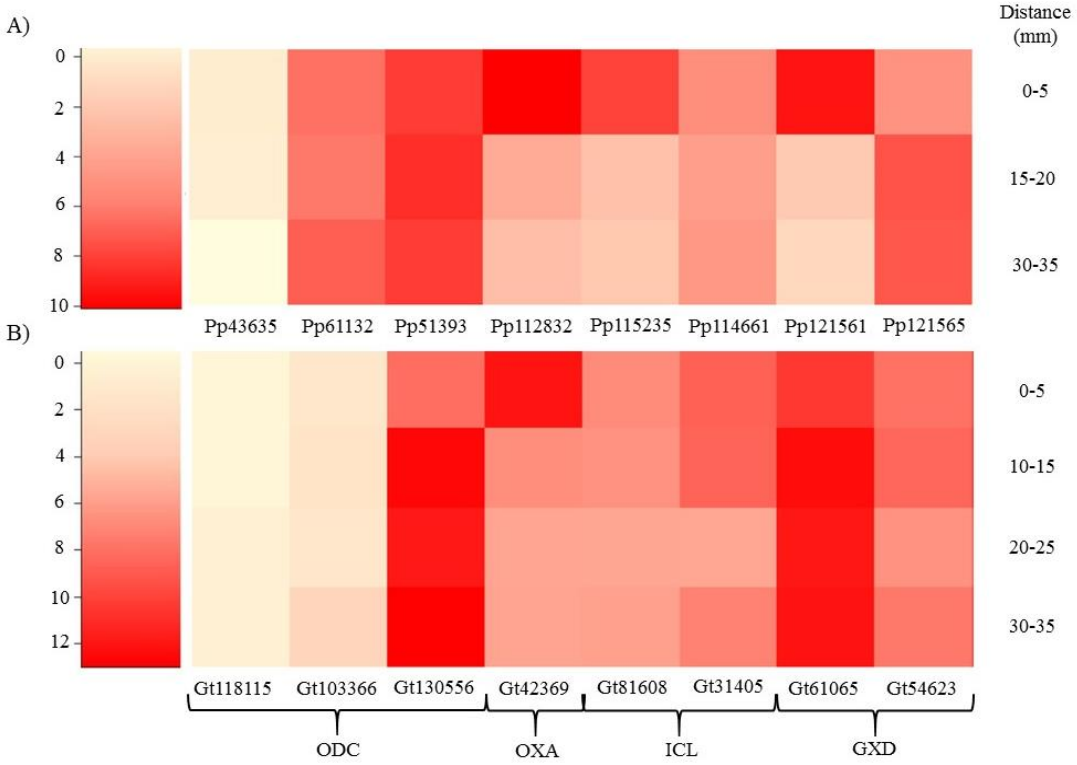

Figure 3.5: Heat maps showing expression levels of oxalate synthesis and oxalate degradation genes relative to actin genes in each fungus in aspen wafer sections degraded by *Postia placenta* (A), and *Gloeophyllum trabeum* (B). Values represented are the $\log_2$ of the relative expression levels normalized to Pp43635 and Gt118115 at 0–5 mm for *P. placenta* and *G. trabeum*, respectively. Genes are identified by their JGI protein ID numbers ODC = oxalate decarboxylase, OXA = oxaloacetase, ICL = isocitrate lyase, GXD = glyoxylate dehydrogenase.

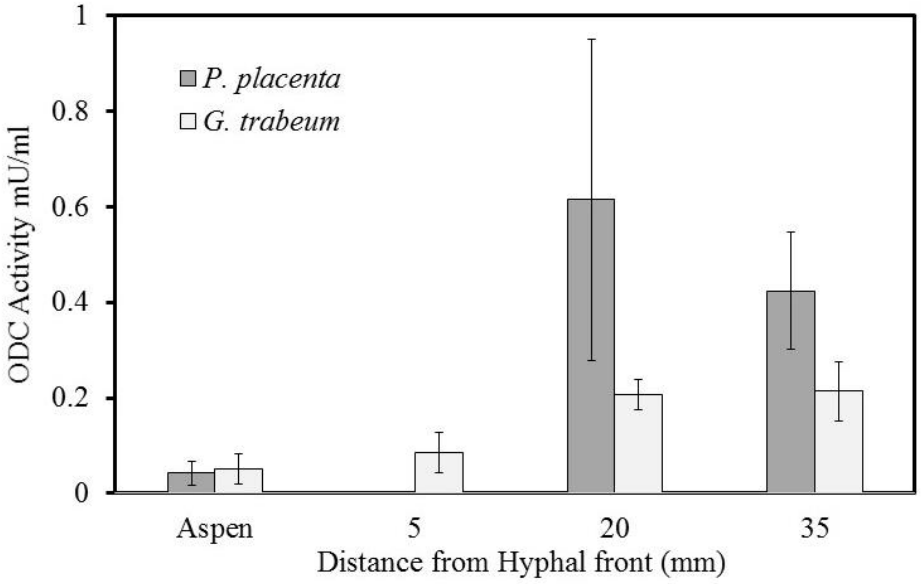

Figure 3.6: Oxalate decarboxylase (ODC) activity of protein extracts from aspen wafers. Oxalate levels present in the enzyme extracts were detected and subtracted from the total detected activity of each sample except for aspen, which shows native oxalate levels in the wood extract. Error bars represent the standard deviation of two assays of a single protein extract.

Makela et al. (2014) determined the phylogenetic relationships among ODCs from *P. placenta* and *G. trabeum*, and among the genes included in that study, two clear orthologs (Pp43635 and Gt118115) and two closely related paralogs in *G. trabeum* (Gt103366 and Gt130556) were tested in our study. On our aspen wafers, the orthologous ODC genes Pp43635 and Gt118115 showed a similar, generally low expression level in all wafer sections, supportive of a similar regulatory pattern in both fungal species. Conversely, the Gt103366 and Gt130556 paralogs show constitutive and late-stage

upregulation, respectively, a distinction that may indicate a functional divergence afforded by gene duplication.

Expression patterns of oxalate synthesis genes vary and may indicate differential induction due to the plurality of physiological roles of oxalate (SHIMADA *et al.* 1997). OXA is upregulated at the hyphal front in both fungi as are the ICL Pp115235 and the GXD Pp121561, where they may function to provide oxalate for iron chelation and modulation of radical oxygen species (ROS). Conversely, the ICLs Gt81608, Gt31405, and Pp114661 and the GXD Gt54623 are constitutively expressed while the GXDs Pp121565 and Gt61065 are upregulated in more degraded wood (Figure 3.4). Constitutive and late stage upregulation are tied to the glyoxylate cycle's role in energy metabolism in brown-rot fungi (MUNIR *et al.* 2001b), with late stage carbon influxes due to cellulose depolymerization causing the latter. Differential regulation of homologous oxalate synthesizing genes has been reported previously in brown-rot fungi. GXD activity in brown-rot fungus *Fomitopsis palustris* is upregulated in the early stages of growth (MUNIR *et al.* 2001a; YOON *et al.* 2002), while expression of GXD from *Fibroporia radiculosa* is induced by a chemical stressor (TANG *et al.* 2013). Conversely, Gt61065 and Gt42369 are constitutively expressed under high and low nitrogen conditions (ZHUANG *et al.* 2015). Further induction studies would be required to more succinctly explain the patterns in aspen wafers.

3.3.4 Oxalate in vitro antioxidant study

The capacity for oxalate to prevent Fenton-mediated cellulolysis and lipid peroxidation has been known for some time, but no study has shown its ability to prevent

activity loss in cellulases (TANAKA 1994; VARELA and TIEN 2003). Treatment of *Trichoderma reesei* cellulases (Celluclast®) with Fenton reagents (1 mM $FeSO_4$, 15 mM H_2O_2) caused a 27.3% reduction in EG specific activity. Addition of oxalate prior to treatment with Fenton's reagent significantly reduced this loss in EG activity once oxalate reached 0.5 mM. Specific activity of EG was fully restored at oxalate levels above 0.75 mM (Figure 3.7). The concentration of Fe^{2+} used in this study was higher than those found in brown-rotted wood as whole, but may be closer to unmeasurable local concentrations created by fungi to facilitate decay (SUZUKI *et al.* 2006; WEI *et al.* 2010).

3.3.5 Oxalate 'staggering' and equilibrium

Our data indicate that oxalate synthesis and decomposition are differentially regulated by the temporal progression of brown-rot wood decay. Some oxalate synthesis genes are induced near the hyphal front, by an increase in EG activity after oxalate levels in wood have peaked. The up-regulation of oxalate synthesis genes such as OXA in the early decay stages may serve to produce an environment that enables brown-rot cellulases to function in the later stages of decay, as well as to initiate Fenton chemistry by mobilizing Fe^{3+}. It is important to note that oxalate is synthesized in glyoxysomes in brown-rot fungi and significant amounts of oxalate near the hyphal front may reside within fungal cells (SAKAI *et al.* 2006). We also cannot resolve the location of oxalate within fungal cells or whether it is bound to wood fibers (HUNT *et al.* 2004) and therefore we cannot know the impact of oxalate detected in this study on the reactivity of Fenton's reagent in wood cell walls. It is possible that the concentration of free oxalate is low in

the front and high farther behind the front; facilitating and inhibiting Fenton chemistry respectively (VARELA and TIEN 2003).

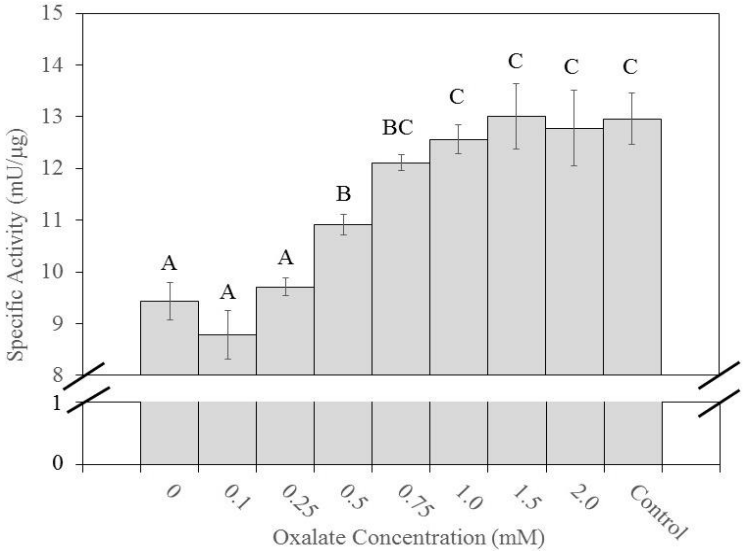

Figure 3.7: In vitro assay for oxalate capacity to prevent protein denaturation. Oxalate's ability to prevent the loss of enzyme activity due to treatment with Fenton reagents (1 mM $FeSO_4$ and 15 mM H_2O_2) is shown by the EG specific activity of each mixture compared to the untreated enzyme (control). Error bars represent standard deviation of three separate reactions. Bars with the same letters indicate that the values are not significantly different from one another ($p < 0.05$).

Once at high levels, oxalate levels were maintained at a relatively stable level across the wafer sections. A similar optimized level for oxalate was observed by Schilling and Jellison (2005) for two brown-rot fungi (*Fomitopsis pinicola* and *Meruliporia incrassata*), where a range of initial oxalate levels were encountered in wood. Both fungi either increased or decreased these oxalate 'spikes' to reach a unified concentration, again likely by upregulation of ODC. An optimized level for oxalate may represent the

need for these brown-rot fungi to balance a maximization of Fenton reactions (by optimizing the Fe^{3+}/Fe^{2+}-oxalate complex ratio; (VARELA and TIEN 2003)) and a minimization of oxidative damage to enzymes and hyphae. This balancing act may be, at least in part, what allows brown-rot fungi to deploy an ROS-driven mechanism with somewhat low specificity.

3.4 Conclusion

We effectively resolved spatially a temporal progression of decay in the brown-rot fungus *Postia placenta* by growing fungi directionally on thin wood wafers. Analysis of wood along the decay gradient identified a zone of non-cellulolytic polysaccharide depolymerization, suggestive of early hemicellulose and cellulose degradation possibly by a non-hydrolytic mechanism. This decay system effectively resolves wood "pretreatment" from later stage saccharification and allowed us to investigate the nature of these poorly described decay mechanisms in brown-rot fungi.

We modified our wood wafer decay system to generate larger samples of degraded wood at each timepoint to perform a larger number of concurrent analyses and extract enough fungal protein for analysis. We found differential regulation of oxalate synthesis/degradation genes and metabolites during brown rot by *Postia placenta* and *Gloeophyllum trabeum*, with both fungi producing oxalate rapidly and then actively regulating its concentrations, coincident with the onset of EGs. This induction of oxalate synthesis may be a function of apical hyphal growth and oxalate decomposition may be stimulated by oxalate accumulation. Optimization of extracellular oxalate during brown

rot is in line with its role in mobilizing Fe^{3+} in oxalate complexes without forming Fenton-inhibiting Fe^{3+}/Fe^{2+}-$(oxalate)_{2,3}$ complexes at higher oxalate concentrations. The absolute optimum, however, may balance the costs of Fenton inhibition with its benefits, given the deleterious reactions of ROS with hyphae and enzymes.

3.5 Supplemental Information

Table S3.1: Genes targeted for expression analysis in *P. placenta* and *G. trabeum* and their respective primer sequences.

Genes (Protein ID)	Direction	Primer Sequences	Product length (bp)	Amplification efficiency
Ppl Actin (108207)	Forward	AGAACTTGACGGAGCGTGGGTA	229	97.72%
	Reverse	AGGAATGCGGGCTGGAAGA		
Ppl ODC1 (43635)	Forward	TAGCACTCAAGTGTCTACGGTCACT	161	91.35%
	Reverse	CGCCATTGTCAAATACCAGCA		
Ppl ODC2 (61132)	Forward	GCGGAACTGTGAAGGTCGTG	124	90.76%
	Reverse	CATTCATCCTGAGTGGGGTGCC		
Ppl ODC3 (51393)	Forward	GTTACGACCGATACCGACCCT	121	72.14%
	Reverse	CATCAGTAGTTGGCGGGGCTA		
Ppl OXA (112832)	Forward	GATTCTATCCCCGGTGGCTC	99	99.32%
	Reverse	GGCGAGCTTGAGACGAGTGA		
Ppl ICL1 (115235)	Forward	ACACATGGCAGGCAAGGTGCT	144	87.49%
	Reverse	TTCGTCGTGATGAGCGTTGC		
Ppl ICL2 (114661)	Forward	TGAGCTGGGACTGGGATCTG	141	89%
	Reverse	CAAGGTCTGGTCGCTTCGTTT		
Ppl GXD1 (121561)	Forward	AAGCCCGACCAGACCCTCTT	177	98.13%
	Reverse	GCCCTCATCGCCCACAAACT		
Ppl GXD2 (121565)	Forward	GTATGTCAACTCGGACCGTGAA	86	90.33%
	Reverse	CGACAGTGATGAACAGGCCCTTG		
Gtr SAR (110117)	Forward	ACACCATTTGGGCCTGTATC	113	94.50%
	Reverse	CCTCTCCATAACCCTGTCTCT		
Gtr OXD1 (118115)	Forward	AAGGAGGTCGCTGGAGTGAACA	164	122.80%
	Reverse	AAGTCGCCTGCGTTGATCGTAG		
Gtr OXD2 (103366)	Forward	CCCGGTGCGATTCGTGAATTGC	101	140%
	Reverse	TTCCTGCCGTCCTGGTCAACTG		
Gtr OXD3 (130556)	Forward	GGCGGGTGTTAATATGCGGCTG	149	91.70%
	Reverse	CGGCACTAACAGTGGCGAGGTA		
Gtr OXA (42369)	Forward	GAGGCCATGCACCTGCTCAAGA	127	89.10%
	Reverse	TCCCTCCAGCGGCAGCATCTAA		
Gtr ICL1 (81608)	Forward	GCAGTTATGAACGAGGCGGAGG	109	90.20%
	Reverse	CCAACACGGTGGAGAACAGGGA		
Gtr ICL2 (31405)	Forward	ACTCGCACCCGTTGGTCACCTT	165	97.20%
	Reverse	AGCCGACCCATTCGCCGACTAT		
Gtr GXD1 (61065)	Forward	ACGGATGTGCTCAAGGCTGTGG	154	96.20%
	Reverse	CGCCGAGGAGACGCATGTTCAT		
Gtr GXD2 (54623)	Forward	TCGAGGTGTTCGTGGATGGAGG	192	98.90%
	Reverse	TGACGCCCAACAGCCGCATT		

Table S3.2: Density and density loss ratios of pooled aspen wafer sections degraded by Postia placenta and *Gloeophyllum trabeum*. These values are picture plotted in Figure 3.2.

	Postia placenta n=6			*Gloeophyllum trabeum* n=9		
Distance from hyphal front (mm)	Time (days)	Density (g/cm^3)	% Density loss	Time (days)	Density (g/cm^3)	% Density loss
5-0	0.0	0.38 ± 0.02	0	0.0	0.40 ± 0.02	0
0-5	1.9 ± 0.29	0.37 ± 0.02	2.1 ± 0.14	1.5 ± 0.18	0.40 ± 0.01	-0.09 ± 0.00
5-10	3.7 ± 0.40	0.38 ± 0.03	0.76 ± 0.06	3.1 ± 0.26	0.39 ± 0.01	2.5 ± 0.01
10-15	5.6 ± 0.50	0.36 ± 0.03	4.7 ± 0.41	4.6 ± 0.32	0.38 ± 0.02	5.6 ± 0.29
15-20	7.4 ± 0.57	0.34 ± 0.02	10.4 ± 0.75	6.2 ± 0.37	0.35 ± 0.02	12.5 ± 0.71
20-25	9.3 ± 0.64	0.32 ± 0.03	16.8 ± 1.6	7.7 ± 0.41	0.32 ± 0.02	19.8 ± 1.4
25-30	11.2 ± 0.70	0.30 ± 0.03	21.7 ± 2.8	9.3 ± 0.45	0.29 ± 0.02	28.4 ± 2.8
30-35	13.0 ± 0.76	0.28 ± 0.03	26.7 ± 3.0	10.8 ± 0.48	0.26 ± 0.01	35.5 ± 3.1

Table S3.3: Average EG activity, total oxalate, and pH of extracts of aspen wafer sections degraded by *Postia placenta* and *Gloeophyllum trabeum*. EG values are averages of three assays of the same protein extract. Total oxalate values are averages of three separate pools of 30 aspen wafer sections. pH values are the average of three separate pools of 30 wafer sections. pH values are averaged from three separate pools of aspen wafer sections. Values in this table were used to calculate values plotted in Figure 3.3. Average values are listed with their associated standard deviations.

Distance from hyphal front (mm)	*Postia placenta*		
	EG specific activity (U/μg)	Total Oxalate (μmol/cm^3)	pH
Aspen	1.51 ± 1.82	12.9 ± 1.39	4.09 ± 0.12
5-0	-0.27 ± 0.19	13.8 ± 1.76	4.03 ± 0.08
0-5	9.62 ± 0.72	34.5 ± 7.08	3.36 ± 0.12
5-10	16.8 ± 1.22	42.1 ± 5.54	3.22 ± 0.06
10-15	21.9 ± 1.41	37.5 ± 3.54	3.06 ± 0.07
15-20	23.3 ± 1.19	36.9 ± 5.01	2.90 ± 0.05
20-25	26.4 ± 1.10	35.1 ± 3.27	2.86 ± 0.06
25-30	27.6 ± 0.95	33.4 ± 5.46	2.81 ± 0.07
30-35	30.8 ± 2.46	31.6 ± 4.10	2.77 ± 0.07
	Gloeophyllum trabeum		
Aspen	1.01 ± 2.53	13.2 ± 3.75	4.09 ± 0.12
5-0	N/A	11.1 ± 5.20	4.21 ± 0.13
0-5	3.89 ± 1.97	24.8 ± 18.1	4.20 ± 0.14
5-10	4.90 ± 0.79	35.3 ± 23.1	3.83 ± 0.18
10-15	12.5 ± 0.32	34.8 ± 21.0	3.44 ± 0.23
15-20	22.2 ± 0.47	28.5 ± 15.2	3.21 ± 0.23
20-25	23.0 ± 0.66	25.4 ± 13.1	3.09 ± 0.18
25-30	27.6 ± 2.41	28.5 ± 11.5	3.04 ± 0.13
30-35	27.6 ± 1.09	24.5 ± 10.7	3.02 ± 0.07

Chapter 4 Analysis of the growth characteristics and secretome dynamics over the course of wood decay in two taxonomically divergent brown-rot fungi

4.1 Introduction

Brown-rot wood-degrading fungi are common pests in lumber and are a dominant agent of wood decay in forests, particularly in conifer-dominated woodlands. These fungi decompose wood via a carbohydrate-selective mechanism, using a combination of free radical oxidation and glycoside hydrolase-mediated saccharification (BALDRIAN and VALASKOVA 2008). Wood oxidation during brown rot is mediated by nonselective hydroxyl radicals, requiring spatial and/or temporal segregation from hydrolytic enzymes to limit deactivation by hydroxyl radicals (HYDE and WOOD 1997).

The overall two-step mechanism is thought to be shared by all brown-rot fungi, despite multiple independent evolutionary origins of brown rot (HIBBETT and DONOGHUE 2001; KORRIPALLY *et al.* 2013). Genomic comparisons, however, suggest that differences in the decay mechanisms driving a twostep oxidative-enzymatic mechanism may exist among brown-rot clades (LUNDELL *et al.* 2014; RILEY *et al.* 2014). Differences among brown-rot species are evident in some measures of decay, such as lignin selectivity indices (SCHILLING *et al.* 2015). There are also examples where fungi in different clades vary in their abilities to utilize certain substrates, such as Antrodia and Gloeophyllum clades; both efficiently degrade wood, but Antrodia clade fungi fail to efficiently degrade

corn stover, unlike *Gloeophyllum trabeum* (KAFFENBERGER and SCHILLING 2013). Although these genomic and phenotypic variations are known, the phylogenetic variations in the brown-rot biochemical mechanisms have not been resolved.

A logical approach to help resolve variations is to better understand spatially the temporal sequence of the two-step brown-rot mechanism to enable comparisons. Brown-rot fungi temporally stagger oxidative and hydrolytic chemistries via differential gene expression, where wood oxidation is followed by glycoside hydrolase upregulation (FLOUDAS *et al.* 2012; ZHANG *et al.* 2016). This staggered pattern was established via both transcriptomics and enzyme assays in *Postia placenta* (Polyporales), but this space-for-time approach has not yet been applied to study the staggered mechanisms of other brown-rot fungi from other distinct clades (ZHANG *et al.* 2016).

In this study, we employed a wood wafer setup to compare the temporal progressions of decay by two taxonomically divergent brown-rot fungi, *Gloeophyllum trabeum* and *Serpula lacrymans*. Specifically, we compared differences in secretome composition, enzymatic activity, and mode of colonization over the course of wood decay. Both fungi are ubiquitous lumber pests, but they evolved from distinct evolutionary lineages, with key differences in plant cell wall deconstruction genes, including the notable presence in *S. lacrymans* of cellobiohydrolases (CBHs) that distinguish its clade (Boletales) from all other brown-rot clades (FLOUDAS *et al.* 2012). *Serpula lacrymans* is also distinct in that it is not commonly observed in nature, unlike the ubiquitous *G. trabeum* (GILBERTSON and RYVARDEN 1986; PALFREYMAN *et al.* 2003). The "dry rot fungus," as *S. lacrymans* is known, can initiate decay with minimal

ground contact, as well as in wood with low moisture content, and perhaps with less of a need for combative ability due to its adaptations to dry environments (JENNINGS and BRAVERY 1991). Our design and analyses therefore test the hypothesis that the agents deployed to create a two-step brown-rot mechanism differ between these fungi.

4.2 Methods

4.2.1 Microcosms setup and harvest

Gloeophyllum trabeum ATCC 11539 and *Serpula lacrymans* S7.3 were cultivated on 60-mm by 25-mm by 3-mm spruce wafers in modified ASTM standard soil block microcosms, as previously described (ZHANG *et al.* 2016). In brief, wafers were propped vertically within microcosms atop a hyphal mat and incubated in the dark at room temperature until fungal hyphae had advanced 45 to 50 mm up the wafers (2 to 3 weeks). Wafers with straight horizontal hyphal fronts were harvested, and average growth rates were determined by dividing total growth up the wafers by the total incubation time, less a 3-day lag (n = 60). Surface hyphae were removed and wafers were sectioned into seven 5-mm sections starting at the hyphal front and extending 35 mm behind it. Wafer sections were chopped into smaller pieces with sterilized razor blades prior to protein or ergosterol extractions.

4.2.2 Protein extraction, purification, and assay

Spruce wafers degraded by either *G. trabeum* or *S. lacrymans* (n = 30 per species) were processed as described above, and sections were pooled with equivalents (i.e., same distance behind the hyphal front) from other wafers. Sections were suspended in 50 ml of

cold 0.5 M NaCl and gently shaken for 24 h at 4°C. The extracts were filtered through Miracloth, centrifuged at 4,000 rpm for 10 min, and filtered through sterile 0.2-μm-pore polyvinylidene difluoride (PVDF) filters. Protein concentrations were determined using a Bio-Rad protein assay kit (Hercules, CA, USA). Cellulases and hemicellulases were measured by the dinitrosalicylic acid (DNS) method using solutions of 1.5% carboxymethyl cellulose (endoglucanase), 2% birchwood xylan (xylanase), and 0.5% locust bean gum (mannanase) (GHOSE 1987). Triplicate portions of protein extract were incubated with substrate at 50°C for 30 min in 50 mM citrate (pH 5.3). The absorbance at 540 nm was measured, and reducing sugars were determined as glucose-, xylose-, and mannose-reducing equivalents for endoglucanase, xylanase, and mannanase activities, respectively.

4.2.3 Mass spectrometry

Extracts from spruce wafer sections 0 to 5, 10 to 15, and 20 to 25 mm from the visible hyphal front were generated as described above and concentrated using 3,000-kDa-cutoff polyether sulfone membranes. Extracts were tricarboxylic acid (TCA)-acetone precipitated and reconstituted in 7 M urea, 2 M thiourea, 0.4 M triethylammonium bicarbonate (TEAB) (pH 8.5), 20% methanol, and 4 mM Tris(2-carboxyethyl)phosphine (TCEP). Twenty-microgram aliquots were reduced for 1 h at 37°C and alkylated in 8 mM methyl methanethiosulfonate. Samples were diluted 4-fold with ultrapure water, mixed with trypsin at 1:50, incubated for 16 h at 37°C, dried, and cleaned with a 4-ml Extract-Clean C18 SPE cartridge from Grace-Davidson (Deerfield, IL), with eluates dried *in vacuo*.

Tryptic peptides were rehydrated in water, acetonitrile, and formic acid at a ratio of 98 to 1.9 to 0.1, respectively. Each sample was subjected to a Paradigm Platinum Peptide Nanotrap precolumn (0.15 by 50 mm, 400-µl volume; Michrom Bioresources, Inc., Auburn, CA, USA), followed by an analytical capillary column (100 µm by 12 cm) packed with C18 resin (5 µm, 200 Å; MagicC18AG; Michrom Bioresources, Inc.) at a flow rate of 600 nl min^{-1}. Peptides were fractionated on a 60-min (5 to 35% acetonitrile) gradient on a Paradigm MS4 high-performance liquid chromatograph (HPLC; Michrom Bioresources, Inc.). Mass spectrometry (MS) was performed on an LTQ mass spectrometer (Thermo Electron Corp., San Jose, CA, USA). Ionized peptides eluting from the capillary column were subjected to an ionizing voltage (1.8 kV) and selected for tandem MS (MS/MS) using a data-dependent procedure alternating between an MS scan and five MS/MS scans for the five most abundant precursor ions. Identified proteins were filtered using Scaffold 4.0 (Proteome Software, Portland, OR, USA). Positive protein identification was restricted to peptides with a 95.0% peptide identification probability threshold against the *S. lacrymans* and *G. trabeum* predicted proteins and a minimum number of 2 observed peptides per protein.

4.2.4 Ergosterol analysis

Total ergosterol, a biomarker used to determine fungal biomass, was extracted from individual spruce wafer sections using established methods (NEWELL *et al.* 1988). Ergosterol was measured by HPLC, using previously described parameters (SCHILLING and JELLISON 2005), with detection of absorbance at 282 nm.

4.3 Results

4.3.1 Secretome composition

In *S. lacrymans*, 93 proteins (identified as peptides exclusively matched to a protein) were identified among all colonized wafer sections. *G. trabeum*, on the other hand, produced 209 proteins in total and about 3 times more proteins than *S. lacrymans* from the section nearest the hyphal front (Figure 1). The proteins identified totaled 65, 81, and 72 in *S. lacrymans* cultures at distances of 0 to 5, 10 to 15, and 20 to 25 mm behind the hyphal front, respectively, and totaled 200, 150, and 120 in the equivalent wafer sections colonized by *G. trabeum*.

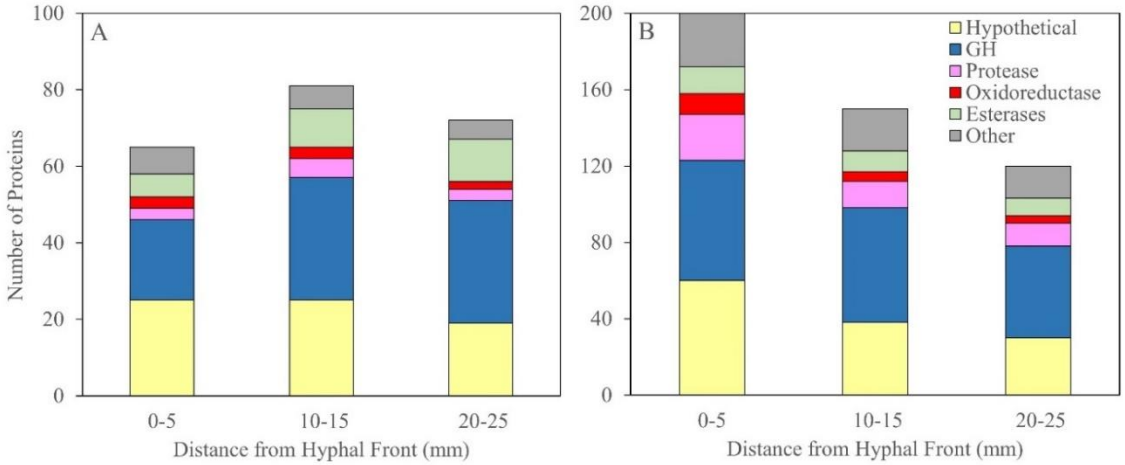

Figure 4.1: Secretome composition in spruce wafer sections degraded by (A) *Serpula lacrymans* and (B) *Gloeophyllum trabeum* expressed as the total number of proteins belonging to one of 6 categories identified in each sample. Note the difference in scale for both fungi due to the higher amount of protein diversity found in *G. trabeum*. GH, Glycoside Hydrolase

Hypothetical proteins and glycoside hydrolases (GHs) were the most abundant protein categories. Hypothetical protein diversity was greatest near the hyphal front for

both fungal species, with 12 and 34 hypothetical proteins found only within 15 mm of the hyphal front in *S. lacrymans* and *G. trabeum* cultures, respectively (Table 4.1). GH diversity followed the same pattern in *G. trabeum* (Table 4.2) but not *S. lacrymans* (Table 4.3). Twenty GHs from *G. trabeum* were exclusive to the first 15 mm behind the hyphal front and consisted of chitinases, non-cellulolytic β-glucanases, hemicellulases, and a GH 28 pectinase (Table 4.2).

Table 4.1: Hypothetical proteins found exclusively in the early decay stages (0-5 and 10-15 mm behind the hyphal front) in spruce wafer extracts from *Serpula lacrymans* and *Gloeophyllum trabeum* cultures. Hypothetical proteins are categorized by functional domains identified by BLAST search to the Swiss-Prot database.

Serpula lacrymans	
Domain[1]	Unique hypothetical proteins[2]
GATase domain	1
Cytoskeletal protein	1
YjgF	1
No domain	9
Total	12
Gloeophyllum trabeum	
Domain	Unique hypothetical proteins
Acyl-CoA binding	1
Aldo-keto reductase	1
Cerato platanin	1
Cupredoxin	1
Delta endotoxin	1
DNAJ	1
Lipase	1
No domain	27
Total	34

[1]Protein domains were identified by BLAST searches of the SWISS PROT database (BATEMAN *et al.* 2015)

[2]Hypothetical protein listed were found in extracts from either 0-5 or 10-15 mm behind the hyphal front.

Table 4.2: Glycoside hydrolases found in extracts of spruce wafer sections degraded by *Gloeophyllum trabeum* and the number of unique peptides identified for each protein in each wafer section extract.

				Unique Peptides[5]		
GT Number[1]	Family[2]	Putative Function[3]	Signal P[4]	0-5	10-15	20-25
81012	1	Beta-glucosidase	no	13	20	15
115191	2	Mannanase	yes	12	13	11
44548	3	Beta-glucosidase	yes	2	0	0
71534	3	Beta-glucosidase	yes	0	6	0
122002	3	Exo-1,4-beta-xylosidase	yes	8	10	7
75899	3	Beta-glucosidase	no	7	8	7
69843	3	Beta-glucosidase	yes	10	13	13
68070	5	Exo-1,3-beta-glucanase	yes	2	0	0
118009	5	Unknown	yes	2	2	0
120257	5	Endo-1,4-beta-glucanase	yes	2	4	2
41779	5	Exo-1,3-beta-glucanase	no	1	4	3
114574	5	Endo-1,4-beta-mannanase	yes	1	3	3
42111	5	Exo-1,3-beta-glucanase	no	2	4	4
135369	5	Endo-1,4-beta-mannanase	yes	3	8	6
59826	5	Exo-1,3-beta-glucanase	no	9	9	7
110405	5	Endo-1,4-beta-mannosidase	yes	3	7	10
63180	5	Endo-1,4-beta-glucanase	yes	6	14	45
149061	10	Endo-1,4-beta-xylanase	yes	3	0	0
122601	10	Endo-1,4-beta-xylanase	yes	6	1	0
138785	10	Endo-1,4-beta-xylanase	yes	3	7	5

107452	10	Endo-1,4-beta-xylanase	yes	15	36	49
138821	12	Endo-1,4-beta-glucanase	yes	8	18	49
73036	13	Amylase	yes	9	0	0
61700	15	Amylase	yes	11	7	7
52752	16	Beta glucan synthesis	no	4	0	0
66072	16	Beta glucan synthesis	no	2	0	0
81698	16	Beta glucan synthesis	no	7	7	2
82316	18	Chitinase	no	2	3	0
122074	18	Chitinase, CBM 5	yes	0	3	0
118998	18	Chitinase, CBM 5	yes	3	3	2
45026	18	Chitinase	no	2	3	3
81165	18	Chitinase, CBM 5	yes	1	5	3
91195	20	Beta-N-acetylglucosaminidase	yes	4	1	0
116582	20	Beta-N-acetylglucosaminidase	yes	2	1	0
81761	27	Alpha-galactosidase, CBM 35	yes	1	2	0
117566	27	Alpha-galactosidase	yes	11	15	10
104965	28	Endo-polygalacturonase	yes	8	3	0
110574	28	Polygalacturonase	yes	2	6	2
54367	28	Exo-polygalacturonase	yes	0	3	3
117232	28	Exo-rhamnogalacturonase	yes	1	3	3
6650	28	Exo-polygalacturonase	no	2	6	4
138836	28	Exo-polygalacturonase	yes	4	6	7
61165	29	Alpha-L-fucosidase	no	3	5	2
46629	30	Unknown	yes	3	4	4
119185	31	Alpha-glucosidase	yes	10	10	9
141329	31	Alpha-xylosidase	yes	10	18	14
81512	35	Beta-galactosidase	no	8	13	10
111095	35	Beta-galactosidase	yes	16	24	19
100356	37	Trehalase	no	0	2	3
69366	43	Unknown, CBM 35	yes	0	3	0
58475	43	Endo-1,5-alpha-L-arabinase	yes	3	3	4
107755	47	Alpha-1,2-mannosidase	yes	6	6	4
111463	51	Alpha-L-arabinofuranosidase	yes	3	6	3
134804	51	Alpha-L-arabinofuranosidase	yes	2	9	4
137578	55	Endo-1,3-beta-glucosidase	no	5	2	1
126879	55	Beta-1,3-glucosidase	yes	8	12	15

39602	71	Endo-1,3-α-glucosidase	yes	2	0	0
113553	72	β-1,3-glycanosyltransferase, CBM 43	yes	3	4	7
68888	74	Xyloglucanase	yes	3	10	7
121201	78	Unknown	yes	2	2	0
136552	78	Unknown	yes	7	6	4
44058	79	Beta-glucuronidase	no	1	6	2
116837	79	Beta-glucuronidase	no	3	11	10
120232	88	Glucuronyl hydrolase	yes	2	2	0
81814	92	Unknown	yes	7	11	10
108097	95	Alpha-fucosidase	yes	6	9	7
121307	115	Alpha-glucuronidase	yes	5	0	0
121308	115	Alpha-glucuronidase	yes	15	20	14

[1]Protein ID numbers from the DOE JGI Mycocosm database (GRIGORIEV *et al.* 2014).

[2]Glycoside hydrolase families as defined in the CAZy database (LOMBARD *et al.* 2014).

[3]Putative functions determined by BLAST searches of SWISS PROT database (BATEMAN *et al.* 2015).

[4]Secretion signals for detected protein sequences were detected using Signal P algorithm (PETERSEN *et al.* 2011).

[5]Unique peptide counts for proteins found in wafer sections 0-5, 10-15, and 20-25 mm from the hyphal front.

Table 4.3: Glycoside hydrolases found in extracts of spruce wafer sections degraded by *Serpula lacrymans* and the number of unique peptides identified for each protein in each wafer section extract.

				Unique Peptides[5]		
SL Number[1]	Family[2]	Putative Function[3]	Signal P[4]	0-5	10-15	20-25
62623	1	Beta-glucosidase	no	3	4	4
107546	2	Beta-mannosidase	yes	4	9	21

158615	3	Beta-glucosidase	no	0	2	1
431585	3	Beta-glucosidase	yes	0	3	4
446061	3	Beta-glucosidase	yes	0	5	4
491435	3	Beta-glucosidase	yes	0	6	10
172091	3	Exo-1,3-beta-xylosidase	no	3	7	8
433208	5	Endo-1,4-beta-glucanase	no	0	2	4
480589	5	Endo-1,4-beta-mannosidase	yes	1	1	3
412480	5	Exo-1,3-beta-glucosidase	yes	1	2	0
349170	10	Endo-1,4-beta-xylanase	yes	3	6	4
361860	20	Beta-N-acetyl-hexosamine	yes	0	2	2
457293	27	Alpha-galactosidase	yes	1	2	3
414701	28	Exo-polygalacturonase	yes	0	1	2
463474	28	Exo-polygalacturonase	yes	1	3	2
463527	29	Alpha-L-fucosidase	no	1	2	2
453109	31	Alpha-glucosidase	yes	1	3	4
451973	31	Unknown	yes	1	4	5
154347	35	Beta-galactosidase	yes	0	3	2
453704	35	Beta-galactosidase	no	2	9	7
167797	35	Beta-galactosidase	yes	3	8	10
431618	37	Unknown	yes	0	2	3
469468	37	Trehalase	yes	1	2	2
445922	43	Unknown, CBM 35 domain	yes	0	3	2
102103	47	Alpha-1,2-mannosidase	yes	7	8	9
412847	51	Alpha-arabinofuranosidase	yes	1	3	3
94292	55	Exo-1,3-beta-glucanase	no	0	0	2
446424	79	Beta-glucuronidase	yes	0	1	2
468146	79	Beta-glucuronidase	yes	1	1	2
361158	92	Unknown	yes	2	4	5
413209	92	Unknown	no	3	6	8
442669	95	Alpha-fucosidase	yes	2	6	8
77415	115	Unknown	yes	1	11	11

[1]Protein ID numbers from the DOE JGI Mycocosm database (GRIGORIEV *et al.* 2014).

[2]Glycoside hydrolase families as defined in the CAZy database (LOMBARD *et al.* 2014).

[3]Putative functions determined by BLAST searches of SWISS PROT database (BATEMAN *et al.* 2015).

[4]Secretion signals for detected protein sequences were detected using Signal P algorithm (PETERSEN *et al.* 2011).

[5]Unique peptide counts for proteins found in wafer sections 0-5, 10-15, and 20-25 mm from the hyphal front.

Oxidoreductases (ORs) were most abundant in the early decay stages in both fungi, and a total of 6 ORs and 1 OR were exclusive to the section 0 to 5 mm from the hyphal front in *G. trabeum* and *S. lacrymans*, respectively (Table 4.4). *S. lacrymans* produced a putative copper radical oxidase in all sections, whereas this class of enzyme was not found in *G. trabeum* cultures. *G. trabeum*, on the other hand, produced a putative glucose-methanol-choline (GMC) oxidoreductase and an auxiliary activity 9 (AA9) family protein in all sections, which were not found in *S. lacrymans* cultures.

4.3.2 Fungal growth, protein secretion, and ergosterol

Serpula lacrymans and *Gloeophyllum trabeum* advanced up spruce wafers during incubation at average rates of 4.6 and 2.6 mm/day, respectively. Total protein in wood extracts was generally higher in *G. trabeum*, rapidly increasing to a maximum of 5 to 10 mm behind the front, followed by a steady decline as wood became more degraded. *S. lacrymans* extracts showed the same rapid increase but at lower levels and without a decline in the later stages (Figure 4.2). Because differences in total protein levels between sections of equal distance from the hyphal front for the two fungi could result from a simple distinction in growth rates (nearly 2 times higher for *S. lacrymans*), ergosterol

profiles for each fungus were measured, showing that fungal biomass closely tracked with protein levels and resulted in nearly flat ergosterol/protein (E/P) ratios in all sections for both fungi (Figure 4.2). The only exception was an increase at 5 to 10 mm in *S. lacrymans*. Overall, E/P ratios were 3.5 to 9.5 times higher in *S. lacrymans* (average, 38.6) than equivalent wafer sections from *G. trabeum* cultures (average, 5.7) (Figure 4.2).

Table 4.4: Total number of proteins divided into 6 functional categories observed in spruce wafer sections (mm from the hyphal front) degraded by Serpula lacrymans and Gloeophyllum trabeum. Values shown in this table are depicted in Figure 4.1. OR, oxidoreductase, GH, glycoside hydrolase.

	Serpula lacrymans				*Gloeophyllum trabeum*			
Category	0-5	10-15	20-25	Average	0-5	10-15	20-25	Average
Other	7	6	5	6.0	28	22	17	22.3
Esterases	6	10	11	9.0	14	11	9	11.3
OR	3	3	2	2.7	11	5	4	6.7
Protease	3	5	3	3.7	24	14	12	16.7
GH	21	32	32	28.3	63	60	48	57.0
Hypothetical	25	25	19	23.0	60	38	30	42.7
Totals	**65**	**81**	**72**	**72.7**	**200**	**150**	**120**	**156.7**

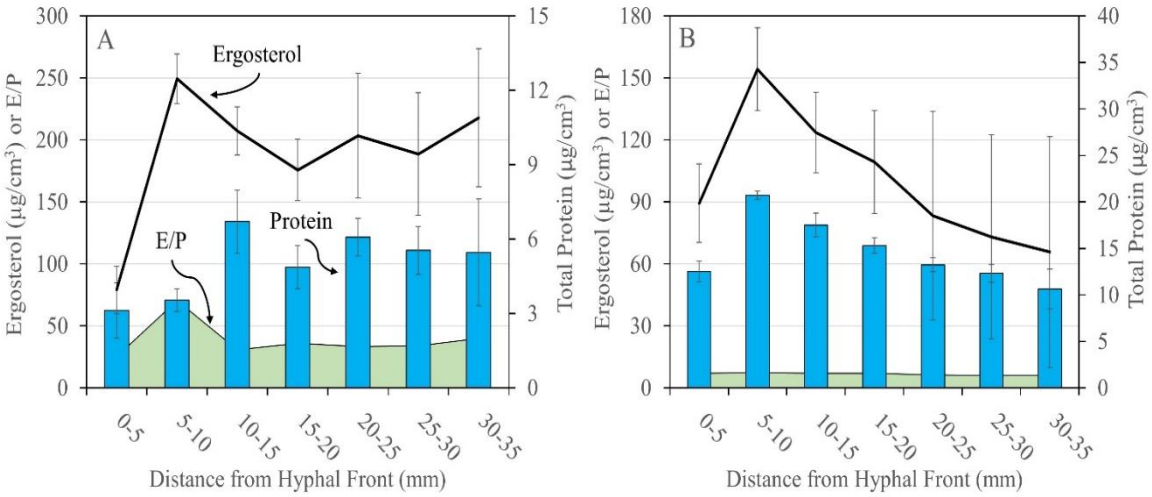

Figure 4.2: Total protein (blue bars) and ergosterol (black lines) extracted from spruce wafer sections degraded by *Serpula lacrymans* (A) and *Gloeophyllum trabeum* (B). Ergosterol/protein ratios (E/P, green area) were calculated from total protein and ergosterol values per wafer section. Error bars for total protein values are standard deviations of three assays of a single protein extract and error bars for total ergosterol are standard deviation of averages of three (*S. lacrymans*) and six (*G. trabeum*) wafer sections. *Ergosterol values found here are higher than those found in nature (SONG et al. 2014) due to dense surface growth on high surface:volume wood wafers.

4.3.3 Endoglucanase- and hemicellulase-specific activities

Endoglucanase- and hemicellulase-specific activities were low in the early stages of decay and increased and then plateaued in more-degraded wood, but the hemicellulase activities of the two test fungi had distinct patterns (Figure 4.3). For *S. lacrymans*, mannanase-specific activity dominated the hemicellulase main-chain depolymerization activity and was much higher in degraded wood than the mannanase activity of *G. trabeum*. Conversely, xylanase activity was higher in more-decayed sections in *G.*

trabeum than in *S. lacrymans* (Figure 4.3). One putative xylanase from GH family 10 and one putative mannanase from GH family 5 were found in S. lacrymans wafer extracts (Table 4.5). Four of each (GH 10 xylanases and GH 5 mannanases) were found in G. trabeum extracts.

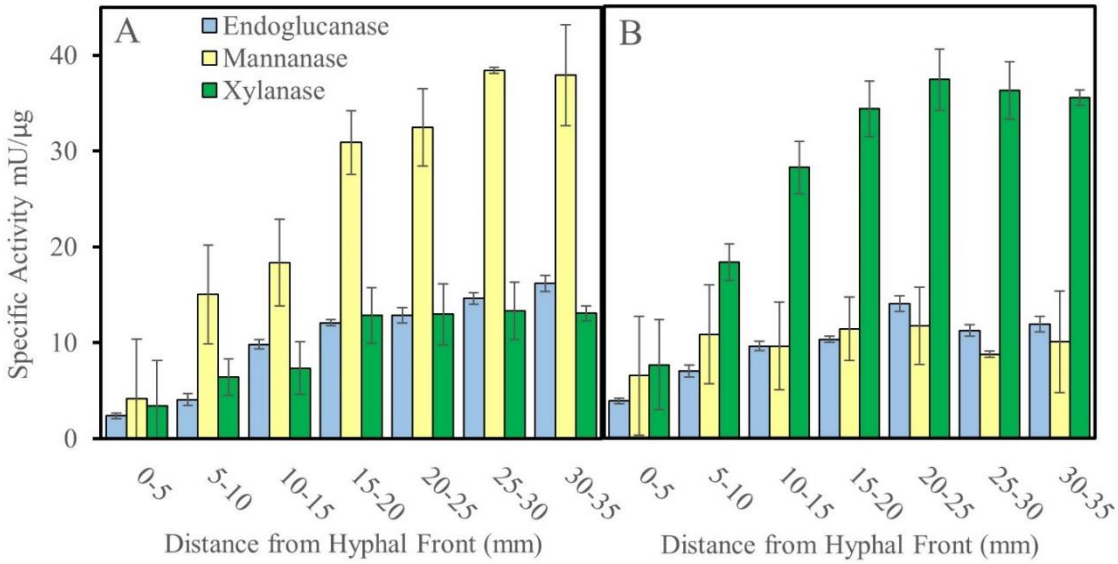

Figure 4.3: Polysaccharide degrading enzyme activity detected in protein extracts of spruce wafer sections degraded by *Serpula lacrymans* (A) and *Gloeophyllum trabeum* (B). Specific activities are the amount of enzyme required to liberate one µmol glucose, mannose, or xylose reducing equivalent per minute per µg of total protein for endoglucanase, mannanase or xylanase values, respectively. Error bars represent standard deviation of three assays of a single protein extract.

Table 4.5: GH 5 putative β-mannanases and GH 10 putative xylanases found in protein extracts of spruce wafers sections degraded by *Serpula lacrymans* and *Gloeophyllum trabeum*. The number of unique peptides for each protein are listed for each wafer section pool (mm from the hyphal front).

GH Family 5		Unique peptides		
Protein ID[1]	Putative function[2]	0-5	10-15	20-25
Serpula lacrymans				
433208	Endo-β-1,4-glucanase	0	2	4
480589	Endo-β-1,4-mannosidase	1	1	3
412480	Exo-β-1,3-glucanase	1	2	0
Gloeophyllum trabeum				
63180	Endo-β-1,4-glucanase	6	14	45
120257	Endo-β-1,4-glucanase	2	4	2
110405	Endo-β-1,4-mannanase	3	7	10
118009	Endo-β-1,4-mannosidase	2	2	0
68070	Exo-β-1,3-glucanase	2	0	0
59826	Exo-β-1,3-glucanase	9	9	7
42111	Exo-β-1,3-glucanase	2	4	4
41779	Exo-β-1,3-glucanase	1	4	3
135369	β-1,4-mannanase	3	8	6
114574	β-mannanase	1	3	3
GH 10 Family		Unique Peptides		
Protein ID[1]	Putative function[2]	0-5 mm	10-15 mm	20-25 mm
Serpula lacrymans				
349170	Endo-β-1,4-xylanase	3	6	4
Gloeophyllum trabeum				
107452	Endo-β-1,4-xylanase	15	36	49
138785	Endo-β-1,4-xylanase	3	7	5
122601	Endo-β-1,4-xylanase	6	1	0
149061	Endo-β-1,4-xylanase	3	0	0

[1]Protein ID numbers shown are from the DOE JGI Mycocosm database (GRIGORIEV *et al.* 2014).

[2]Putative functions were determined by BLAST searches of the SWISS PROT database (BATEMAN *et al.* 2015).

4.4 Discussion

S. lacrymans and *G. trabeum* had enzyme secretion patterns consistent with a two-step decay mechanism as observed in *P. placenta* (ZHANG *et al.* 2016), showing greater oxidoreductase diversity at the hyphal front and increased endoglucanase and hemicellulase activities farther behind the hyphal front. Some GHs were exclusively produced at the hyphal front by *G. trabeum*, including a putative GH 28 pectinase. In *P. placenta*, a GH 28 was the most highly upregulated transcript during wood colonization, suggesting that early pectin decomposition is shared by *P. placenta* and *G. trabeum* (ZHANG *et al.* 2016).

While consistent with a two-step decay mechanism, the colonization strategies of *S. lacrymans* and *G. trabeum* differed. This included a difference in the number of proteins observed, with *S. lacrymans* producing less than half (44%) of the number of proteins found in *G. trabeum*. The greatest distinction was near the hyphal front, where *G. trabeum* produced a more than 3 times greater variety of proteins than *S. lacrymans*. The discrepancy may be a result of differing growth rates, as each 5-mm section of wood represents approximately 1 and 1.9 days of growth/protein secretion for *S. lacrymans* and *G. trabeum*, respectively. These differences may be due to a difference in water translocation efficiency between the two fungi (JENNINGS and BRAVERY 1991), despite relatively constant moisture contents (30 to 35%) along the wafers once the wood is colonized. Hyphae in the slower-growing fungus (*G. trabeum*) may include a wider age

range in sections of equal distance from the hyphal front, resulting in a higher diversity of proteins.

Based on microscopic analysis of wafer sections degraded by *Postia placenta* (ZHANG *et al.* 2016), section age should coincide with increased fungal biomass. This held true for *S. lacrymans*, where older sections had high relative ergosterol levels, but in *G. trabeum*, we found the opposite. The ergosterol/protein values were also 7 times greater for *S. lacrymans* than for *G. trabeum*. Although there is a caveat when testing sequenced monokaryotic strains rather than dikaryotic strains, this distinction suggests that there may be a fundamental difference in biomass versus protein investment by these two fungi.

In addition to protein quantity, secretome composition also varied between the two fungi and was particularly notable among hypothetical proteins at the hyphal front, where *G. trabeum* produced over 2 times the number of proteins found at the *S. lacrymans* hyphal front. The number of hypothetical proteins in *G. trabeum* decreased by half from 5 to 25 mm behind the hyphal front; none of these have a proven biological function, but some are significantly homologous to characterized basidiomycete proteins. GT_129666, for example, is 39% identical to volvatoxin 2 (VVA2), a membrane-binding cytolytic toxin found in *Volvariella volvacea* (LIN *et al.* 2004; WENG *et al.* 2004), and could be employed as a combative protein toxin in *G. trabeum*. Protein toxins may serve to clear territory for *G. trabeum*, and high hypothetical protein diversity near the hyphal front may be a result of a combative, rather than a stress tolerance, strategy that would likely characterize *S. lacrymans*. Pore-forming proteins are known to be produced by

other wood-degrading basidiomycetes, such as *Laetiporus sulphureus*, and these may be common tools of combat in fungi (TATENO and GOLDSTEIN 2003); however, this conjecture requires further support.

The later stages of decay were also characterized by differing secretome compositions, particularly in the hemicellulase profiles of the two fungi. Most notably, *S. lacrymans* produced greater mannanase-specific activity despite the presence of only one putative GH5 mannanase (SL_480589), compared to four GH 5 mannanases in the *G. trabeum* secretome. Greater mannanase abundance may partly explain this discrepancy, or there may be a structural difference leading to increased catalytic potential among GH 5 mannanases in *S. lacrymans.* The cause of the discrepancy in hemicellulase profiles remains unresolved, but the reason behind observed patterns may also relate to species niches. In nature, *S. lacrymans* is found on glucomannan-rich conifer wood (WHITE *et al.* 1997) and thus may have evolved more efficient enzymes for glucomannan conversion. *Gloeophyllum trabeum*, which produced greater xylanase activity despite growth on a xylan-poor substrate, is more of a substrate generalist, with niches including xylan-rich angiosperm wood (GILBERTSON and RYVARDEN 1986). *S. lacrymans* also produced no cellobiohydrolase in this study, consistent with previous work failing to identify CBH in wood protein extracts and showing only low levels of expression despite its existence in the genome sequence. These results suggest that CBH plays only a minor, if any, role in decay by *S. lacrymans* (EASTWOOD *et al.* 2011).

These differences in the *S. lacrymans* and *G. trabeum* secretomes suggest that there are variations in the biochemical routes to brown rot, and this was evident in the

oxidoreductase profiles of the two fungi. *Serpula lacrymans* produced a putative copper radical oxidase not found in *G. trabeum*, and *G. trabeum* instead produced a putative GMC oxidoreductase and a xyloglucan-specific AA9 family protein (KOJIMA *et al.* 2016), a class of protein encoded in the *S. lacrymans* genome but not secreted on spruce wood (LUNDELL *et al.* 2014). Those differences suggest that these fungi rely on different electron sources for H_2O_2 production for the brown-rot mechanism, and they partially explain the enhanced xylanase activity in *G. trabeum* (DANIEL *et al.* 2007; KERSTEN and CULLEN 2014).

Overall, this work supports a two-step brown-rot decay mechanism common in *S. lacrymans* and *G. trabeum*, a strategy seen in other brown-rot fungi (ZHANG *et al.* 2016) and white-rot fungi, where the secretion of enzymatic oxidants is more prolific in the early decay stages (HORI *et al.* 2014; KUUSKERI *et al.* 2016). Given our data, we propose that multiple biochemical manifestations of brown rot exist among the independent lineages of brown rot, driven by species-specific niches. This makes the brown-rot mechanism difficult to reconstruct as a single mechanism but also indicates the presence of a more diverse pool of catabolic enzymes among brown-rot fungi for various applications. It also implies that the broad outcome of brown rot must be, in part, predictable as a function of environment, given the convergence among taxa.

Chapter 5 Brown rot-type fungal decomposition of sorghum bagasse: Variable success and mechanistic implications

5.1 Introduction

Renewable biofuel and bio-based products are an avenue towards energy independence and rural economic growth in southern Africa (GASPARATOS *et al.* 2015). In the case of bioethanol in southern Africa, the predominant plant feedstock is water-intensive sugar cane (DIAZ-CHAVEZ and JAMIESON 2010), but changes in Sub-Saharan climate are predicted to result in dryer conditions and demand more diverse crop options in order for agriculture to adapt (SERDECZNY *et al.* 2016). Sweet stem sorghum (*Sorghum bicolor*) is a native African plant grown for sugar that is more tolerant of arid climates and saline soils (ZEGADA-LIZARAZU and MONTI 2012; REGASSA and WORTMANN 2014), making it an attractive alternative bioenergy crop for southern Africa, and its residues post-sugar extraction (bagasse) are an attractive biomass crop for many different bio-based product options. The lignocellulose in extracted sorghum bagasse could be utilized for silage or as a feedstock for biofuels and bioproducts, given efficient deconstruction (CAI *et al.* 2013). The sugars locked in sorghum bagasse, however, are more difficult to liberate than those extractable in hot water, requiring harsher pretreatments to liberate fermentable sugars (RABEMANOLONTSOA and SAKA 2016).

To better understand how sorghum bagasse could be deconstructed using milder, bio-based techniques, it is logical to study how sorghum is deconstructed by

lignocellulose-degrading fungi. For this study, we chose to assess the mechanisms of lignocellulose-degrading 'brown-rot' fungi, a current research focus due to their carbohydrate-selective extraction pathways and their consolidation of oxidative pretreatments with enzymatic saccharification, two steps that remain separate in industrial processing (ZHANG *et al.* 2016). In addition to a relevant bioprocessing system, investigating brown rot of sorghum is logical due to the varying abilities to degrade lignin and monocot grasses (KAFFENBERGER and SCHILLING 2013), something that is rarely tested among decomposer fungi associated with wood substrates. Brown-rot fungi are polyphyletic (HIBBETT and DONOGHUE 2001), and while some characteristics such as early hemicellulose removal are common among brown-rot fungi (HIGHLEY 1987; SCHILLING *et al.* 2012), their genomes harbor significant variability (FLOUDAS *et al.* 2012; RILEY *et al.* 2014), and brown-rot fungi can be found in a wide variety of niches in nature (GILBERTSON and RYVARDEN 1986). This implies variability in decay mechanisms among brown-rot fungal clades, a useful model system for probing decay pathways for an understudied feedstock such as sweet stem sorghum bagasse as well as offering a useful context for probing fungal biochemical variability.

For our study, we chose to focus specifically on *Gloeophyllum trabeum* and *Serpula lacrymans* from two distinct clades (Gloeophyllaceae and Coniophoraceae, respectively). *S. lacrymans* has several key genomic distinctions from *G. trabeum*. These include the retention of exo-acting cellobiohydrolase (CBH) cellulase genes, but, like *Postia placenta*, the absence of carbohydrate esterase family 1 (CE 1), a family containing feruloyl esterases (EC 3.1.1.73) that might be involved in decoupling xylan

from lignin, particularly in the decay of grasses (CREPIN *et al.* 2003). We have also seen on wood substrates (spruce, (PRESLEY and SCHILLING 2017)) that *S. lacrymans* preferentially produced mannanase activity and *G. trabeum* produced higher xylanase activity, despite causing a similar type of decay. Sorghum, like other Poaceae substrates (VOGEL 2008), is a xylan-rich substrate that would require *S. lacrymans* to alter its mannanase-dominant glycoside hydrolase profile in order to survive, as well as decoupling xylan from lignin by the hydrolysis of ferulic acid esters. Xylan is barrier to most of the utilizable carbon in plant biomass (ZHAO *et al.* 2012), and failure by fungi to remove it could result in starvation and associated cell autolysis (NITSCHE *et al.* 2012).

In this study, *G. trabeum* and *S. lacrymans* were compared for their ability to grow on water-extracted sweet stem sorghum biomass, the bagasse substrate (post-extracted) most relevant to sorghum bioconversion. The fungi were grown for 7, 14, and 21 days and the loss of major structural carbohydrates, relative to sorghum not inoculated with fungi, was measured along with polysaccharide-degrading enzyme activity and ergosterol contents. Decay strategies were compared to previous patterns generated on wood, as well as to other work showing variable decay patterns on other grass substrates.

5.2 Methods

5.2.1 Sorghum collection and preparation

Sweet stem sorghum (Sorghum bicolor) stalks were grown outside of East London, South Africa, maintained on Agricultural Research Council of South Africa research plots, and were harvested in May 2016. Four stalks were cut into ~2 cm long

sections near the top of the stalks (< 2 cm diameter). The stalk sections were dried at 70˚C and then extracted in water at 90˚C with 5 exchanges of fresh water. This approach removes some hemicellulose, along with other more soluble sugars, and is a more biotechnologically-relevant substrate, as post-extracted bagasse. After extraction, the stems were dried at 70˚C and stored until further use.

5.2.2 Fungal cultivation and decay microcosms

Serpula lacrymans S7.3 and Gloeophyllum trabeum ATCC 11539 cultures were maintained on potato dextrose agar. Agar plugs (1 cm dia) from plates colonized by either fungus were used to inoculate modified soil block jars, as previously described (PRESLEY and SCHILLING 2017). Extracted sorghum sections were vacuum-impregnated with water, sterilized (121˚C, 16 psi, 1 hour), and cooled. Four sections were added to each soil block microcosm after allowing the fungus to colonize for 2 weeks, and then the microcosms were incubated at room temperature in the dark for 7, 14, and 21 days. Sorghum sections prepared in parallel but not inoculated were used as control material for characterization.

5.2.3 Protein extraction, purification, and activity assays

At each timepoint, degraded and non-degraded sorghum discs were chopped into smaller pieces by hand, suspended in 80 ml of extraction buffer (50 mM acetate, 0.5 M NaCl, 0.05% Tween 80, pH 5.0), and then extracted at 4˚C with gentle shaking for 24 hours. Two replicate extracts of four pooled sorghum discs at each timepoint were used generate to generate protein extracts for each fungus. Coarse material was filtered using a polyester mesh, dried at 70˚C, and reserved for chemical analysis. The filtrate was

centrifuged (4000 g, 30 min) to remove particulates, filtered through 0.2 µm polyethersulfone (PES) filters, and exchanged into 50 mM citrate buffer pH 5.0 through 10 kDa PES membranes. Protein concentration was determined using a Bio-Rad protein assay kit (Hercules, CA, USA).

Cellulase and hemicellulase specific activities were measured by the dinitrosalicylic acid (DNS) method using solutions of 1.5% carboxymethyl cellulose (for endoglucanase activity), 2% Birchwood xylan (xylanase), and 0.5% locust bean gum (mannanase) (GHOSE 1987). Protein extracts were incubated with substrate at 50˚C in 50 mM citrate pH 5.0 in triplicate. The absorbance at 540 nm was measured after color development, and reducing sugars were determined as glucose, xylose, and mannose reducing equivalents for endoglucanase, xylanase, and mannanase activities, respectively. Activities for β-glucosidase and β-xylosidase were determined by measuring the release of 4-nitrophenol (4NP) from 4-nitrophenol-β-glucoside (4NPG) and 4-nitrophenol-β-xylopyranoside (4NPX), respectively. Reactions were carried out in 10 mM 4NP-substrate in 50 mM citrate, pH 5.0 at 50˚C and were quenched with 2 volumes of 0.2 M Na_2CO_3. Absorbance at 400 nm was measured to determine free 4NP.

5.2.4 Ergosterol extraction and assay

Total ergosterol was measured to use as a biomarker for fungal biomass and was extracted from three separate sorghum sections for each fungus at 7, 14, and 21 days of decay and from non-degraded sorghum using established methods (NEWELL *et al.* 1988). Ergosterol was measured by HPLC using a PhenomenexTM (Torrance, CA, USA) 4µ

Hydro-RP 80a column by detection at 282 nm using previously described methods (SCHILLING and JELLISON 2005).

5.2.5 Sorghum mass loss, density and compositional analyses

Mass loss was determined for sorghum degraded for 7, 14, and 21 days and density of degraded and non-degraded sorghum sections were determined in triplicate by measuring the mass of water displaced by submerging fully-hydrates sorghum sections in excess water (g cm^{-3}). Degraded and non-degraded sorghum biomass previously extracted for protein was milled to 40 mesh in a Wiley mill. Sorghum powder was hydrolyzed in dilute acid and the concentration of glucan, xylan, and arabinan were measured by HPLC using an Aminex HPX87-P column (Bio-Rad, Hercules, CA) according to standard procedures (SLUITER *et al.* 2008). The % loss of each component was calculated from original component mass calculated using average mass losses at each timepoint.

5.3 Results

5.3.1 Decay rates and fungal biomass on sorghum

Gloeophyllum trabeum degraded sorghum more completely than *S. lacrymans*, causing nearly 5x greater mass loss (37.8% vs. 7.9%, respectively) after 21 days of decay (Table 5.1). As typical of brown rot, early-stage strength loss was evident and residues were easily crumbled in the hand, more so for sorghum incubated with *G. trabeum*. Despite differences in degradative ability, ergosterol levels, a proxy for fungal biomass, did not differ at equivalent timepoints between the fungi and indicated ample

colonization but minimal substrate degradation for *S. lacrymans* (Table 5.1). Total protein amounts were also similar between the two fungi at most equivalent timepoints, ranging from 71-107 μg cm^{-3} of biomass (Table 5.1).

Table 5.1: Ergosterol (E), Protein (P), and ergosterol/protein ratios (E/P) for sorghum sections degraded by *Gloeophyllum trabeum* and *Serpula lacrymans* for 7, 14, 21 days. Protein and Ergosterol levels are standardized to cm^3 of biomass.

	Gloeophyllum trabeum				*Serpula lacrymans*			
	Mass loss %[a]	E μg cm^{-3} [a]	P μg cm^{-3} [b]	E/P	Mass loss %	E μg cm^{-3}	P μg cm^{-3}	E/P
7 days	2.4 (1.8)	73.3 (44.5)	98.1 (30.8)	0.7	2.0 (1.0)	76.3 (60.8)	107.6 (26.4)	0.7
14 days	30.8 (5.1)	205.0 (59.1)	98.5 (31.1)	2.1	3.1 (1.2)	73.0 (54.2)	71.3 (12.7)	1.0
21 days	37.8 (3.7)	215.0 (33.9)	78.3 (16.5)	2.7	7.9 (3.6)	235.6 (71.0)	74.6 (7.1)	3.2
Sorghum Avg	23.7 (18.7)	164.4 (79.1)	94.5 (22.6)	1.9	4.4 (3.1)	128.3 (93.0)	112.5 (21.6)	1.6
Spruce Avg[c]	N/A	99.8 (31.3)	14.6 (3.5)	6.7	N/A	188.8 (53.6)	5.0 (1.3)	38.6

[a] Standard deviation of three biological replicates is shown in parentheses.

[b] Standard deviation of three assays of an extract of 8 sorghum discs is shown in parentheses.

[c] Values adapted from Presley and Schilling 2017.

5.3.2 Sorghum carbohydrate losses

The undegraded sorghum biomass was composed of 39.9% glucan, 16.2% xylan, an 4.3% arabinan. Xylan was removed more rapidly from sorghum than glucan by both species, with 24.5% and 29% xylan loss after 7 days of decay compared to 3.2% and 5% glucan loss over the same period by *G. trabeum* and *S. lacrymans*, respectively (Figure 5.1). Arabinan loss at 7 days for both species tended to be higher than glucan, but not significantly at 95% confidence (Tukey's HSD, $p>0.05$). Glucan removal proceeded rapidly in the later stages of decay in *G. trabeum*, but this was not the case in *S. lacrymans*, reaching 38.4% loss by 21 days of decay in the former, and only 5.3% loss in the latter.

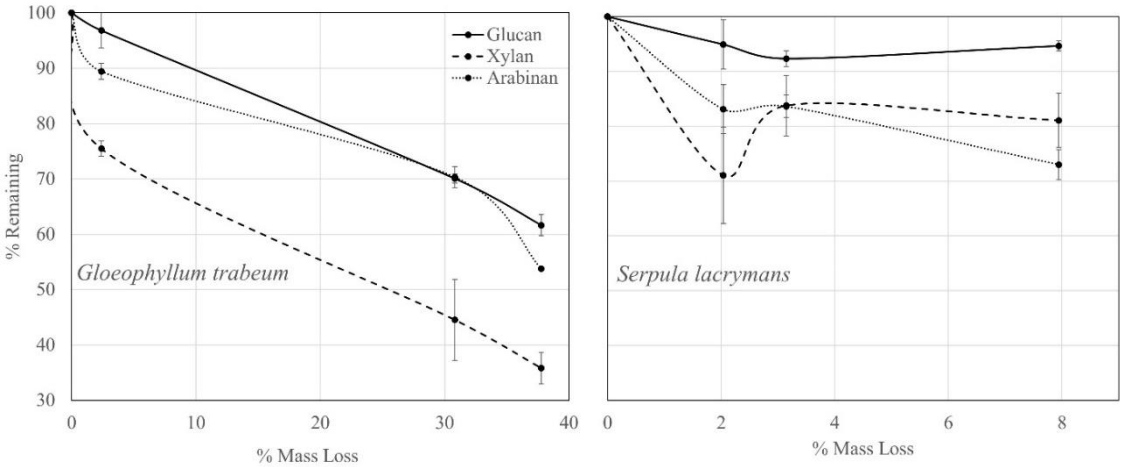

Figure 5.1: Major structural carbohydrate removal from sorghum biomass over a 21-day progression of decay for Gloeophyllum trabeum and Serpula lacrymans. Error bars are +/- standard error of three replicate assays of each of two replicate extracts.

In relative terms (% of calculated original polymer mass), xylan was the most labile polysaccharide for *G. trabeum*, and 62.2% of the original xylan was lost after 21 days of decay (Figure 1). In absolute terms (mg of polymer), the mass of glucan and xylan removed by *G. trabeum* did not differ significantly until after 21 days of decay, where the total mass of glucan and xylan lost were 81 mg and 54.7 mg, respectively. *S. lacrymans* removed relatively more xylan and arabinan than glucan by 21 days of decay, and did not remove either of the major hemicelluloses preferentially. The mass of polysaccharide components removed over time did not differ significantly from one another for sorghum degraded by *S. lacrymans* indicating no sugar preference. *S. lacrymans* also degraded lower percentages of all components than *G. trabeum*, collectively explaining low mass loss values.

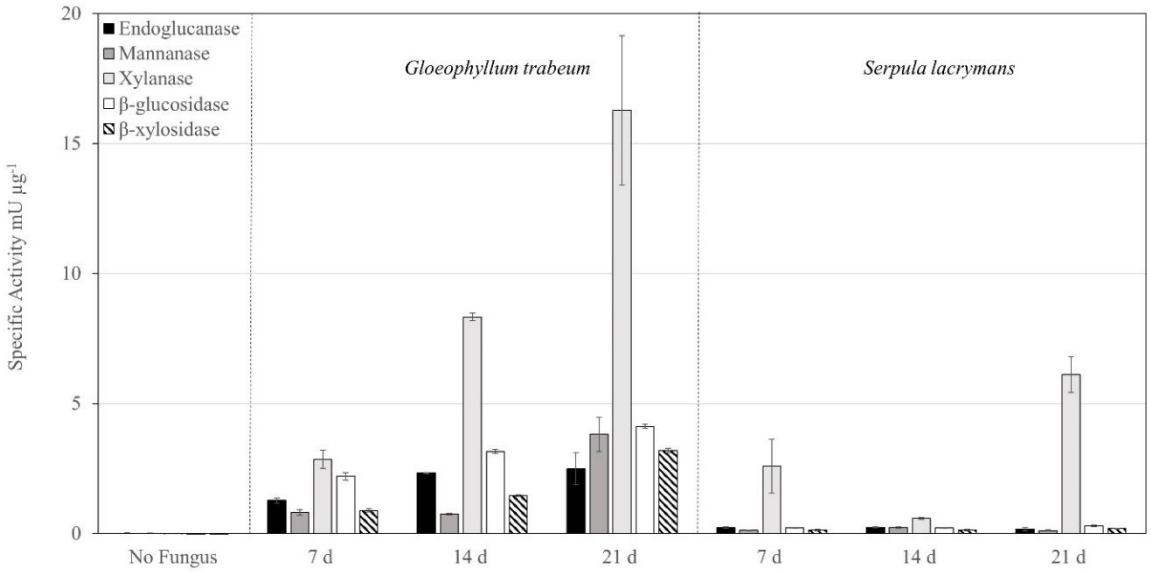

Figure 5.2: Endoglucanase, Xylanase, Mannanase, β-glucosidase, and β-xylosidase specific activities of protein extracts from sorghum sections degraded by Gloeophyllum trabeum and Serpula lacrymans for 7, 14, and 21 days and undegraded sorghum biomass. Error bars are +/- standard error of three replicate assays of each of two replicate extracts.

5.3.3 Enzyme activities

In *G. trabeum* extracts, most enzyme activities increased from early to late stages of decay except for endoglucanase activity, which remained flat throughout decay stages (Figure 5.2) ($p>0.05$, Tukey's HSD). In *S. lacrymans*, enzyme activities tended to be much lower, despite similar levels of total protein to *G. trabeum*. All measured activities in *S. lacrymans*, except for xylanase at 21 days, were not significantly above non-degraded controls ($p>0.05$, Tukey's HSD). In line with patchy growth patterns observed in *S. lacrymans*, xylanase activity at 7 days was highly variable between the two replicate extractions, with activity from one extract matching that of non-degraded controls. For both fungi, xylanase was the highest polysaccharide-degrading enzyme activity. Despite this, β-xylosidase (BXL) activity was lower than β-glucosidase (BGL) activity in *G. trabeum* extracts.

5.4 Discussion

In this study, the brown-rot fungus *G. trabeum* (Gloeophyllales) effectively degraded sorghum while the fungus *S. lacrymans* (Boletales) struggled to release carbohydrates from the substrate. This variability in apparent recalcitrance of the sorghum substrate is an important result, but the variability between the fungi is also informative. Brown-rot fungi are often assumed to prefer conifer substrates (gymnosperms) rather than angiosperm substrates in nature, and it is notable that *G. trabeum* is commonly found on the wood of both conifers and angiosperms (GILBERTSON and RYVARDEN 1986). This lack of substrate specificity for *G. trabeum* might help explain, coarsely, its superiority to *S. lacrymans* on sorghum, although these substrate

associations are poorly understood and often do not persist outside of a natural setting. Wood-degrading fungi that are host-specific in the field are often capable of growing and deconstructing a wider range of substrates when grown in culture (HIGHLEY 1973a; VALASKOVA and BALDRIAN 2006). Instead, these results suggest a broader variability in fungal deconstruction pathways among the brown-rot types.

Successful growth on xylan-rich sorghum by *G. trabeum* may be due in part to high xylanase activity, a trait that would also enable decay of angiosperm wood whose hemicellulose is dominated by xylan. Both of our test fungi initiated the decomposition process by removing xylan, reflecting the protective role of xylan in shielding glucan from enzymatic hydrolysis (ZHAO *et al.* 2012). Similar to the distinction between these fungi previously on spruce wood (PRESLEY and SCHILLING 2017), xylanase specific activities were approximately 3x higher on average for *G. trabeum* than for *S. lacrymans*. It is plausible that *G. trabeum* has more responsive xylanase induction than *S. lacrymans*, stimulated by endoxylanase-produced xylo-, di- and oligosaccharides as in other fungal species (HALTRICH *et al.* 1996; ZHANG and SCHILLING 2017). In *G. trabeum*, BXL activity after 7 days was considerably lower than xylanase activity, implying that the majority of xylanase activity at the early decay stages is due to endo-acting xylanases required to liberate β-xylosidase substrates (BIELY *et al.* 2016).

Differences in the degradative capacity of brown-rot fungi may also be explained by the number and types of lignocellulose-degrading genes in their genomes that would be effective on a grass substrate. Along with *S. lacrymans, Postia placenta* and *Fomitopsis pinicola* have been shown ineffective in degrading a wide range of Poaceae

substrates (KAFFENBERGER and SCHILLING 2013). Grasses contain hemicelluloses that are like sorghum, primarily consisting of glucuronoarabinoxylan with ferulic acid ester linkages between xylan and lignin (KUMAR *et al.* 2009). Among the types of genes involved in the degradation of grass polysaccharides, CE 1 feruloyl esterases (FAE) (EC 3.1.1.73) are absent in the genomes of *P. placenta* and *F. pinicola* (Table 5.2) 14. Absence of FAE activity has also been demonstrated in cultures of *Postia placenta,* indicating a minimal capacity to hydrolyze ferulic acid esters in lignocellulose 31. In contrast, *G. trabeum* is known to effectively degrade Poaceae substrates 9 and possesses a CE 1 that it actively secretes on wood 17, suggesting CE 1 proteins could be the basis of the phenotypic difference we observed in this study.

Table 5.2: Number of copies of gene families with activity on glucuronoarabinoxylan, cellulose, and mixed linkage glucan present in the genomes of seven brown-rot fungi. The major taxonomic affiliations are shown, SL, *Serpula lacrymans*, CP, *Coniophora puteana*, WC, *Wolfiporia cocos*, PP, *Postia placenta*, FP, *Fomitopsis pinicola*, GT, *Gloeophyllum trabeum*, DP, *Dacryopinax sp.*

		Brown Rot Species[3]						
Relevant Activity[1]	Family[2]	CP	SL	PP	FP	WC	GT	DP
AXE/FE	CE 1	0	0	0	0	0	1	0
AXE	CE 4	9	6	2	3	4	5	11
AXE	CE 5	1	0	0	0	0	0	0
4MGU	CE 15	0	0	1	1	1	1	1
AE	CE 16	7	4	4	8	6	7	3
BGL/BXL/BGU	GH 1	3	3	2	2	1	5	1
BGU/ABF	GH 2	5	3	3	4	3	4	3
BGL/BXL/ABF/B3G/B4G	GH 3	13	10	6	12	8	11	9

EGL/EXL/BGL/B3G/EBG	GH 5	21	21	17	19	18	19	24
EGL/CBHII	GH 6	2	1	0	0	0	0	0
EGL/CBHI/E34G	GH 7	2	0	0	0	0	0	0
EGL/BGL/E34G/EBG/CBH	GH 9	1	1	0	0	0	1	1
EXL	GH 10	3	1	3	2	4	3	3
EGL/E34G	GH 12	4	2	2	2	2	2	1
E3G/E34G	GH 16	24	20	24	28	19	29	14
E3G/E34G	GH 17	4	2	2	3	2	2	3
E34G	GH 26	0	0	0	0	0	0	4
EXG/BGL/BGU/BXL	GH 30	7	2	3	10	2	3	4
BXL/ABF/EXL	GH 43	6	2	1	7	1	6	5
EGL	GH 45	1	0	0	1	0	1	1
EGL/EXL/BXL/AAF	GH 51	3	1	1	4	4	4	2
E3G/B3G	GH 55	5	6	3	3	3	2	2
EGL/EXG	GH 74	0	1	0	0	0	1	0
BGU	GH 79	4	6	2	3	3	6	7
E3G	GH 81	1	0	0	0	0	1	0
ABF	GH 93	1	0	0	0	0	0	0
AGU	GH 115	2	1	1	1	2	2	2
E3G	GH 128	9	5	5	4	2	6	2
E346G	GH 131	2	2	0	1	0	1	1

[1]Each abbreviation represents an EC number indicating the specificity of an enzyme in each family. 4MGU, 4-O-methylglucuronyl methylesterase (EC 3.1.1.-), ABF, α-arabinofuranosidase (EC 3.2.1.55), AE, Acetylesterase (EC 3.1.1.6), AXH arabinoxylan arabinofuranohydrolase (EC 3.2.1.55), AXE, Acetylxylan esterase (EC 3.1.1.72), AGU, α-glucuronidase (EC 3.2.1.131), B3G, β-1,3-glucosidase (EC 3.2.1.58), B4G, β-1,4-glucosidase (EC 3.2.1.74), BGL, β-glucosidase (EC 3.2.1.21), BGU, β-glucuronidase (EC 3.2.1.31), BXL, β-xylosidase (EC 3.2.1.37), CBHII, cellobiohydrolase (EC 3.2.1.91),

CBHI, cellobiohydrolase reducing end (EC 3.2.1.176), E34G, Endo-β-1,3-1,4-glucananse (EC 3.2.1.73/3.2.1.6), E364G, Exo-β-1,3-1,6 and endo-β-1,4-glucanase (EC 3.2.1.-), E3G, Endo-β-1,3-glucanase (EC 3.2.1.39), EXG, Exo-β-1,4-glucanase (EC 3.2.1.74), EGL, Endo-β-1,4-glucanase (EC 3.2.1.4), EXL, Endo-β-1,4-xylanase (EC 3.2.1.8), FE, Feruloyl esterase (3.1.1.73)

[2]CE, carbohydrate esterase, GH, glycoside hydrolase

[3]Gene counts are adapted from (RILEY *et al.* 2014).

Despite differences in degradative ability, both fungi produced similar amounts of ergosterol, a proxy for total fugal biomass (NEWELL *et al.* 1988), as well as different amounts of secreted protein on sorghum when compared at equivalent timepoints. Ergosterol/protein ratios (E/P) for the two fungi did not differ significantly at any decay stage, unlike previous observations on spruce where *G. trabeum* produced relatively more protein and less ergosterol (lower E/P) than *S. lacrymans* (PRESLEY and SCHILLING 2017). These patterns in E/P are likely explained by increased protein investments on sorghum, particularly for *S. lacrymans*; however, polysaccharide-degrading enzyme specific activity was on average 13x lower on sorghum biomass compared to spruce, whereas the same discrepancy was less than 4x lower for *G. trabeum*. The differences in specific activity may be linked to the relative inability of *S. lacrymans* to metabolize sorghum, causing C-starvation, cell autolysis, and the dilution of secreted protein with cellular protein as seen in C-starved cultures of *Paxillus involutus* and *Aspergillus niger* (NITSCHE *et al.* 2012; ELLSTROM *et al.* 2015). It indicates that quantifying protein investments as a 'trait,' including nitrogen-use efficiencies, might yield very different

trait values for the same wood-degrading fungi, depending on the substrates used to calculate these values.

5.5 Conclusion

This study highlights differences in the biodegradative ability and decay mechanisms among phylogenetically disparate brown-rot fungi. *S. lacrymans*, like some other brown-rot fungi, may have general difficulty degrading grass substrate. The more generalist substrate associations of *G. trabeum*, however, may impart an ability to more easily degrade grasses. The early hemicellulose selectivity, in terms of industrial relevance, suggests that pretreatment methods such as dilute acid that target carbohydrates may be effective in sweet sorghum lignocellulose conversion. In terms of fungal biology, the discrepancies may be linked to the presence of fungal genes coding for products that target xylan-lignin bonds and xylan, itself. This would be useful to explore in other brown-rot clades, as well, and may help explain substrate-specificities among wood-degrading fungi.

Chapter 6 Comparing the temporal process of wood metabolism among white and brown-rot fungi by coupling secretomics with enzyme activities

6.1 Introduction

Wood-degrading basidiomycete fungi and their metabolic pathways for plant biomass decomposition are of biotechnological interest and are a principle determinant soil quality and CO_2 evolution rates in nature (BARDGETT *et al.* 2008; A'BEAR *et al.* 2014). Wood decomposition is a dynamic process where decomposer species composition (RAJALA *et al.* 2011; HISCOX *et al.* 2015a) and the 'signature' physiochemical modifications they make to wood substrates (KUUSKERI *et al.* 2016; ZHANG and SCHILLING 2017) change over time, ultimately determining the fate of wood-bound carbon. Considerable interspecific variation in decay mechanisms is apparent among related species (MACDONALD *et al.* 2012), and some variations may relate to time-dependent up/down regulation patterns (PRESLEY and SCHILLING 2017). Better resolution of temporal changes in basidiomycete wood decay mechanisms can therefore help identify processes that drive broader interspecific variations in the decay mechanisms of these important fungi.

Wood-degrading fungi are traditionally categorized as carbohydrate-selective brown-rot (BR) fungi and lignin-degrading white-rot (WR) fungi (HATAKKA and HAMMEL 2010). As a general rule, WR fungi produce lignin-degrading peroxidases

(HOFRICHTER *et al.* 2010) and a greater diversity of glycoside hydrolase (GH) families (FLOUDAS *et al.* 2012) than BR fungi. Comparative genomics studies have, however, identified variable copy numbers for different classes of ligninolytic enzymes and other oxidases among species (FLOUDAS *et al.* 2012; RUIZ-DUENAS *et al.* 2013). The white-rot fungus *Trametes versicolor* (Polyporales), as a relevant example to the work we will present here, is known to produce large amounts of laccase 13 and to possess in its genome lignin peroxidases (LiPs), versatile peroxidases (VPs), dye de-colorizing (DyPs), and short Manganese peroxidases (MnPs). On the other hand, the white-rot fungus *Stereum hirsutum* (Russulales) possesses only 'atypical' MnPs and laccases among its ligninolytic genes (FLOUDAS *et al.* 2012), a feature that does not apparently limit its ability to degrade lignin and that leaves *S. hirsutum* lumped with *T. versicolor* within a single rot 'type.' This lumping into two rot type 'bins,' however, is increasingly viewed as oversimplified, and genomic (RILEY *et al.* 2014) and proteomic (ZHU *et al.* 2016) studies indicate that rot types generally lie along a spectrum. Individual species within BR and WR groups vary considerably in the enzymes they produce to degrade wood (MACDONALD *et al.* 2012; PRESLEY and SCHILLING 2017).

These decay mechanisms are also dynamic over time, and this temporal variability is essential in how these mechanisms proceed. Temporal aspects of regulation are not evident from genomic DNA sequences, and are likely controlled via gene networks so they can only be evaluated via RNA transcripts rather than genomes. Using a recent transcriptomics study as an example for BR fungi, a directional colonization design using wood wafers showed that early stages of BR involve a unique set of

differentially-regulated oxidoreductases along with high pectinase expression (ZHANG *et al.* 2016). This temporal sequencing may loosen lignocellulose ahead of secretion of enzymes, providing better ingress for hemicellulases and cellulases, degrading pit membranes to improve cell-to-cell growth (BLANCHETTE 1995), and separating pectin from cellulose (DICK-PEREZ *et al.* 2011). This 'pretreatment' would leave cellulose microfibrils more accessible to degradative enzymes that are upregulated after an initial delay (XIAO and ANDERSON 2013).

Transcriptomics, however, is also limited in linking genes to their function, and gene products apparent in secretomes can provide more insight into the metabolites participating in lignocellulose deconstruction. These techniques are less quantitative than measuring expression levels, but are inherently valuable 'downstream' measurements post-translation and can be coupled with enzyme activity assays in many cases to complement spectral counts of amino acids. This approach has, for example, shown that WR fungi make early investments in peroxidase secretion (HORI *et al.* 2014) that are followed by an accumulation and increased activity of GHs, a pattern similar to BR fungi (PRESLEY and SCHILLING 2017). These integrated secretome and specific activity assessments have also been used to distinguish growth versus protein investments as a function of time among distinct wood-degrading clades within the BR fungi (PRESLEY and SCHILLING 2017). This approach had not yet been coupled, however, with the higher-resolution temporal approaches to make intra-strain comparisons within and among rot types.

In our study, growth characteristics and temporal dynamics among secretomes of four relevant WR and BR fungi were compared on thin sections of aspen wood. Two BR and two WR fungi were grown on aspen wafers vertically, forcing a gradient of decay along the length of the wafer starting at the advancing hyphal front (ZHANG *et al.* 2016). Thin cross sections were taken along the advancing hyphal front to compare secretome characteristics over a progression of decay, tracking relative biomass investments and matching spectral counts via mass spectrometry with enzyme specific activity assays. Our results contribute valuable secretome datasets that were generated using the high-resolution temporal sequence on solid wood and including four fungi commonly used as models in biochemical studies. Our results also confirm several key mechanistic patterns that were inferred previously from less-resolved time series or transcriptomic studies. Two novel insights also emerged from our results, as well, highlighting distinct temporal regulation of pectinases between BR and WR fungi and revealing two distinct peroxidase pathways the WR fungi tested.

6.2 Methods

6.2.1 Microcosm set-up and harvest

Two BR fungi (*Postia placenta* MAD-698 and *Gloeophyllum trabeum* ATCC 11539) and two WR fungi (*Stereum hirsutum* FP-91666 and *Trametes versicolor* A1-ATF (taken from the personal collection of Dr. Jonathan Schilling) were cultivated on 60 x 25 x 3 mm aspen wafers in modified ASTM standard soil block microcosms, as previously described (ZHANG *et al.* 2016; PRESLEY and SCHILLING 2017). Wafers with straight, horizontal hyphal fronts were harvested, surface hyphae were removed, and were

cross-sectioned into seven 5-mm sections starting at the hyphal front and extending 35 mm behind it. Wafer sections were chopped into smaller pieces with sterilized razor blades prior to protein or ergosterol extractions. Growth rates were calculated as the total distance traveled by fungal hyphae divided by the total number of days of incubation less a three-day (*P. placenta*, *G. trabeum*, and *S. hirsutum*) and two-day (*T. versicolor*) lag period.

6.2.2 Protein extraction and biochemical assays

Aspen wafer sections from equivalent distances from the advancing hyphal front (0-5 mm to 30-35 mm) degraded by each of the species mentioned above were pooled and chopped with sterile razor blades prior to extraction. Chopped sections were extracted with 80 ml of cold extraction buffer (0.5 M NaCl, 50 mM acetate, 0.05% tween 80, pH 5.0) for 24 hours at 4˚C with gentle shaking. Extracts were filtered through polyester cloth, centrifuged at 4000 x g for 30 minutes to remove solid particles, and filtered through sterile 0.2 µm PVDF filters. Extracts were exchanged into 0.05 M citrate pH 5.0 and concentrated using Vivaspin Polyethersulfone (PES) 10 kDa cutoff membranes prior to freezing at -20˚C. Protein concentrations of extracts were determined using a BioRad protein assay kit (Hercules, California, USA).

Protein extracts of wafer section pools (12 wafers) from all seven separate sections along the hyphal front were assayed for various polysaccharide-degrading enzyme and ligninolytic oxidase activities. Cellulases and hemicellulase activities were measured by the dinitrosalicylic acid (DNS) method using solutions of 0.5%

polygalacturonic acid (pectinase), 1.5% carboxymethyl cellulose (endoglucanase), 2% Birchwood xylan (xylanase), and 0.5% locust bean gum (mannanase) (GHOSE 1987). Triplicate portions of protein extracts were incubated with substrate solutions in 50 mM citrate pH 5.0 at 50˚C and quenched with DNS development solution. Reactions were developed at 90˚C and absorbance at 540 nm was measured and used to determine reducing sugars as galacturonic acid, glucose, xylose, and mannose reducing equivalents for pectinase, endoglucanase, xylanase, and mannanase activity, respectively. One unit was defined as the amount of enzyme required to produce 1 µmol of reducing sugar per minute. β-1,4-glucosidase (BGL), β-1,4-galactosidase (BGA), β-1,4-xylosidase (BXL), and β-1,4-N-acetylglucosaminidase (BNG) activities were determined by measuring the release of 4-nitrophenol (4NP) from 4-nitrophenol-β-glucopyranoside, 4-nitrophenol-β-galactopyranoside, 4-nitrophenol-β-xylopyranoside, and 4-nitrophenol-N-acetyl-β-glucosamine, respectively. Reactions were carried out in (4NPX) 10 mM 4NP-substrate in 50 mM citrate, pH 5.0 at 50˚C and were quenched with 2 volumes of 0.2 M Na_2CO_3. Absorbance at 400 nm was measured to quantify free 4NP, and 1 unit is defined as the amount of enzyme required to produce 1 µmol of free 4NP per minute under these conditions.

Protein extracts from WR fungi were also assayed for laccase and laccase + general peroxidase activity. Laccase and laccase + general peroxidase activities were measured by monitoring the oxidation of 2,2’-azino-bis 3-ethylbenzothiazoline-6-sulphonic acid (ABTS) at 420 nm (ε= 36000 $M^{-1}cm^{-1}$). Reactions were carried out in 5 mM ABTS for laccase and 5 mM ABTS, 1 mM H_2O_2, and 1 mM $MnCl_2$ for laccase +

general peroxidase. Both reactions were carried out at 20˚C in 50 mM citrate buffer pH 5.0, and one unit was defined as the amount of enzyme needed to oxidize 1 µmol of ABTS per minute under these conditions.

6.2.3 Mass Spectrometry

Purified protein extract from pools of 30 wafer sections from 0-5, 15-20, and 30-35 mm behind the advancing hyphal front for each fungus were used for LC-MS/MS-based proteomics. Extracts were TCA/acetone precipitated, pelleted, and reconstituted in saturated guanidine-HCl. The protein concentration of each cellular extract was determined by BCA assay (SMITH *et al.* 1985). For each sample, processing replicates were performed; 50 µg of protein was aliquoted to low-retention Eppendorf tubes for downstream sample processing. All samples were incubated for 30 minutes at 60 ºC with tris(2-carboxyethyl)phosphine (Bond-Breaker TCEP, Thermo Fisher Scientific, Rockford, IL) to reduce disulfide bonds. Alkylation of cysteine residues was performed by treatment with 50 mM iodoacetamide, which was added from a 500 mM iodoacetamide, 500 mM ammonium bicarbonate stock solution. After addition of iodoacetamide, all samples were incubated at room temperature in the dark for 40 min on a rocker. Each sample was then diluted to 0.9 M urea with 500 mM ammonium bicarbonate. To each 50 µg sample, 0.1 µg of mass spectrometry grade trypsin (Promega Corp., Madison, WI) was added and incubated overnight at 37 ºC. Peptides were extracted from each sample using solid phase extraction with Discovery C18 50 mg resin columns (Supelco, St. Louis, MO). Each column was activated with 2 ml of methanol followed by equilibration with 6 ml of 18 mΩ water. The sample was applied to the

column and then the column was washed with 8 ml of 50 mM ammonium bicarbonate. Peptides were eluted with two 0.9 ml washes of 40% acetonitrile. Samples were dried using a centrifugal concentrator (Thermo Scientific, Asheville, NC) and stored at -20 C until LC/MS analysis.

Peptides were solubilized in 150 µl solvent A (0.1% formic acid). For LC/MS analysis, 5 µl of sample was injected onto a Jupiter C18 resin reverse-phase column (3 µm particle size, 35 cm long, 75 µm inner diameter; Phenomenex, Torrance, CA). The peptides were eluted at 0.3 µl min-1 with an Agilent (Santa Clara, CA) 1200 high-performance liquid chromatograph with solutions of solvent A and 0.1% formic acid in acetonitrile (solvent B) using the following conditions: 0 to 30 min, isocratic at 100% solvent A; 30 to 32 min, linear gradient to 8% solvent B; 32 to 50 min, linear gradient to 12% solvent B; 50 to 105 min, linear gradient to 35% solvent B; 105 to 127 min, linear gradient to 60% solvent B; 127 to 130 min, linear gradient to 95% solvent B; and isocratic at 95% solvent B for 5 min. Eluted peptides were introduced into an Orbitrap XL mass spectrometer (Thermo Fisher, Waltham, MA) by electrospray ionization.

Spectra were collected in a data-dependent mode, with the five most intense ions in each survey scan selected for collisional induced dissociation in the five subsequent scans. Spectra were deconvoluted using the DeconMSn software (MAYAMPURATH *et al.* 2008) to more accurately assign parent ion mass and ion charge state, and then searched against predicted peptides derived from the fungal genome sequences via MS-GF+ (software used to analyze tandem mass spectra data, (KIM and PEVZNER 2014)), using a 20 ppm parent ion mass tolerance in searches of tryptic peptides with a variable post-

translational modification of oxidized methionine. A Q value cut off (≤0.01) was utilized to obtain a ~1% false discovery rate (FDR) at each individual data set level, as assessed from a decoy identification search utilizing the reverse fungal genome sequence.

6.2.4 Ergosterol analysis

Total ergosterol was measured as a biomarker for fungal biomass and was extracted from 5 mm sections taken along the advancing hyphal front of three separate aspen wafers for each fungus. Ergosterol was extracted using established methods (NEWELL *et al.* 1988) and measured by HPLC using a PhenomenexTM (Torrance, CA, USA) 4µ Hydro-RP 80a column by detection at 282 nm using previously described methods (SCHILLING and JELLISON 2005).

6.3 Results

6.3.1 Secretome composition along hyphal fronts

Secretome composition changed from undegraded to degraded wood sections in BR and WR fungi (Figure 6.1). All fungi showed an increase in the proportion of glycoside hydrolases (GHs) identified from 0-5 mm to 30-35 mm from the hyphal front, ranging from 5.0-23.3% at 0-5 mm to 15.5-31.7% at 30-35 mm. The total number of GH spectra observed at each timepoint supports this trend, with GHs at least doubling and at most increasing 447-fold from 0-5 to 30-35 mm from the hyphal front in all species (Table 6.1). GH families 3, 5, 10, 18, and 28 were found among all fungi, while GH 55 was unique to *P. placenta*, *G. trabeum* produced only GHs in common with other fungi, GH 45 was unique to *S. hirsutum*, and GH 30, 43, 53, and 131 were exclusively produced

in *T. versicolor* extracts. GH 16 was found exclusively in BR fungi in this study, while GH 6, 7, 72, and 92 were found exclusively in WR fungi. Each fungus produced one GH 28 pectinase (PP 111730, GT 120615, SH 125789, and TV 125789) exclusively at 0-5 mm behind the hyphal front (Tables S6.1-6.4). In addition, WR fungi produced two (SH 150302 and 130790) and one (TV 74031) GH 28 pectinases exclusively at 30-35 mm in *S. hirsutum* and *T. versicolor* extracts, respectively. In addition to GH 28 proteins, both *G. trabeum* and *T. versicolor* produced GH 35 β-galactosidases, the former also produced a CE 8 pectin methylesterase, and the latter also produced a GH 53 putative β-1,4-galactanase (Tables S6.2 and S6.4).

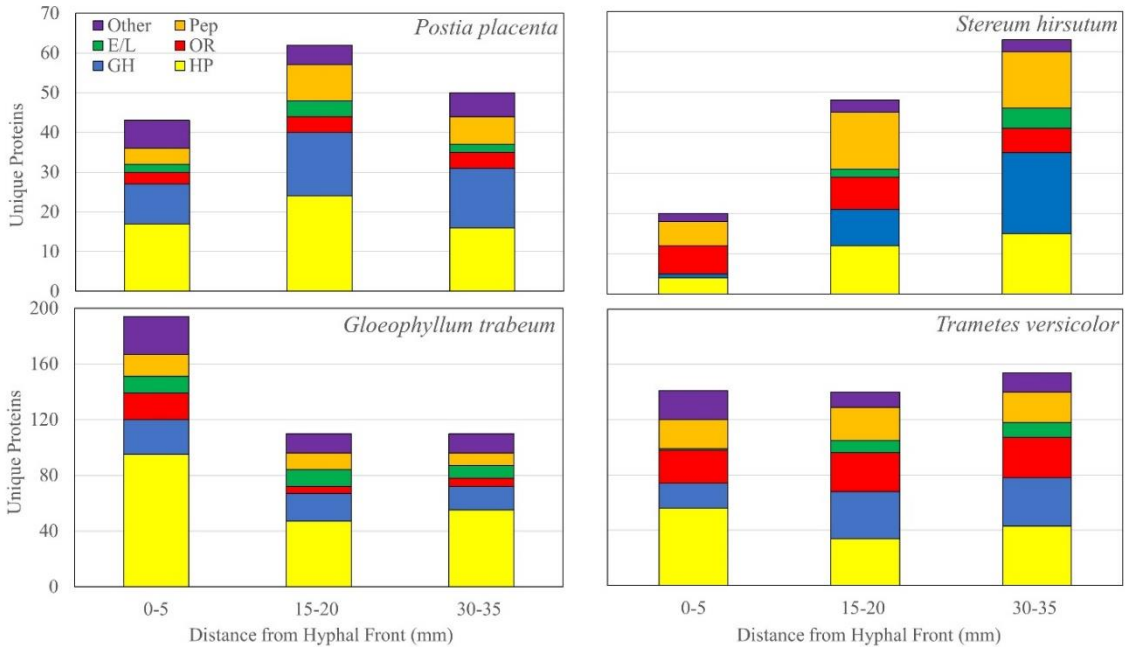

Figure 6.1: Total number of unique proteins identified in protein extracts of aspen wafer sections 0-5, 15-20, and 30-35 mm from the advancing hyphal front degraded by brown-rot (Postia placenta, Gloeophyllum trabeum) and white-rot (Stereum hirsutum, Trametes versicolor) fungi. HP, hypothetical protein, GH, glycoside hydrolase, OR, oxidoreductase, E/L, esterase lipase, Pep, peptidase.

Table 6.1: Total number of observations (proxy for abundance) of proteins in each of six categories from degraded aspen wafer section extracts taken 0-5, 15-20, and 30-35 mm behind the advancing hyphal front each fungus. Number of observations were quantified from equal portions of protein from each section type among samples from each fungus. GH, glycoside hydrolase, OR, oxidoreductase.

Category	Total number of observations											
	Postia placenta			*Gloeophyllum trabeum*			*Trametes versicolor*			*Stereum hirsutum*		
	0-5	15-20	30-35	0-5	15-20	30-35	0-5	15-20	30-35	0-5	15-20	30-35
Hypothetical	143	336	352	5566	1122	468	805	625	363	8	126	186
GH	194	329	485	502	1053	1070	279	820	848	1	30	447
OR	17	64	32	1006	100	9	995	511	365	55	302	168
Esterase/Lipase	156	270	316	220	482	303	1	63	55	0	86	136
Peptidase	20	28	16	403	374	198	875	2052	1226	28	240	323
Other	53	62	68	947	65	33	311	147	109	26	88	74

Esterases and lipases constituted a much smaller portion of the secretome of all fungi (0-10%), but were generally a greater proportion of early decay stage (0-5 mm) extracts in BR fungi (4.7-6.2%) as opposed to WR fungi (0-0.7%). These trends are supported by the total number of observations of esterases/lipases 0-5 mm behind the hyphal for BR (156-220) and WR fungi (0-1) (Table 6.1). All four fungi produced CE family 16 proteins, while CE 10 was only found in *P. placenta* extracts, CE 4 and 8 were

only found in G. trabeum extracts, and CE 12 was only found in *S. hirsutum* extracts (Tables S6.1-6.4). CE 1 and CE 15 were found in extracts from all fungi except for *P. placenta*.

Oxidoreductases (OR) constituted a larger proportion of WR protein extracts compared to BR fungi, constituting up to 35% and 20% of all identified proteins in *S. hirsutum* and *T. versicolor*, respectively, compared to 8.0% and 9.8% for *P. placenta* and *G. trabeum*, respectively (Figure 6.1). This difference is primarily driven by MnPs and laccases found in *S. hirsutum* and *T. versicolor* and to LiPs and DyPs in extracts of the latter (Table 6.2). Secreted oxidoreductases were found exclusively in 0-5 mm sections of *P. placenta* (Pp 130360) and *G. trabeum* (Gt 95549 and 130320) extracts (Tables S6.5 and S6.6), but their functions are not known.

Table 6.2: Laccases and peroxidases found in aspen wafer extracts and the number of observations found in protein extracts 0-5, 15-20, and 30-35 mm behind the advancing hyphal fronts of white-rot fungi. Number of observations were quantified from equal portions of protein from each section type among samples from each fungus. MnP, manganese peroxidase, LiP lignin peroxidase, DyP, dye decolorizing peroxidase.

	Trametes versicolor					*Stereum hirsutum*			
		Observations[3]					Observations[3]		
Protein ID[1]	Name[2]	0-5	15-20	30-35	Protein ID[1]	Name[2]	0-5	15-20	30-35
51375	MnP 1, short	53	1	1	134504	MnP, atypical	4	62	13
112835	MnP 2, short	2	5	4	134527	MnP, atypical	0	25	1
131080	MnP 3, short	11	0	0	142136	MnP, atypical	3	2	0

130496	MnP 4, short	211	38	30	161701	MnP, atypical	0	8	0
43477	MnP 5, short	0	3	0	171838	MnP, atypical	28	51	0
51455	MnP 6, short	53	10	5	129431	Laccase 5	1	3	0
51457	MnP 9, short	0	0	0	86228	Laccase 6	1	0	0
43576	LiP 1	8	42	41	135975	Laccase 13	1	0	0
43578	LiP 2	6	34	66					
52333	LiP 6	0	0	0					
134226	LiP 9	12	69	34					
114944	LiP 12	0	0	0					
146232	Laccase 2	41	0	0					
138261	Laccase 3	62	27	14					
115295	Laccase 4	16	0	0					
48870	DyP 1	174	57	33					
48874	DyP 2	109	4	7					

[1]Protein ID numbers shown are from the DOE JGI Mycocosm database (GRIGORIEV *et al.* 2014).

[2]Putative functions were determined by BLAST searches of the SWISS PROT database (BATEMAN *et al.* 2015).

[3]Spectral counts for proteins found in wafer sections 0-5, 15-20, and 30-35 mm from the hyphal front.

6.3.2 Enzyme activities

Specific activity of plant polysaccharide-degrading enzymes showed no consistent pattern along the advancing hyphal front among all fungi. BR fungi produced equal or greater CAZyme specific activities compared to WR fungi (Figures 6.2 and 6.3), despite secreting a reduced suite of GHs (Tables S6.1-6.4). Endoglucanase specific activity increased significantly ($p<0.05$, Tukey's HSD) from 0-5 mm to 30-35 mm only in *P.*

placenta, with the same pattern holding for xylanase specific activity in *G. trabeum* and *S. hirsutum* (Figure 6.2). *P. placenta* xylanase specific activity increased above controls only 5-20 mm behind the hyphal front, then declined. *P. placenta* was also the only fungus to express mannanase specific activity above control levels in all sections ($p<0.05$, Tukey's HSD) (Figure 6.2), probably because of the high abundance of GH 5 proteins in its secretome, which constituted 29-31% of all GH observations (Table S6.1). Pectinase specific activity tended to be highest near the hyphal front (0-5 mm and 5-10 mm), although levels in WR fungi also reached similar levels in more degraded wood (30-35 mm) (Figure 6.2).

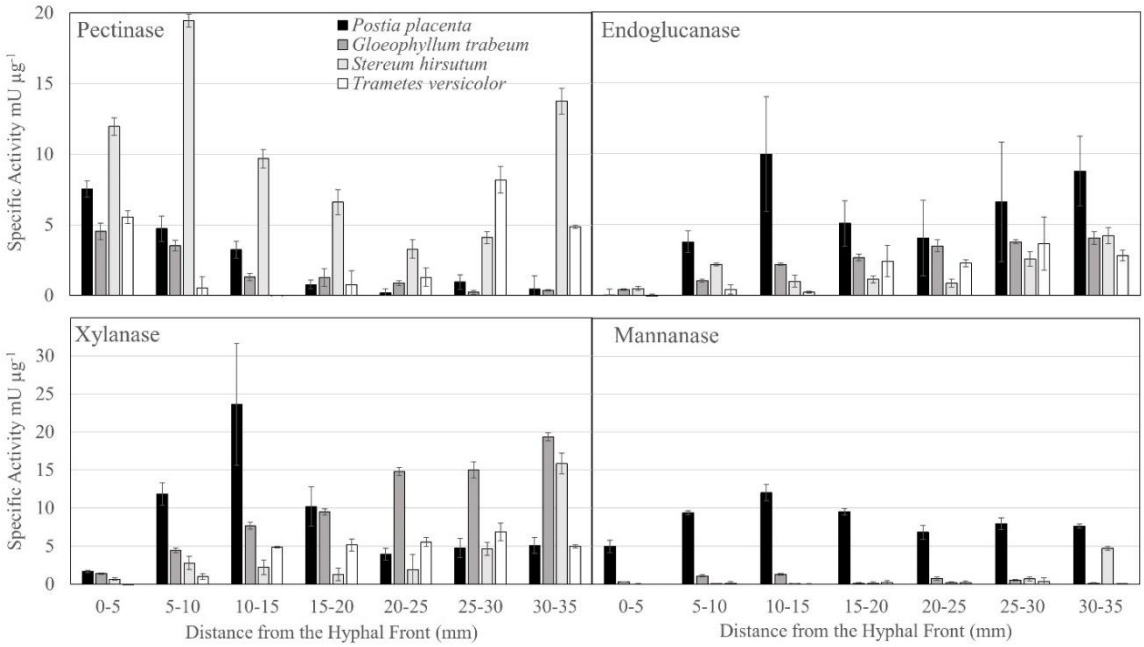

Figure 6.2: Polysaccharide-degrading enzyme activities from aspen wafer section extracts along the advancing hyphal fronts of white-rot and brown-rot fungi. Error bars are standard deviations of three assays of one extract of a pool of 12 separate wafers.

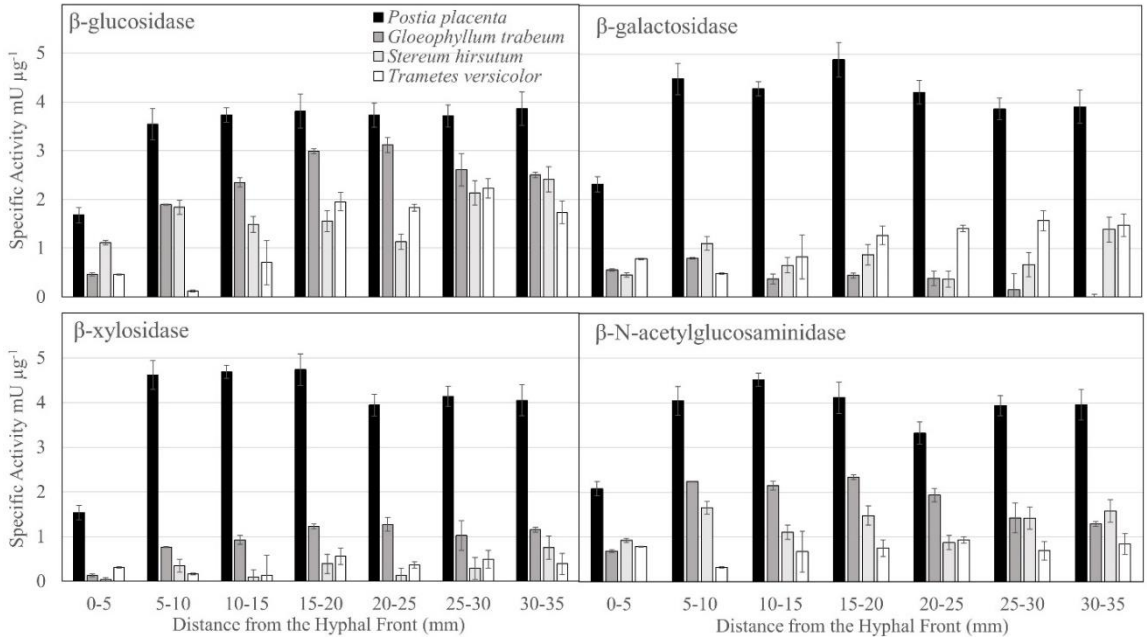

Figure 6.3: Oligo- and di-saccharide degrading enzyme specific activity from aspen wafer section extracts along the advancing hyphal fronts of white and brown-rot fungi. Error bars are standard deviations of three assays of one extract of a pool of 12 separate wafers.

Among oligo- and disaccharide-degrading (BGL, BGA, BXL, and BNG) specific activities, BGA in *G. trabeum* was the only one highest near the hyphal front, concurrent with the production of a GH 35 exclusively at the hyphal front (Figure 6.3, Table S6.2). BXL and BNG specific activity for *T. versicolor* were the only activities that remained constant among all sections ($p>0.05$, Tukey's HSD) (Figure 6.3). Increases in specific activity from undegraded to degraded sections were seen for all four activities in *P.*

placenta, for BGL, BXL, and BNG in *G. trabeum*, for all four activities in *S. hirsutum*, and for BGL and BGA in *T. versicolor*. Consistent with these trends, both WR fungi produced a putative GH 3 β-glucosidase exclusively after the earliest decay stage (Tables S6.3 and S6.4). Despite producing the highest oligo- and disaccharide-degrading enzyme activities, *P. placenta* only produced one GH 3 in all extracts, but this protein constituted 38-49% of all GH observations in *P. placenta* extracts (Table S6.1), suggesting high abundance.

The most dramatic difference between BR and WR secretome activity, was among ORs. Laccase and general peroxidase activity were only measurable in extracts from WR fungi. Laccase specific activity was above controls only near the hyphal front in *S. hirsutum* extracts, but remained flat throughout decay, ranging from 0.17-0.01 mU µg-1 (Figure 6.5). *T. versicolor* on the other hand, produced 7-11 times greater laccase activity than *S. hirsutum* 0-10 mm behind the hyphal front (1.17-1.69 mU µg-1), before dropping to levels not distinguishable from controls in all other sections (0.14-0.06 mU µg-1) (Figure 6.4). H_2O_2 and Mn^{2+} were added to laccase assays to determine the additive effect of peroxidases present in the secretome. Their addition drastically increased (3- to 65-fold) ABTS oxidation in samples taken 5-30 mm behind the *S. hirsutum* hyphal front. In *T. versicolor* extracts, the difference in activity due to peroxide was less pronounced, and increases (15-fold) were only seen at 10-15 mm (Figure 6.4).

6.3.3 Growth rates and ergosterol analysis

Fungal growth rates were comparable for *P. placenta*, *G. trabeum*, and *S. hirsutum*, advancing up the wafers at 2.7, 3.2, and 2.7 mm day-1, respectively, whereas *T.*

versicolor grew notably faster at 5.3 mm day-1. Each 5-mm wafer section is equivalent to 2 days of growth for *P. placenta* and *S. hirsutum*, 1.5 days for *G. trabeum*, and about 1 day for *T. versicolor*. Relatively slow growth by *P. placenta* and *S. hirsutum* did not result in increased ergosterol levels or protein secretion due to increased residence time at each 5-mm section (Figure S6.1).

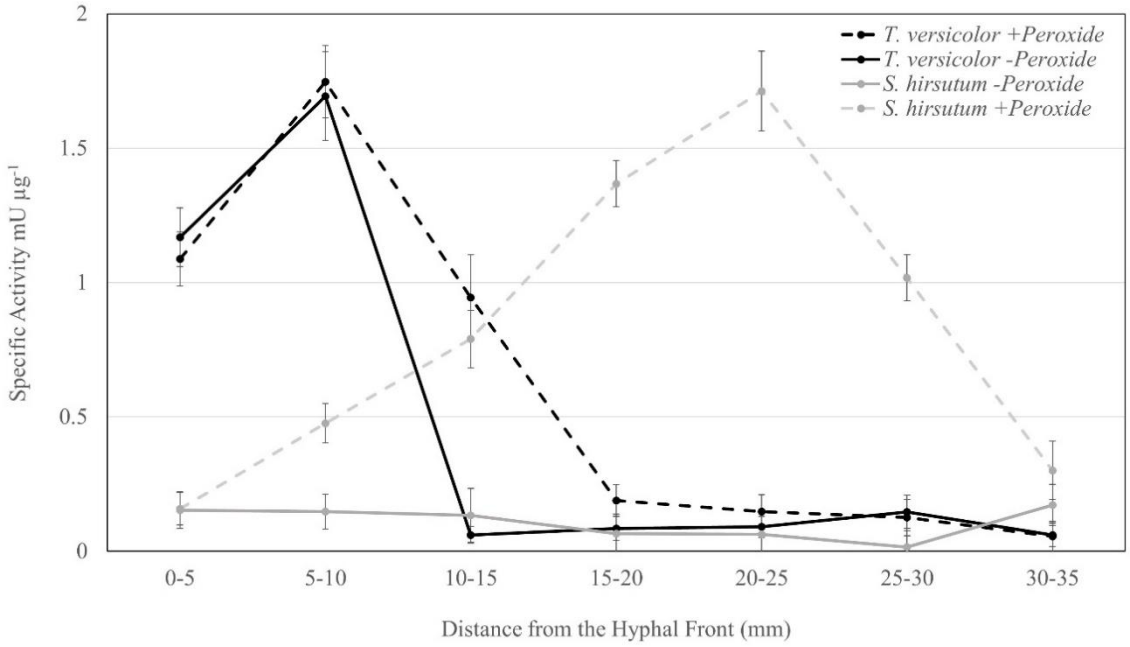

Figure 6.4: Laccase activity from aspen wafer extracts of sections taken along the advancing hyphal front of aspen wafers degraded by *Trametes versicolor* (black) and *Stereum hirsutum* (grey). Activities were measured with (dashed lines) and without (solid lines) the addition of hydrogen peroxide and Mn^{2+} to determine the addition ABTS-oxidase activity of peroxidases in the extracts.

6.4 Discussion

This study reveals secretome changes on a scale of 1-2 days, comparable or higher resolution than previous studies of secretome dynamics in wood decay fungi (HORI *et al.* 2014; ZHU *et al.* 2016). Early pectin metabolism (Figure 6.2) and GH 28 secretion (Tables S6.1-6.4), persisted across all rot types and species in this study despite the low (<2%) pectin content of aspen wood (WILLFOR *et al.* 2009). This supports prior observations in our group of high pectinase expression seen in early decay stages by *Postia placenta* (ZHANG *et al.* 2016), and this pattern suggests early stage pectinolysis may be necessary to convert wood lignocellulose enzymatically without harsh pretreatments. Consistent with previous studies (HORI *et al.* 2014; KUUSKERI *et al.* 2016; ZHANG *et al.* 2016; PRESLEY and SCHILLING 2017), increases in non-pectinolytic GH abundance (Figure 6.1, Table 6.1) and most CAZyme specific activities (Figures 6.2 and 6.3) increased as wood became more degraded. Our work suggests this sequence is universal among WR and BR fungi, and is likely a necessary "pretreatment" due to pectin's close association with hemicellulose and cellulose in the plant cell wall (DICK-PEREZ *et al.* 2011), where its removal allows GHs to access cell wall polysaccharides (XIAO and ANDERSON 2013). The early dissolution of pectin-rich pit membranes (CHOAT *et al.* 2008) may also contribute to this pattern as pits are an avenue of early wood colonization by decay fungi (BLANCHETTE 1995). However, later decay stages of WR decay also show heightened pectinase activity and GH 28 secretion, which may result from the dissolution of the lignin and pectin-rich middle lamellae seen in some types of WR (BLANCHETTE 1991).

It is well established that WR fungi secrete a more diverse suite of GHs than BR fungi (FLOUDAS *et al.* 2012; RILEY *et al.* 2014). However, the presence of a more diverse hemicellulose and cellulose-degrading arsenal in WR fungi (LAFOND *et al.* 2012) does not appear to drive increases in endoglucanase and hemicellulase specific activity compared to BR fungi (Figure 6.2 and 6.3), and the difference must be driven by abundance or enzyme turnover. Protein quantitation using spectral counting indicates that the most abundant glycoside hydrolases in WR fungi were GH 6 and 7 proteins, averaging 44% and 20% of all GH observations in the middle (15-20 mm) and late stages (30-35 mm) of decay, respectively (Tables S6.3 and S6.4). BR fungi produced greater amounts of GH 3 and 5 proteins, with these averaging 27% and 18% of all mid-late stage GH observations, respectively, compared to 1% and 3% in WR fungi, respectively. Indeed, BR fungi may compensate for losses in GH diversity by secreting their remaining GH suite in greater abundance than their WR counterparts. *G. trabeum* was a particularly heavy producer of GH 10 xylanases, and this family of enzymes constituted just over 51% of all GH observations by the latest decay stage (Table S6.2). This pattern is supported by the high xylanase activity in *G. trabeum* (Figure 6.2) extracts and suggests that different brown-rot species may have different carbohydrate preferences, possibly leading to chemical variability in the decay substrate among species.

In addition to losses of several GH families, BR fungi are also known to lack lignin-degrading peroxidases (FLOUDAS *et al.* 2012) and phenol oxidase (laccase) activity (JORGENSEN and VEJLBY 1953). However, an uncharacterized cupredoxin domain-containing protein secreted by *P. placenta* (Pp 130360) and two FAD-binding domain-

containing proteins secreted by *G. trabeum* (Gt 95549 and 130320) (Data S6.5 and S6.6) early during decay may participate in an oxidative "pretreatment" phase of the BR decay mechanism (KEREM *et al.* 1999). These BR ORs bear little homology to any functionally characterized proteins and merit further investigation.

WR fungi are unified as a group by the presence of lignin degrading enzymes including laccases and peroxidases, but this study identifies some of the mechanistic diversity among WR species. Lignin degrading OR activity in WR fungi followed different patterns in *S. hirsutum* and *T. versicolor*. Early secretion of ORs is known from other WR fungi (HORI *et al.* 2014; KUUSKERI *et al.* 2016), but the types of peroxidases produced by the two WR fungi in this study differed. The only peroxidase secreted by *S. hirsutum* were 5 atypical MnPs, the only type in its genome (FLOUDAS *et al.* 2012), while *T. versicolor* secreted 5 LiPs, 6 short MnPs (RUIZ-DUENAS *et al.* 2013), and 2 DyPs (LIERS *et al.* 2010). Despite this disparity, H_2O_2-dependent ABTS oxidase activity in *S. hirsutum* extracts was greater and produced over a larger timespan (5-30 mm) (Figure 6.4), supporting the functionality of atypical MnPs (HILDEN *et al.* 2014), and suggesting that they may be more effective than *T. versicolor* MnPs. Variation in oxidoreductases between *S. hirsutum* and *T. versicolor* could be one of the determinants of their ecological signatures. Both fungi are early secondary wood colonizers (CHAPELA and BODDY 1988; BODDY and HISCOX 2016), but pre-colonization of beech wood with either fungus produces disparate fungal successional patterns (HISCOX *et al.* 2015a). This effect has been attributed to the production of biocidal secondary metabolites by *S. hirsutum*

(HEILMANN-CLAUSEN and BODDY 2005), but in light of this study, variations in decay mechanism and decay residue chemistry may also determine successor communities.

Overall, this study shows that the temporal changes in cultural characteristics and secretome composition during aspen wood decay are shared among BR and WR fungi. Early wood degradation likely requires hydrolysis of pectin, a barrier to access structural polysaccharides. Aside from pectinases, most plant-degrading GHs become more prominent as wood is more thoroughly degraded. Several ORs of BR fungi present in rotting wood remain uncharacterized while WR oxidoreductases such as laccase and MnP are most active in early and intermediate decay stages, respectively. This work highlights some of the differences in the physiology of WR and BR fungi as well as interspecific variations in decay mechanisms, which may drive niche specialization and the ecological signatures of each species. We have also identified the importance of pectinolysis in early biological wood pretreatment and pectin removal may be an important initiation step to facilitate fully enzymatic conversion of lignocellulose.

6.5 Supplemental Information

Table S6.1: Carbohydrate esterase (CE) and glycoside hydrolase (GH) families identified in aspen wafer sections degraded by *Postia placenta* taken from 0-5, 15-20, 30-35 mm from the advancing hyphal front.

Protein ID[1]	CE/GH[2]	Putative Function[3]	Signal P[4]	Observations[5]		
				0-5	15-20	30-35
20448	CE 10	Lipase	No	6	7	0
125801	CE 16	Acetylesterase	Yes	14	17	12
108959	CE 16	Acetylesterase	Yes	0	2	0
106710	CE 16	Unknown	No	0	2	0
107557	GH 3	β-glucosidase	No	69	124	132
103675	GH 5	Endo-β-1,4-glucanase	Yes	13	16	27
95568	GH 5	Endo-β-1,4-mannosidase	Yes	0	5	0
115648	GH 5	Endo-β-1,4-glucanase	Yes	15	48	46
121831	GH 5	Endo-β-1,4-mannanase	No	16	24	32
113670	GH 10	Endo-β-1,4-xylanase	Yes	3	1	0
112658	GH 12	Endo-β-1,4-glucanase	Yes	0	0	2
113112	GH 15	Glucoamylase	Yes	0	0	1
54949	GH 16	β-glucan synthesis	No	0	1	0
112941	GH 16	Endo-β-1,3(4)-glucanase	Yes	0	6	4
116903	GH 16	Endo-β-1,3(4)-glucanase	Yes	0	3	0
44128	GH 18	Chitinase	No	0	0	1
128150	GH 27	α-galactosidase	Yes	9	67	53
111730	GH 28	Pectinase	Yes	13	0	0
115593	GH 47	α-1,2-mannosidase	Yes	0	4	2
100251	GH 51	α-arabinofuranosidase	No	2	1	14
105490	GH 55	Endo-β-1,3-glucanase	Yes	0	7	6
108648	GH 55	Exo-β-1,3-glucanase	Yes	1	6	3
119394	GH 55	Exo-β-1,3-glucanase	Yes	0	5	5
111332	GH 79	β-glucuronidase	No	0	5	18

[1]Protein ID numbers from the DOE JGI Mycocosm database (GRIGORIEV *et al.* 2014).

[2]Carbohydrate esterase and glycoside hydrolase families as defined in the CAZy database (LOMBARD *et al.* 2014).

[3]Putative functions determined by BLAST searches of SWISS PROT database (BATEMAN *et al.* 2015).

[4]Secretion signals for detected protein sequences were detected using Signal P algorithm (PETERSEN *et al.* 2011).

[5]Unique peptide counts for proteins found in wafer sections 0-5, 15-20, and 30-35 mm from the hyphal front.

Table S6.2: Carbohydrate esterase (CE) and glycoside hydrolase (GH) families identified in aspen wafer sections degraded by *Gloeophyllum trabeum* taken from 0-5, 15-20, 30-35 mm from the advancing hyphal front.

Protein ID[1]	GH/CE[2]	Putative Function[3]	Signal P[4]	Observations[5]		
				0-5	15-20	30-35
117128	CE 1	Acetyl xylan esterase	Yes	0	16	16
32318	CE 4	Chitin deacetylase	Yes	5	0	0
112531	CE 8	Pectinesterase	Yes	10	1	0
46545	CE 15	4-O-methyl-glucuronyl methylesterase	Yes	17	195	150
48624	CE 16	Acetylesterase	Yes	20	42	5
56205	CE 16	Acetylesterase	Yes	9	16	0
115191	GH 2	β-mannanase	Yes	26	19	5
69843	GH 3	β-glucosidase	Yes	55	128	55
75899	GH 3	β-glucosidase	No	9	0	0
122002	GH 3	Exo-β-1,4-xylosidase	Yes	75	94	46
114574	GH 5	Endo-β-1,4-mannanase	Yes	2	8	0
110405	GH 5	Endo-β-1,4-mannanase	Yes	4	18	0
135369	GH 5	Endo-β-1,4-mannanase	Yes	0	6	0
63180	GH 5	Endo-β-1,4-glucanase	Yes	14	64	35
140289	GH 10	Endo-β-1,4-xylanase	Yes	0	1	3
46499	GH 10	Endo-β-1,4-xylanase	No	81	359	545
138821	GH 12	Xyloglucan specific endo-β-1,4-glucanase	Yes	6	175	328

61700	GH 15	Glucoamylase, CBM20	Yes	1	0	0
52752	GH 16	β-glucan synthesis	No	2	0	0
122074	GH 18	Chitinase	Yes	0	5	0
116582	GH 20	β-N-acetylglucosaminidase	Yes	28	13	0
77583	GH 20	β-N-acetylglucosaminidase	Yes	14	0	0
117566	GH 27	α-galactosidase	Yes	14	14	1
110574	GH 28	Pectinase	Yes	22	17	2
120615	GH 28	Pectinase	Yes	23	0	0
138836	GH 28	Pectinase	Yes	0	0	1
6650	GH 28	Pectinase	No	8	0	0
141329	GH 31	α-xylosidase	Yes	2	0	0
111095	GH 35	β-galactosidase	Yes	12	0	0
112205	GH 47	Mannosyl oligosaccharide α-1,2-mannosidase	Yes	7	0	0
121307	GH 115	Unknown	Yes	4	1	2
121308	GH 115	Unknown	Yes	55	90	42

[1]Protein ID numbers from the DOE JGI Mycocosm database (GRIGORIEV *et al.* 2014).

[2]Carbohydrate esterase and glycoside hydrolase families as defined in the CAZy database (LOMBARD *et al.* 2014).

[3]Putative functions determined by BLAST searches of SWISS PROT database (BATEMAN *et al.* 2015).

[4]Secretion signals for detected protein sequences were detected using Signal P algorithm (PETERSEN *et al.* 2011).

[5]Unique peptide counts for proteins found in wafer sections 0-5, 15-20, and 30-35 mm from the hyphal front.

Table S6.3: Carbohydrate esterase (CE) and glycoside hydrolase (GH) families identified in aspen wafer sections degraded by *Stereum hirsutum* taken from 0-5, 15-20, 30-35 mm from the advancing hyphal front.

Protein ID[1]	GH/CE[2]	Putative Function[3]	Signal P[4]	Observations[5]		
				0-5	15-20	30-35
127673	CE 1	Acetyl xylan esterase, CBM 1	Yes	0	0	4
172051	CE 12	Rhamnogalacturonan acetyl esterase	Yes	0	0	3
96554	CE 15	Glucuronyl esterase, CBM 1	Yes	0	0	14
104030	CE 16	Acetylesterase	Yes	0	0	1
161774	CE 16	Acetylesterase	Yes	0	1	0
144289	GH 3	β-glucosidase	Yes	0	0	2
65746	GH 5	Endo-β-1,4-glucanase	Yes	0	2	8
136401	GH 5	Endo-β-1,4-glucanase/acyl-activating enzyme, CBM 1	Yes	0	0	6
165557	GH 5	Endo-β-1,4-glucanase, CBM 1	Yes	0	0	2
92249	GH 6	Cellobiohydrolase, CBM 1	Yes	0	16	197
62237	GH 7	Cellobiohydrolase	Yes	0	4	123
159684	GH 10	Endo-β-1,4-xylanase	Yes	0	1	0
49403	GH 10	Endo-β-1,4-xylanase, CBM1	Yes	0	0	5
91607	GH 10	Endo-β-1,4-xylanase, CBM 1	Yes	0	0	6
58599	GH 15	Glucoamylase, CBM 20	Yes	0	0	8
123978	GH 15	Glucoamylase, CBM 20	Yes	0	0	2
49482	GH 18	Unknown, CBM 5	Yes	0	0	2
159752	GH 18	Unknown, CBM 5	Yes	0	1	0
61806	GH 18	Unknown, CBM 5	No	0	0	3
91437	GH 18	Chitinase, CBM 5	Yes	0	0	3
98572	GH 20	β-hexosaminidase	Yes	0	0	0
125789	GH 28	Endopolygalacturonase	Yes	1	0	0
150302	GH 28	Exopolygalacturonase	Yes	0	1	2
130790	GH 28	Polygalacturonase	Yes	0	0	67
97697	GH 45	Unknown	Yes	0	0	1
82112	GH 72	β-1,3-glucanosyl transferase, CBM 43	Yes	0	1	6

117496	GH 72	β-1,3-glucanosyl transferase, CBM 43	Yes	0	0	1
112437	GH 75	Endo-chitosanase	Yes	0	2	0
128057	GH 79	β-glucuronidase	Yes	0	2	2
77852	GH 92	Unknown	Yes	0	0	1

[1]Protein ID numbers from the DOE JGI Mycocosm database (GRIGORIEV *et al.* 2014).

[2]Carbohydrate esterase and glycoside hydrolase families as defined in the CAZy database (LOMBARD *et al.* 2014).

[3]Putative functions determined by BLAST searches of SWISS PROT database (BATEMAN *et al.* 2015).

[4]Secretion signals for detected protein sequences were detected using Signal P algorithm (PETERSEN *et al.* 2011).

[5]Unique peptide counts for proteins found in wafer sections 0-5, 15-20, and 30-35 mm from the hyphal front.

Table S6.4: Carbohydrate esterase (CE) and glycoside hydrolase (GH) families identified in aspen wafer sections degraded by *Trametes versicolor* taken from 0-5, 15-20, 30-35 mm from the advancing hyphal front.

				Observations[5]		
Protein ID[1]	GH/CE[2]	Putative Function[3]	Signal P[4]	0-5	15-20	30-35
141077	CE 1	Acetyl xylan esterase, CBM 1	Yes	0	1	0
112899	CE 15	Glucuronyl esterase	No	0	2	10
70662	CE 16	Acetylesterase	Yes	0	0	1
168624	CE 16	Acetylesterase	Yes	0	8	4
39742	CE 16	Acetylesterase, CBM 1	Yes	0	7	6
61724	GH 2	β-mannosidase	Yes	0	0	2
67879	GH 3	Exo-β-1,4-xylosidase	Yes	14	11	3

132011	GH 3	Exo-β-1,4-xylosidase	Yes	10	7	6
127171	GH 3	β-glucosidase	No	0	3	1
151588	GH 3	β-glucosidase	No	0	1	0
68557	GH 3	β-glucosidase, CBM 1	Yes	0	1	2
33056	GH 5	Endo-β-1,4-glucanase, CBM 1	No	0	5	14
151848	GH 5	Endo-β-1,4-glucanase, CBM 1	Yes	0	3	0
150608	GH 5	Endo-β-1,4-glucanase, CBM 1	Yes	0	1	2
63826	GH 6	Cellobiohydrolase	Yes	10	306	334
110790	GH 7	Cellobiohydrolase	Yes	0	1	0
112163	GH 7	Cellobiohydrolase	Yes	4	103	225
124366	GH 7	Cellobiohydrolase	Yes	0	8	4
125941	GH 7	Cellobiohydrolase	Yes	2	128	80
33948	GH 10	Endo-β-1,4-xylanase	Yes	0	21	0
38102	GH 10	Endo-β-1,4-xylanase, CBM 1	Yes	0	6	8
136117	GH 12	Endo-β-1,4-glucanase	Yes	0	22	23
50178	GH 12	Xyloglucan-specific endo-β-1,4-glucanase	Yes	8	0	0
18215	GH 18	Chitinase	No	0	3	0
158931	GH 18	Chitinase, CBM 5	Yes	0	1	0
135976	GH 20	β-hexosaminidase	Yes	20	16	4
175547	GH 20	β-hexosaminidase	Yes	3	2	2
60477	GH 27	α-galactosidase	Yes	0	1	0
74031	GH 28	Endopolygalacturonase	Yes	0	0	1
62650	GH 28	Rhamnogalacturonase	Yes	0	1	0
52416	GH 28	Pectinase	Yes	45	41	47
171861	GH 28	Pectinase	Yes	89	0	0
66957	GH 30	Unknown	Yes	0	5	7
58033	GH 31	α/β-glucosidase	Yes	2	0	0
37024	GH 35	β-galactosidase	Yes	0	7	13
58222	GH 43	Endo-α-1,5-L-arabinofuranosidase	Yes	4	0	0
145953	GH 43	Unknown, CBM 35	Yes	0	6	7
131501	GH 47	Mannosyl oligosaccharide α-1,2-mannosidase	Yes	7	2	4
59914	GH 51	α-L-arabinofuranosidase	Yes	14	11	3

143650	GH 53	Endo-β-1,4-galactanase	Yes	0	0	0
68341	GH 72	β-1,3-glucanosyltransferase, CBM 43	Yes	0	0	0
26555	GH 79	β-glucuronidase	Yes	2	2	0
40820	GH 92	Unknown	Yes	0	0	1
43566	GH 92	Unknown	Yes	12	24	20
75494	GH 92	Unknown	Yes	23	2	0
49304	GH 115	Unknown	Yes	10	66	28
175614	GH 131	Unknown	Yes	0	1	3
46975	GH 131	Unknown, CBM 1	Yes	0	2	4

[1]Protein ID numbers from the DOE JGI Mycocosm database (GRIGORIEV *et al.* 2014).

[2]Carbohydrate esterase and Glycoside hydrolase families as defined in the CAZy database (LOMBARD *et al.* 2014).

[3]Putative functions determined by BLAST searches of SWISS PROT database (BATEMAN *et al.* 2015).

[4]Secretion signals for detected protein sequences were detected using Signal P algorithm (PETERSEN *et al.* 2011).

[5]Unique peptide counts for proteins found in wafer sections 0-5, 15-20, and 30-35 mm from the hyphal front.

Table S6.5: Putative oxidoreductases identified in aspen wafer sections degraded by *Postia placenta* taken from 0-5, 15-20, 30-35 mm from the advancing hyphal front.

				Observations[4]		
Protein ID[1]	OR Description	Putative Function[2]	Signal P[3]	0-5	15-20	30-35
130360	Oxidoreductase	Unknown	Yes	1	0	0
127365	NADH-cytochrome b5 reductase	NADH-cytochrome b5 reductase	No	15	57	25

130375	NADH-cytochrome b5 reductase	NADH-cytochrome b5 reductase	No	0	5	6
108489	GMC oxidoreductase	Choline dehydrogenase	Yes	0	1	0
129494	Cytochrome p450	Cytochrome p450	No	0	0	0
116836	Thioredoxin	Thioredoxin	No	1	1	0
49651	Cytochrome p450	Cytochrome p450	No	0	0	1

[1]Protein ID numbers from the DOE JGI Mycocosm database (GRIGORIEV *et al.* 2014).

[2]Carbohydrate esterase and Glycoside hydrolase families as defined in the CAZy database (LOMBARD *et al.* 2014).

[3]Putative functions determined by BLAST searches of SWISS PROT database (BATEMAN *et al.* 2015).

[4]Secretion signals for detected protein sequences were detected using Signal P algorithm (PETERSEN *et al.* 2011).

[5]Unique peptide counts for proteins found in wafer sections 0-5, 15-20, and 30-35 mm from the hyphal front.

Table S6.6: Putative oxidoreductases identified in aspen wafer sections degraded by *Gloeophyllum trabeum* taken from 0-5, 15-20, 30-35 mm from the advancing hyphal front.

Protein ID[1]	OR Description	Putative Function[2]	Signal P[3]	Observations[4] 0-5	15-20	30-35
135963	Cytochrome b5-like	Cytochrome b5	No	10	0	0
141118	Cytochrome p450	Cytochrome P450 monooxygenase	No	0	1	0

139255	Cytochrome p450 reductase	Cytochrome p450 reductase	No	0	1	0
113068	Aldo/keto reductase	NAD(P)H-xylose reductase	No	9	0	0
75656	Aldo/keto reductase	Glycerol 2 dehydrogenase	No	0	0	0
75987	Aldo/keto reductase	Glycerol 2 dehydrogenase	No	7	0	0
111441	Aldo/keto reductase	Unknown	No	14	0	0
78681	α-aminoadipate reductase	α-aminoadipate reductase	No	1	0	0
80932	Nitrate reductase	Nitrate reductase	No	0	0	1
140776	Oxidoreductase	Unknown	No	4	0	0
95549	FAD binding oxidoreductase	Solanopyrone synthase	Yes	10	0	0
130320	FAD-binding oxidoreductase	Unknown	Yes	9	0	0
107788	FMN-binding oxidoreductase	NADPH oxidase	No	0	0	0
46992	Glutathione peroxidase	Glutathione peroxidase	No	26	0	0
65654	Glyoxal oxidase	Glyoxal oxidase	Yes	2	0	0
74773	GMC oxidoreductase	Choline dehydrogenase	Yes	6	0	0
116849	Nitrate reductase	Nitrate reductase	No	1	1	0
65680	Thioredoxin reductase	Thioredoxin reductase	No	45	0	0
109378	FAD-dependent oxidoreductase	FAD-dependent monooxygenase	No	1	0	0
110868	FAD-dependent oxidoreductase	FAD-linked sulfhydryl oxidase	No	1	0	0
82473	GMC oxidoreductase	Pyranose dehydrogenase	Yes	1	0	0
82515	FAD-containing polyamine oxidase	Polyamine oxidase	Yes	5	6	0

134939	Thioredoxin	Thioredoxin	No	838	91	8
62178	Thioredoxin reductase	Thioredoxin reductase	No	16	0	0

[1]Protein ID numbers from the DOE JGI Mycocosm database (GRIGORIEV *et al.* 2014).

[2]Carbohydrate esterase and Glycoside hydrolase families as defined in the CAZy database (LOMBARD *et al.* 2014).

[3]Putative functions determined by BLAST searches of SWISS PROT database (BATEMAN *et al.* 2015).

[4]Secretion signals for detected protein sequences were detected using Signal P algorithm (PETERSEN *et al.* 2011).

[5]Unique peptide counts for proteins found in wafer sections 0-5, 15-20, and 30-35 mm from the hyphal front.

Table S6.7: Putative oxidoreductases identified in aspen wafer sections degraded by *Stereum hirsutum* taken from 0-5, 15-20, 30-35 mm from the advancing hyphal front.

Protein ID[1]	OR Description	Putative Function[2]	Signal P[3]	Observations[4]		
				0-5	15-20	30-35
74329	Cellobiose dehydrogenase	Cellobiose dehydrogenase	Yes	0	0	3
76915	CRO	Glyoxal oxidase	Yes	17	146	128
135975	Laccase, SHlcc13	Laccase	Yes	1	0	0
129431	Laccase, SHlcc5	Laccase-4	Yes	1	3	0
86228	Laccase, SHlcc6	Laccase	Yes	1	0	0
99490	LPMO	LPMO	Yes	0	0	2
121343	LPMO, CBM 1	LPMO	Yes	0	5	21
134504	MnP, short	Versatile peroxidase	Yes	4	62	13
134527	MnP, short	Versatile peroxidase	Yes	0	25	1

142136	MnP, short	Versatile peroxidase	Yes	3	2	0
161701	MnP, short	Versatile peroxidase	Yes	0	8	0
171838	MnP, short	Versatile peroxidase	Yes	28	51	0

[1]Protein ID numbers from the DOE JGI Mycocosm database (GRIGORIEV *et al.* 2014).

[2]Carbohydrate esterase and Glycoside hydrolase families as defined in the CAZy database (LOMBARD *et al.* 2014).

[3]Putative functions determined by BLAST searches of SWISS PROT database (BATEMAN *et al.* 2015).

[4]Secretion signals for detected protein sequences were detected using Signal P algorithm (PETERSEN *et al.* 2011).

[5]Unique peptide counts for proteins found in wafer sections 0-5, 15-20, and 30-35 mm from the hyphal front.

Table S6.8: Putative oxidoreductases identified in aspen wafer sections degraded by *Trametes versicolor* taken from 0-5, 15-20, 30-35 mm from the advancing hyphal front.

Protein ID[1]	OR Description	Putative Function[2]	Signal P[3]	Observations[4] 0-5	15-20	30-35
45408	Cellobiose dehydrogenase	Cellobiose dehydrogenase, CBM 1	Yes	0	3	10
61229	CRO	Aldehyde oxidase	No	0	1	1
115556	CRO	Glyoxal oxidase	Yes	0	13	2
116129	CRO	Glyoxal oxidase	Yes	2	9	1
117805	CRO	Glyoxal oxidase	Yes	5	60	30
118266	CRO	Glyoxal oxidase	Yes	8	27	13
136392	CRO	Glyoxal oxidase	Yes	0	33	7
130016	CRO	Glyoxal oxidase	Yes	55	6	4

143158	Cytochrome b5	Cytochrome b5	No	21	0	0
48870	DyP1	Dye decolorizing peroxidase	No	174	57	33
48874	DyP2	Dye decolorizing peroxidase	No	109	4	7
30062	GAPDH	GAPDH	No	1	0	0
73596	GMC oxidoreductase	Cellobiose dehydrogenase	Yes	0	2	1
44509	Isopropyl malate dehydrogenase	Isopropyl malate dehydrogenase	No	42	0	0
146232	Laccase, TvLac2	Laccase-2	Yes	41	0	0
138261	Laccase, TvLac3	Laccase	Yes	62	27	14
115295	Laccase, TvLac4	Laccase	Yes	16	0	0
43576	Lignin peroxidase 1	Lignin peroxidase	Yes	8	42	41
114944	Lignin peroxidase 12	Ligninase C	Yes	0	0	0
43578	Lignin peroxidase 2	Lignin peroxidase	Yes	6	34	66
52333	Lignin peroxidase 6	Ligninase C	Yes	0	0	0
134226	Lignin peroxidase 9	Ligninase C	Yes	12	69	34
71674	LMPO, CBM1	LPMO	Yes	0	0	0
34184	LPMO	LPMO	Yes	0	1	0
162601	LPMO	LPMO	Yes	0	23	19
162729	LPMO	LPMO	Yes	0	2	1
36998	LPMO	LPMO	Yes	0	33	16
51004	LPMO	LPMO	Yes	0	4	4
51375	Mn peroxidase 1	Mn Peroxidase 3	Yes	53	1	1
112835	Mn peroxidase 2	Mn Peroxidase 3	Yes	2	5	4
131080	Mn peroxidase 3s	Mn Peroxidase 3	Yes	11	0	0
130496	Mn peroxidase 4s	Mn Peroxidase 3	Yes	211	38	30

43477	Mn peroxidase 5	Mn peroxidase	Yes	0	3	0
51455	Mn peroxidase 6	Mn peroxidase 3	Yes	53	10	5
51457	Mn peroxidase 9	Mn peroxidase	No	0	0	0
174721	GMC oxidoreductase	Pyranose 2 oxidase	No	19	3	0
32746	Thioredoxin	Thioredoxin	No	51	1	21
156571	Thioredoxin	Thioredoxin	No	5	0	0
68124	Xylose reductase	xylose reductase	No	28	0	0

[1]Protein ID numbers from the DOE JGI Mycocosm database (GRIGORIEV *et al.* 2014).

[2]Carbohydrate esterase and Glycoside hydrolase families as defined in the CAZy database (LOMBARD *et al.* 2014).

[3]Putative functions determined by BLAST searches of SWISS PROT database (BATEMAN *et al.* 2015).

[4]Secretion signals for detected protein sequences were detected using Signal P algorithm (PETERSEN *et al.* 2011).

[5]Unique peptide counts for proteins found in wafer sections 0-5, 15-20, and 30-35 mm from the hyphal front.

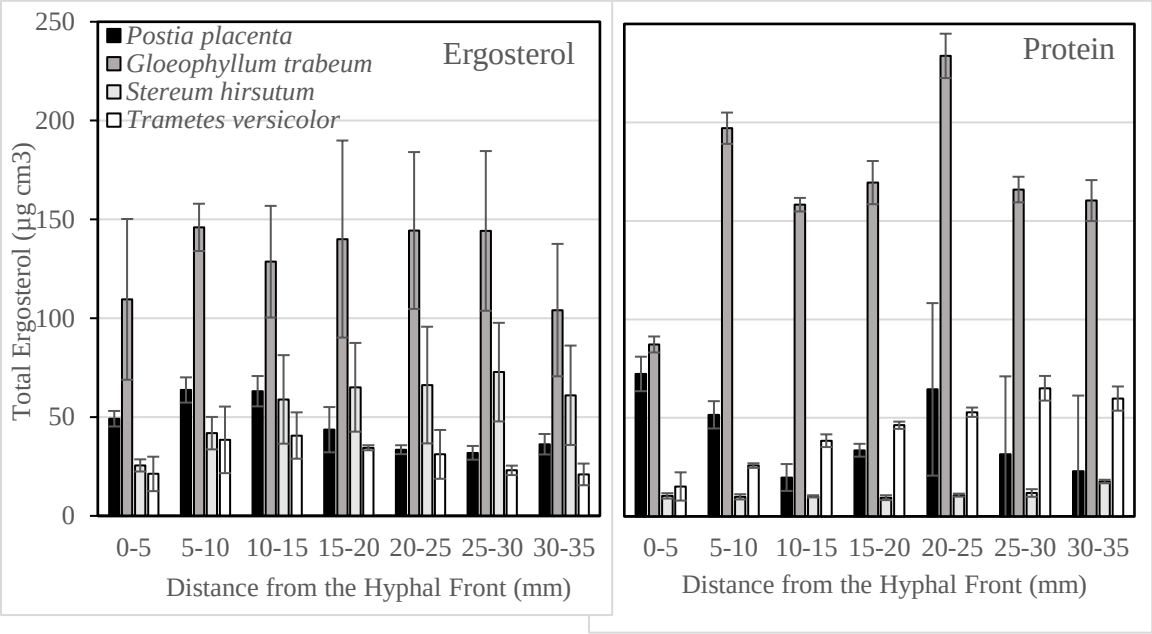

Figure S6.1: Total ergosterol and protein isolated from 5 mm wafer sections along an advancing hyphal front on aspen wafers. Values were standardized to the volume of wood from which it was extracted. Ergosterol error bars are +/- one standard deviation of three replicate wafer sections and protein error bars are standard deviations of three assays of a single extract of 12 wafer sections.

Chapter 7 Comparative proteomics and transcriptomics of the interaction between two model wood-degrading basidiomycetes identifies interaction mediators and resolves two distinct interaction strategies

7.1 Introduction

Wood-degrading basidiomycetes live in complex microbial communities with up to thousands of other fungal species in a single piece of degrading wood (RAJALA *et al.* 2012), which requires them to express combative strategies to survive in wood. These interactions help modulate CO_2 evolution rates from wood (HISCOX *et al.* 2015b) and are thus important processes that regulate global carbon cycles. Interspecific interactions induce characteristic physical, biochemical, and chemical alterations that are observable and measurable in synthetic interaction cultures (BODDY 2000), where they can be resolved from non-combative physiological characteristics.

Study of in vitro basidiomycete interspecific interactions implicates some fungal cell wall-degrading classes of glycoside hydrolases (GHs) in mediating interactions, but has shown mixed involvement of plant cell wall-degrading GHs. Fungal cell walls are composed of a mixture of chitin and branched β-glucans that are degraded by serval GH families including GH 16 β-glucanases, GH 18 chitinases, and GH 20 β-N-acetyl-glucosaminidases (MARTIN *et al.* 2007; LANGNER and GOHRE 2016). In the basidiomycete *Phanerochaete chrysosporium,* GH 18 chitinases are induced in

interspecific interaction (KARLSSON *et al.* 2016), indicating their role in degrading opponent cell walls. Plant cell wall-degrading GH expression, on the other hand, is induced in some ascomycete fungi (ATANASOVA *et al.* 2013), but remains unchanged during interspecific interactions of some basidiomycetes (EYRE *et al.* 2010; ARFI *et al.* 2013), suggesting a diversion of resources away from wood metabolism.

However, several oxidative enzymes that are known to function in plant cell degradation and are common in basidiomycete secretomes are also induced during basidiomycete interspecific interactions. Laccase activity is widely induced in interspecific interaction of basidiomycetes (BALDRIAN 2004; SNAJDR *et al.* 2011) as are ligninolytic peroxidase activity in some white-rot species (HISCOX *et al.* 2010), but the biological function of these enzymes in interactions is not known. Some laccases, for example, are known to be part of the cell wall proteome of filamentous fungi (LIU and FREE 2016), where they likely function in melanin synthesis from endogenous phenolics (CORDERO and CASADEVALL 2017). Like secreted laccases with degradative functions, cell wall-associated laccases possess canonical secretion signals (UPADHYAY *et al.* 2016b), localizing them to melanin-synthesizing endosomes where they polymerize melanin monomers (UPADHYAY *et al.* 2016a). Laccase-synthesized melanins function as a protective barrier against oxidants generated in response to fungal competitors (SILAR 2005; KUES and RUHL 2011; CORDERO and CASADEVALL 2017). Laccases can also degrade toxic metabolites produced by competitors during interactions (HISCOX and BODDY 2017), which is an important biological function unrelated to carbon assimilation in interactions laden with antimicrobial metabolites.

Basidiomycetes are known as rich sources of secondary metabolites (SMs) from identification of SM-synthesizing genes in their genomes (RILEY *et al.* 2014) and from isolation of SMs from basidiomycete cultures. The biological function of most SMs are unknown, but some SMs are produced in response to fungal competitors (HISCOX and BODDY 2017) including terpenes (HYNES *et al.* 2007; EVANS *et al.* 2008; EL ARIEBI *et al.* 2016) and orsellinic acid-derived polyketides (YAO *et al.* 2016) where they presumably function in antibiosis. *Gloeophyllum* species are wood degrading basidiomycetes known to produce several terpenes such as gloeophyllins (RASSER *et al.* 2000; HAN *et al.* 2015) and orsellinic acid-based polyketides such as oosponols (SONNENBICHLER *et al.* 1997; RASSER *et al.* 2000) in axenic culture and during interactions (SONNENBICHLER *et al.* 1993; SONNENBICHLER *et al.* 1994), suggesting a role in antibiosis. *Gloeophyllum trabeum* is a well-studied model brown-rot fungus whose genome encodes several SM synthesis genes predicted to produce SM scaffolds of known *Gloeophyllum* metabolites (SONNENBICHLER *et al.* 1994; LACKNER *et al.* 2012; WAWRZYN *et al.* 2012), but their role in mediating interspecific combat is not known. Extensive prior work characterizing *G. trabeum* physiology in axenic culture provides baseline data for studying alterations in response to competitors along with the diversity of SM-synthesizing genes makes it an ideal system to study the role of these genes in facilitating basidiomycete interactions.

In this study, we investigated the mechanisms of interaction between two model brown-rot fungi, *Gloeophyllum trabeum* and *Postia placenta* on aspen wood wafers using comparative proteomics and transcriptomics. The two fungi were grown in opposition to one another to simulate interspecific interactions and the secreted protein and RNA were

extracted within and around the interacting hyphae. The proteome composition and plant and fungal polysaccharide-degrading activity was compared to actively growing hyphae of single species cultures as were gene expression profiles from equivalent locations to allow the overlay of transcriptomics, proteomics, and enzyme activity data. This work identifies several proteins that are important in mediating basidiomycete interspecific interactions, and identifies two different interaction strategies in the species tested.

7.2 Methods

7.2.1 Culture conditions and interaction microcosms

Gloeophyllum trabeum ATCC 11539 and *Postia placenta* MAD 698-R were maintained on malt extract agar and 1 cm diameter agar plugs were used to inoculate soil block microcosms as previously described (PRESLEY and SCHILLING 2017). Sterile 19 mm aspen blocks were degraded for 4 weeks in soil block jars for each species and then were used as inoculum for interaction microcosms. Interactions were simulated by placing one *G. trabeum* and one *P. placenta* block opposing one another in empty soil microcosms and laying a 60 x 23 x 3 mm aspen wafer (largest face in cross section) across the top of the two blocks (Figure 7.1). Fungal hyphae grew together until they met in the center of the wafer, forming an interaction zone which was then sampled along with surrounding hyphae for protein and RNA as described below.

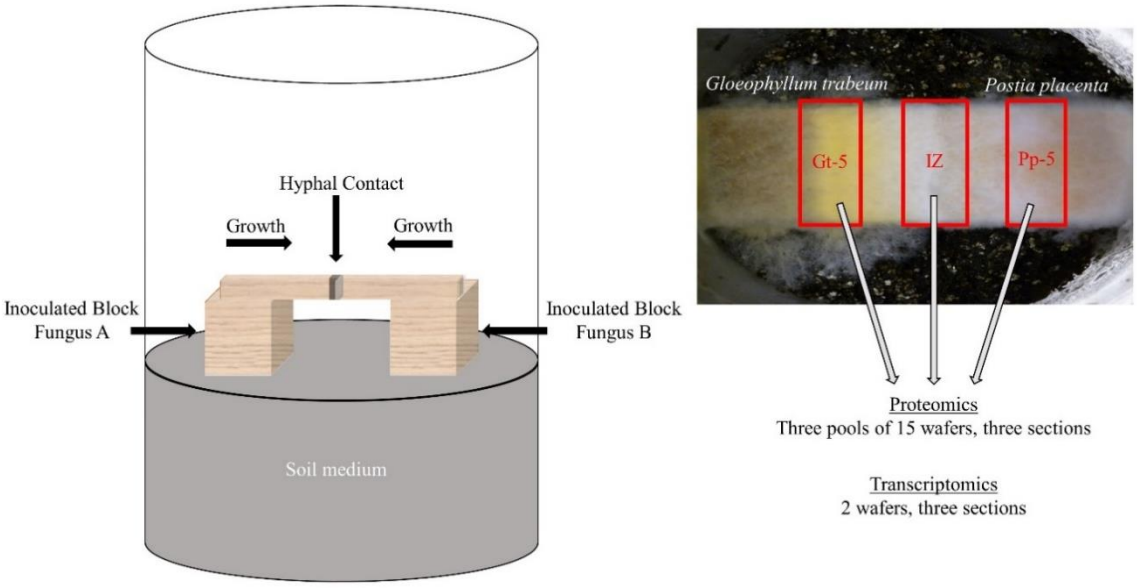

Figure 7.1: Competition microcosms used to simulate interspecific interactions between Gloeophyllum trabeum and Postia placenta in this study. Pre-inoculated wood blocks for each species are used as inoculum for each end of a thin aspen wafer placed across them. The two species grow together and contact in the middle of the wafer where the interaction zone and surrounding hyphae 5 mm outside of the interaction zone is sampled for protein and RNA for proteomic and transcriptomic analysis.

7.2.2 Protein extraction and purification

Interaction wafers were sampled for protein at three sections, one consisting a 10-mm section surrounding the interacting hyphae (IZ), and one 10-mm section 5 mm behind the boundary of the interaction zone toward each species (Gt-5 and Pp-5). Undegraded aspen wood was extracted as a control. For protein extracts, three replicate pools of 15 interaction wafers were extracted with 100 ml of cold extraction buffer (0.5 M NaCl, 0.05 acetate, 0.05% tween 80, pH 5.0) for 24 hours at 4˚C with gentle shaking. Extracts were filtered through polyester cloth, centrifuged at 4000 x g for 30 min, and

filtered through 0.2 µm sterile PVDF filters. Extracts were exchanged into 0.05 M citrate pH 5.0 and concentrated using Vivaspin Polyethersulfone (PES) 10 kDa cutoff membranes prior to freezing at -20˚C. Protein concentrations of extracts were determined using a BioRad protein assay kit (Hercules, California, USA).

7.2.3 Biochemical assays

Interaction protein extracts were assayed for poly, oligo, and disaccharide-degrading activity and compared to previously generated values for single species cultures on aspen wood 0-5 mm from the advancing hyphal front (Gt/Pp0-5) and 15-20 mm behind the hyphal front (Gt/Pp15-20) (Presley et al. in review). Endoglucanase (EG), xylanase (Xyl), laminarinase (Lam), and pectinase (Pec) activity were measured in triplicate using the DNS assay for reducing sugars (GHOSE 1987). Reactions were done at 50˚C in 0.05 M citrate at pH 5.0 using 1.5% carboxymethyl cellulose (EG), 2 % birchwood xylan (Xyl), 0.25% laminarin (Lam), and 0.5% polygalacturonic acid (Pec) as substrates. Color was developed at 90˚C and absorbance of developed reactions was measured at 540 nm. Units were defined as the amount of enzyme required to liberate 1 µmol of glucose, xylose, glucose, or galacturonic acid reducing equivalents per minute under the above conditions for EG, Xyl, Lam, and Pec activity, respectively.

β-glucosidase (BGL) and β-N-acetylglucosaminidase (BNAG) were measured in triplicate by monitoring the liberation of 4-nitrophenol from 4-nitrophenyl-β-D-glucoside and 4-nitrophenyl-β-D-N-acetylglucosamine, respectively. Reactions were carried out in 10 mM of substrate and 0.05 M citrate, pH 5.0 at 50˚C and quenched with 2 volumes of

0.2 M Na_2CO_3. Absorbance at 400 nm of quenched reactions was measured and one unit of activity was defined as the amount of enzyme required to liberate 1 µmol of 4NP per minute in the above conditions.

7.2.4 Mass spectrometry

Portions of the same protein extracts used for biochemical assays were reserved for proteomics analysis after extraction and purification as above. Three separate extracts of pools of 15 interaction wafers were analyzed for proteomic studies. Extracts were TCA/acetone precipitated, pelleted, and reconstituted in saturated guanidine-HCl. The protein concentration of each cellular extract was determined by BCA assay (SMITH *et al.* 2017). For each sample, processing replicates were performed; 50 µg of protein was aliquoted to low-retention Eppendorf tubes for downstream sample processing. All samples were incubated for 30 minutes at 60 ºC with tris(2-carboxyethyl)phosphine (Bond-Breaker TCEP, Thermo Fisher Scientific, Rockford, IL) to reduce disulfide bonds. Alkylation of cysteine residues was performed by treatment with 50 mM iodoacetamide, which was added from a 500 mM iodoacetamide, 500 mM ammonium bicarbonate stock solution. After addition of iodoacetamide, all samples were incubated at room temperature in the dark for 40 min on a rocker. Each sample was then diluted to 0.9 M urea with 500 mM ammonium bicarbonate. To each 50 µg sample, 0.1 µg of mass spectrometry grade trypsin (Promega Corp., Madison, WI) was added and incubated overnight at 37 ºC. Peptides were extracted from each sample using solid phase extraction with Discovery C18 50 mg resin columns (Supelco, St. Louis, MO). Each column was activated with 2 ml of methanol followed by equilibration with 6 ml of 18

mΩ water. The sample was applied to the column and then the column was washed with 8 ml of 50 mM ammonium bicarbonate. Peptides were eluted with two 0.9 ml washes of 40% acetonitrile. Samples were dried using a centrifugal concentrator (Thermo Scientific, Asheville, NC) and stored at -20 C until LC/MS analysis.

Peptides were solubilized in 150 µl solvent A (0.1% formic acid). For LC/MS analysis, 5 µl of sample was injected onto a Jupiter C18 resin reverse-phase column (3 µm particle size, 35 cm long, 75 µm inner diameter; Phenomenex, Torrance, CA). The peptides were eluted at 0.3 µl min-1 with an Agilent (Santa Clara, CA) 1200 high-performance liquid chromatograph with solutions of solvent A and 0.1% formic acid in acetonitrile (solvent B) using the following conditions: 0 to 30 min, isocratic at 100% solvent A; 30 to 32 min, linear gradient to 8% solvent B; 32 to 50 min, linear gradient to 12% solvent B; 50 to 105 min, linear gradient to 35% solvent B; 105 to 127 min, linear gradient to 60% solvent B; 127 to 130 min, linear gradient to 95% solvent B; and isocratic at 95% solvent B for 5 min. Eluted peptides were introduced into an Orbitrap XL mass spectrometer (Thermo Fisher, Waltham, MA) by electrospray ionization.

Spectra were collected in a data-dependent mode, with the five most intense ions in each survey scan selected for collisional induced dissociation in the five subsequent scans. Spectra were deconvoluted using the DeconMSn software (MAYAMPURATH *et al.* 2008) to more accurately assign parent ion mass and ion charge state. Spectra were then searched against predicted peptides derived from the fungal genome sequences via MS-GF+ (software used to analyze tandem mass spectra data, (KIM and PEVZNER 2014)),

using a 20 ppm parent ion mass tolerance in searches of tryptic peptides with a variable post-translational modification of oxidized methionine. A Q value cut off (≤0.01) was utilized to obtain a ~1% false discovery rate (FDR) at each individual data set level, as assessed from a decoy identification search utilizing the reverse fungal genome sequence.

7.2.5 RNA extraction and RNA-seq

Sections equivalent to those described above for protein extraction from two replicate wood wafers (about 200 mg each) were snap frozen in liquid nitrogen and ground to powder prior to extraction in 2 ml of TRIzol (Life Technologies). Samples were purified using an RNeasy minikit (Qiagen, Inc.) with on-column DNase digestion. RNA quality was monitored using an Agilent Bioanalyzer (Agilent Technologies) and only RNA samples with RNA integrity numbers >8 were used for RNA-seq. RNA-seq was performed as previously described (ZHANG *et al.* 2016) on a HiSeq 2500 system (Illumina) and duplicate samples of each type, IZ, Gt-5, and Pp-5, were sequenced. RNA-seq was performed at the University of Minnesota Genomics Center.

RNA-seq data analysis was performed on the Galaxy platform (https://usegalaxy.org/) using described procedures for differential expression analysis (TRAPNELL *et al.* 2012). Raw reads were cleaned with Trimmomatic (v0.3) and mapped against the *P. placenta* MAD698-R (v1.0) and *G. trabeum* ATCC11539 (v1.0) genomes together using TopHat (v2.0.13). Previously generated RNA-seq data from single species cultures of both species grown on equivalent on aspen wafers were used for comparison to data generated in this study (ZHANG *et al.* 2016)(Zhang et al. in review). Expression

levels found at the leading hyphal edge of fungal cultures on aspen and 5 mm outside of the IZ toward each species were compared to expression levels found at the IZ. Reference transcript models from the JGI database were used to determine differences in expression levels (RPKM) in pairwise comparisons among samples using Cuffdiff (Galaxy Tool Version 2.2.1.3) using geometric normalization. FDR was set at <0.05. Transcripts with 4-fold greater or less RPKM values in the IZ sample relative to other samples were identified.

7.2.6 Secondary metabolite synthesis gene expression analysis and cluster identification

Basidiomycete secondary metabolite (SM) scaffold-synthesizing genes including polyketide synthases (PKSs) (LACKNER *et al.* 2012), sesquiterpene synthases (STSs) (WAWRZYN *et al.* 2012), non-ribosomal peptide synthases (NRPSs) (KALB *et al.* 2013), and NRPS-like reductases (AFRs) (BRANDENBURGER *et al.* 2016) were identified in the *G. trabeum* and *P. placenta* genomes. SM synthesis gene clusters analysis was performed with anti-smash fungal version (WEBER *et al.* 2015) and gene clusters of upregulated SM genes were identified. Relative expression levels of genes in SM clusters of interest in the IZ were determined relative to levels previously found at the leading hyphal front of single species cultures (ZHANG *et al.* 2016)(Zhang et al. in review).

7.3 Results

7.3.1 Secretome composition of interacting and non-interacting hyphae

Secreted proteins isolated from the interaction zone (IZ) and from 5 mm outside it toward each species (Gt/Pp-5) were compared to those found in single species cultures 0-5 mm (Gt/Pp0-5) and 15-20 mm (Gt/Pp15-20) behind an actively growing hyphal front. Interaction microcosms

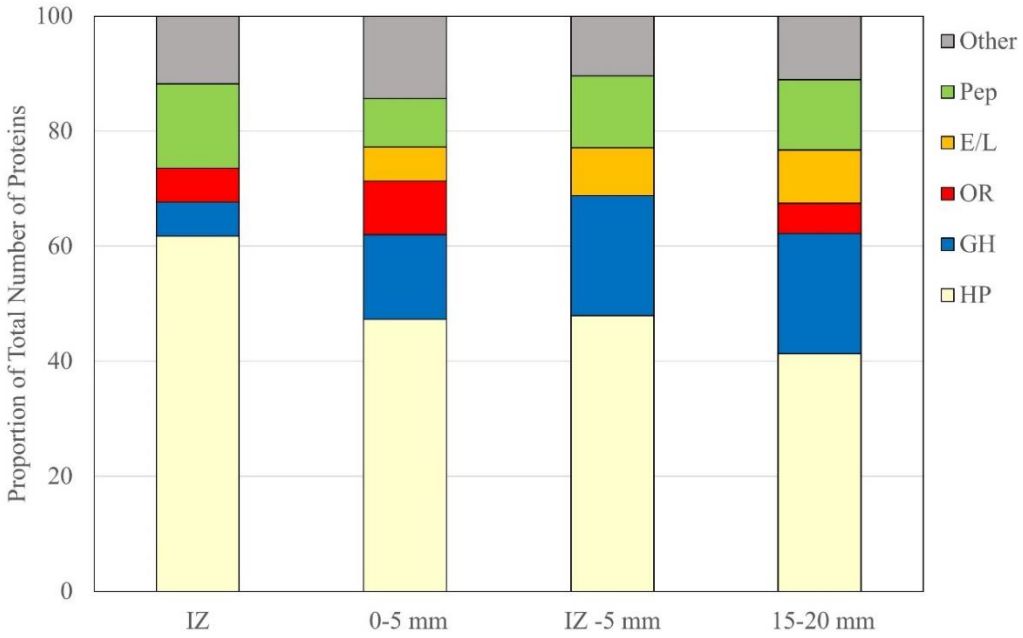

Figure 7.2: Combined secretome compositions from *Gloeophyllum trabeum* and *Postia placenta* interaction and non-interaction cultures for interacting hyphae (IZ), 0-5 mm behind the hyphal front of single species cultures, 5 mm outside of the interaction zone (IZ-5 mm), and 15-20 mm behind the hyphal front of single species cultures. HP; hypothetical protein, GH; glycoside hydrolase, OR; oxidoreductase, E/L; esterase lipase, Pep; peptidase.

showed a reduced diversity of secreted protein compared to single species cultures. Only 36 unique proteins were identified in the IZ, 26 from *G. trabeum* and 10 from *P. placenta*, compared to 194 and 42 unique proteins identified in Gt0-5 and Pp0-5 extracts, respectively. 33 and 15 unique proteins were identified in Gt-5 and Pp-5 extracts, respectively whereas 110 and 62 unique proteins were found in Gt15-20 and Pp15-20 extracts, respectively. Glycoside hydrolases (GHs) as a proportion of all proteins were lower in IZ extracts (6%) than in Gt/Pp-5 extracts (21%) and all single species culture extracts (15-21%) (Figure 7.2). Although GH production in the IZ was reduced, a GH 115 putative α-glucuronidase not found in single species cultures was produced outside (*G. trabeum* and *P. placenta*) and within (*G. trabeum*) the IZ (Tables S7.1-7.3). One of these (Gt 121308) was produced in particularly high abundance and it constituted 20% of all protein observations of proteins in the Gt-5 extracts.

No esterases/lipases were identified in extracts of interacting hyphae while this group of enzymes composed 8% and 6-9% of the proteins found in extracts outside the interaction zone and in single species cultures, respectively. Extracts from the interaction zone were primarily composed of hypothetical proteins (62%), compared to 48% and 41-47% in non-interacting and single species cultures, respectively. Several proteins, 7 from *G. trabeum* and 8 from *P. placenta*, were exclusively found in the interacting hyphae (Table 7.1). The majority of these were uncharacterized hypothetical proteins, but both fungi produced a putative acid protease exclusive to the interaction. None of the proteins exclusive to the interaction contained secretion signals identified by Signal P (PETERSEN *et al.* 2011).

Table 7.1: Proteins found exclusively in protein extracts of the interaction zone between *Gloeophyllum trabeum* and *Postia placenta*.

Gloeophyllum trabeum			
Protein ID[1]	Name	Putative Function[2]	Observations[3]
101772	Hypothetical protein	no strong hits	1
91843	Hypothetical protein	Pumilo domain	1
128123	Hypothetical protein	no strong hits	1
108762	Hypothetical protein	no strong hits	7
81033	Metallophosphatase	Metallophosphatase	1
136352	Protease, Acid	Acid protease	4
112815	Ribosomal protein S15	Ribosomal S37	1

Postia placenta			
Protein ID	Name	Putative Function	Observations
1183565	AB hydrolase	Lipase	2
105721	FAD-oxidoreductase	FAD-binding protein	4
92184	Hypothetical protein	no strong hits	1
99255	Hypothetical protein	no strong hits	7
93455	Hypothetical protein	no strong hits	1
98779	Hypothetical protein	no strong hits	11
96562	Hypothetical protein	no strong hits	36
1127001	Protease, Acid	Polyporopepsin	3

[1]Protein ID numbers from the DOE JGI Mycocosm database (GRIGORIEV *et al.* 2014).

[2]Putative functions determined by BLAST searches of SWISS PROT database (BATEMAN *et al.* 2015).

[3]Number of observations in LC-MS/MS experiment (spectral counts)

7.3.2 Enzyme activities

Six enzyme specific activities, pectinase (Pec), endoglucanase (EG), xylanase (Xyl), β-glucosidase (BGL), Laminarinase (Lam), and β-N-acetylglucosaminidase (BNAG), were measured on protein extracts from interaction cultures (IZ and Gt/Pp-5)

and were compared to those from single species cultures (Gt/Pp0-5 and 15-20) (Figure 7.3). Extracts of the IZ showed the highest pectinase specific activity, 3-fold and 2-fold higher than those found at Gt0-5 mm and Pp0-5, respectively despite the lack of identification of any known pectinases in IZ extracts. Laminarinase specific activity was also significantly higher in IZ extracts than all except Gt-5 and Pp15-20 mm despite the identification of only two GHs, both produced by *G. trabeum*, in the IZ, a GH 115 (Gt 121308) and a GH 3 (Gt 69843). All other measured activities were generally low in IZ extracts, but some plant polysaccharide-degrading activities increased to levels equivalent to those found in single species cultures in Gt-5 extracts only (Figure 7.3).

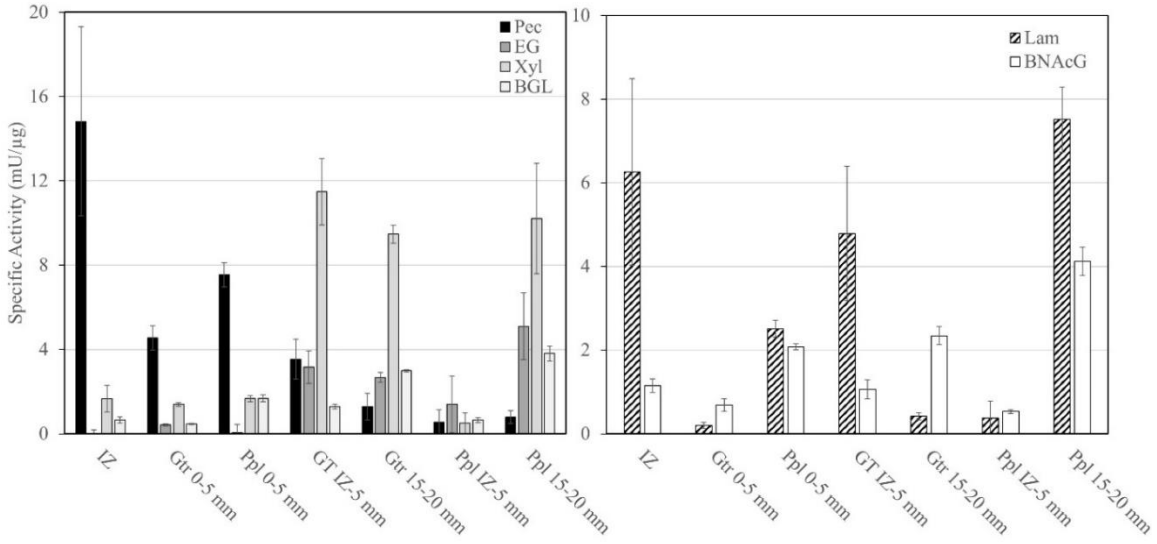

Figure 7.3: Enzyme specific activities from proteins extracts from interacting hyphae (IZ) and 5 mm behind interacting hyphae (-5 mm) of *Gloeophyllum trabeum* (Gtr) and *Postia placenta* (Ppl) grown in opposition on aspen wood along with specific activities from single species cultures on aspen wood 0-5 mm and 15-20 mm behind the advancing culture margin. Pec, Pectinase, EG, Endoglucanase, Xyl, Xylanase, BGL, β-glucosidase, Lam, Laminarinase, BNAcG, β-N-Acetylglucosaminidase.

7.3.3 Transcriptional profiling of interacting hyphae

RNA-seq was used to compare gene expression levels in the IZ to surrounding hyphae and single species cultures for each species. Of the genes that are 4-fold upregulated in the IZ relative to Gt0-5 and Pp0-5 (Figure 7.4A), a greater proportion are oxidoreductases (ORs) (16.0% and 34.6%, respectively) than are 4-fold upregulated in Gt0-5 (6.3%) and in Pp0-5 (8.7%) relative to the IZ (Figure 7.4B). *G. trabeum* upregulated a greater number of secondary metabolite (SM) synthesizing genes (eight) in the IZ relative to Gt0-5 than *P. placenta* did relative to Pp0-5 (one). *P. placenta* 4-fold upregulated more proteases (eight) in the IZ relative to Pp0-5 than *G. trabeum* did relative to Gt0-5 (three) (Figure 7.4A). Similar patterns were seen when gene expression levels in the IZ were compared to non-interacting hyphae around it (Gt/Pp-5). Of the genes that are 4-fold upregulated in the IZ relative to Gt-5 and Pp-5 (Figure 7.5A), a greater proportion are ORs (14.2% and 19.0%, respectively) than are 4-fold upregulated in Gt-5 (10.1%) and Pp-5 (11.5%) relative to the IZ (Figure 7.5B).

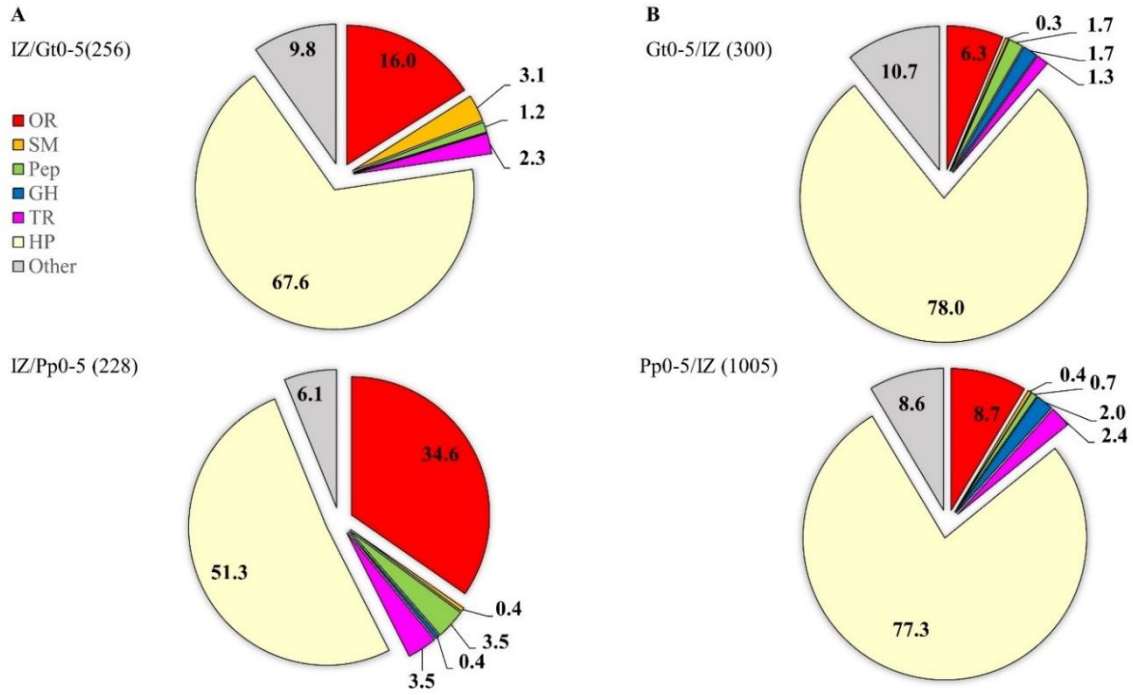

Figure 7.4: (A) Genes 4-fold upregulated in the interaction zone (IZ) compared to the leading hyphal front of single species cultures of *Gloeophyllum trabeum* (Gt0-5) *Postia placenta* (Pp0-5). (B) Genes 4-fold upregulated at the leading hyphal front of single species cultures compared to the IZ. Categories are represented as proportions of all genes 4-fold upregulated and the total number of genes upregulated are in parentheses. OR; oxidoreductase, SM; secondary metabolite synthesizing genes, Pep; peptidases, GH; glycoside hydrolases, TR; transporter, HP; hypothetical protein.

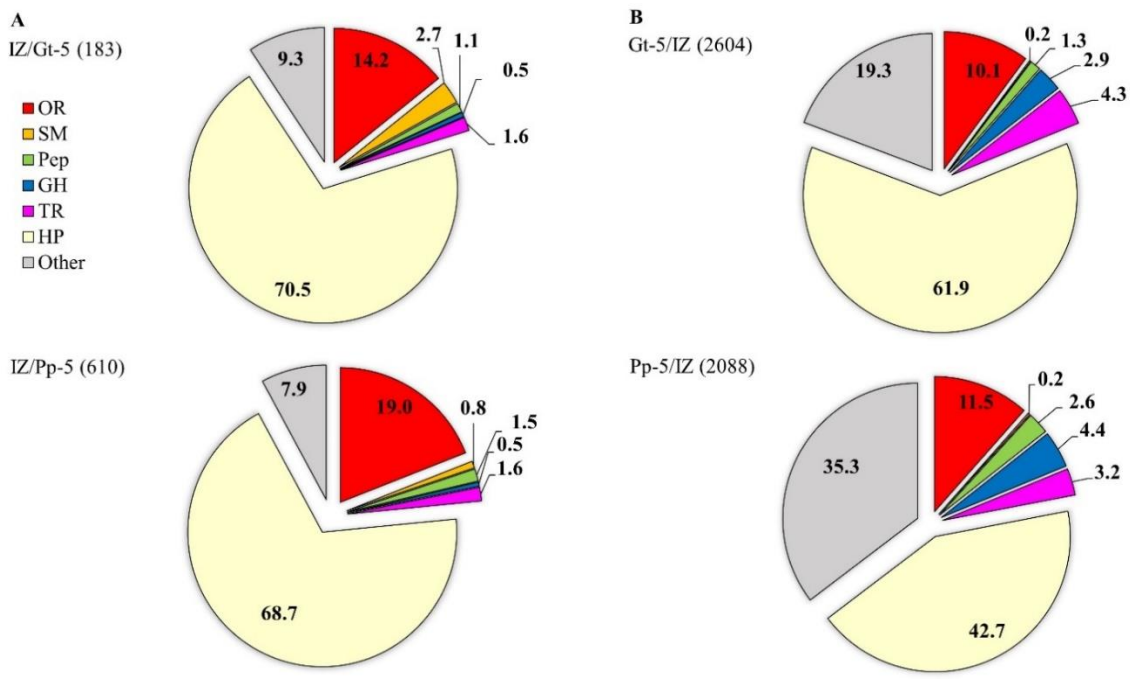

Figure 7.5: (A) Genes 4-fold upregulated in the interacting hyphae (IZ) relative to hyphae 5 mm outside the IZ (Gt/Pp-5) in *Gloeophyllum trabeum* (Gt) or *Postia placenta* (Pp). (B) Genes 4-fold upregulated outside of the IZ relative to the IZ. Categories are represented as proportions of all genes 4-fold upregulated and the total number of genes upregulated are in parentheses. OR; oxidoreductase, SM; secondary metabolite synthesizing genes, Pep; peptidases, GH; glycoside hydrolases, TR; transporter, HP; hypothetical protein.

Consistent with proteomic data, the 25 most highly upregulated *G. trabeum* genes in the IZ relative to Gt0-5 were mostly hypothetical proteins (seventeen). This group also included a laccase, an oxalate decarboxylase, an O-methyl transferase, a polyketide synthase, and a hydrophobin (Table 7.2). The 25 most highly upregulated genes in the IZ relative to the *P. placenta* hyphal front included fewer hypothetical proteins (five), a greater abundance of uncharacterized ORs (fourteen) including putative cytochrome

p450s and an aryl alcohol dehydrogenase, and a peptidase (Table 7.2). A greater number of GHs were upregulated outside of the IZ or in single species cultures than within the IZ. In *G. trabeum,* 5 and 76 GHs were at least 4-fold upregulated in Gt0-5 and Gt-5, respectively relative to the IZ, compared to 0 and 1 at least 4-fold upregulated in the IZ relative to Gt0-5 and Gt-5, respectively. In *P. placenta*, 20 and 92 GHs were at least 4-fold upregulated in Pp0-5 and Pp-5, respectively relative to the IZ, whereas 1 and 3 GHs were at least 4-fold upregulated in the IZ relative to Pp0-5 and Pp-5, respectively. In addition, no carbohydrate esterases were 4-fold or more upregulated in the IZ relative to Gt/Pp0-5 or Gt/Pp-5 samples. Hypothetical proteins were the largest category of upregulated proteins among all comparisons, ranging from 42.7-78.0% of all genes 4-fold upregulated (Figure 7.4 and 7.5).

Table 7.2: Top 25 genes most highly upregulated in interacting hyphae (IZ) compared to the leading hyphal edge (Gt/Pp 0-5) of single species cultures of *Gloeophyllum trabeum* (Gt) and *Postia placenta* (Pp). RPKM values for each gene at each condition is shown with the $\log_2$ of the ratio of IZ.

Most upregulated in IZ/GtrHF						Most upregulated in IZ/PplHF					
Protein ID[1]	Name[2]	RPKM IZ	RPKM Gt0-5[3]	$\log_2$ IZ/Gt0-5	Signal P[4]	Protein ID[1]	Name[2]	RPKM IZ	RPKM Pp0-5[5]	$\log_2$ IZ/Pp0-5	Signal P[4]
137245	Hypothetical protein	492.6	0.4	10.1	no	63488	Oxidoreductase	211.1	0.7	8.3	no
92695	Hypothetical protein	3599.5	8.8	8.7	19-20	60565	Oxidoreductase	129.4	0.5	8.0	no
103366	Oxalate decarboxylase	463.5	1.5	8.2	19-20	105320	Hypothetical protein	65.6	0.3	7.9	22-23
44870	Hypothetical protein	721.6	3.9	7.5	21-22	105721	Oxidoreductase	257.9	1.5	7.4	no
48004	Vacuolar protein	14.4	0.1	7.4	no	47260	Oxidoreductase	389.2	2.6	7.2	no
95418	Hypothetical protein	203.6	1.4	7.2	15-16	35307	Oxidoreductase	545.3	4.3	7.0	no

134059	Hypothetical protein	5481.2	69.5	6.3	23-24	54275	Hypothetical protein	94.8	1.0	6.6	20-21
95488	Hypothetical protein	130.7	1.8	6.2	no	48020	Cytochrome p450	154.3	1.8	6.4	no
114641	O-methyl transferase	3051.3	45.2	6.1	no	45365	Uncharacterized transporter	49.1	0.8	5.9	no
134822	Hypothetical protein	404.2	6.3	6.0	19-20	126377	Oxidoreductase	156.9	2.9	5.8	no
104526	Hypothetical protein	245.2	3.9	6.0	19-20	92340	Cytochrome p450	77.6	1.5	5.7	27-28
96525	Hypothetical protein	159.9	2.8	5.8	no	46594	Aryl alcohol dehydrogenase	79.3	1.5	5.7	no
104708	Oxidoreductase	741.1	13.8	5.7	no	116256	Potassium channel	45.0	0.9	5.7	no
112738	Hypothetical protein	500.8	9.4	5.7	no	126381	Protease, acid	82.2	1.6	5.6	26-27
129354	Hypothetical protein	587.6	11.3	5.7	19-20	105719	Cytochrome p450	68.3	1.6	5.5	27-28
113399	Oxidoreductase	840.4	16.9	5.6	no	106360	Hypothetical protein	69.5	1.7	5.4	no
45373	Hypothetical protein	98.3	2.0	5.6	21-22	103283	Expansin-like protein	25.3	0.6	5.3	20-21
67066	Hypothetical protein	1826.5	37.4	5.6	no	99672	Oxidoreductase	31.1	0.8	5.2	no
94357	Hypothetical protein	58.7	1.2	5.6	17-18	100325	Hypothetical protein	150.3	4.0	5.2	20-21
50822	Polyketide synthase I	184.0	4.0	5.5	no	63451	Oxidoreductase	67.6	2.0	5.1	no
19724	Hydrophobin	2085.5	46.0	5.5	no	45316	Hypothetical protein	121.7	4.1	4.9	no
50761	Hypothetical protein	695.6	15.5	5.5	no	61173	Oxidoreductase	188.3	6.4	4.9	no
101772	Hypothetical protein	372.3	8.8	5.4	25-26	91006	Alcohol dehydrogenase	125.1	4.3	4.9	no
130426	Laccase 2	47.0	1.1	5.4	20-21	115141	Lipase	204.6	7.2	4.8	26-27
17704	Hypothetical protein	149.8	3.8	5.3	no	45371	Oxidoreductase	33.2	1.2	4.8	no

[1]Protein ID numbers from the DOE JGI Mycocosm database (GRIGORIEV *et al.* 2014).

[2]Putative functions determined by BLAST searches of SWISS PROT database (BATEMAN *et al.* 2015).

[3]Gt0-5 RPKM value adapted from (Zhang et al. in review).

[4]Secretion signals for detected protein sequences were detected using Signal P algorithm (PETERSEN *et al.* 2011).

[5]Pp0-5 RPKM values adapted from (ZHANG *et al.* 2016).

7.3.4 Secondary metabolite synthesizing genes in *G. trabeum*

G. trabeum upregulated several SM-synthesizing genes in the IZ whereas *P. placenta* upregulated fewer members of this group in the IZ. Proteins upregulated in the IZ by *G. trabeum* included two polyketide synthases (PKSs), four sesquiterpene synthases (STSs), one non-ribosomal peptide synthases (NRPSs)-PKS hybrid, and two NRPS-like proteins (Figure 7.6). AntiSMASH (WEBER *et al.* 2015) SM cluster analysis identified seven gene clusters in which these nine upregulated proteins are located in the *G. trabeum* genome and most are located near cytochrome p450s, other ORs, and/or membrane transporters. One of the PKSs, Gt116317, shares high homology with characterized basidiomycete orsellinic acid synthases (LACKNER *et al.* 2012). Upregulated sesquiterpene cyclases share greatest homology with protoilludene synthases (Gt117331 and Gt78472) and sativene synthases (Gt131990 and Gt79917).

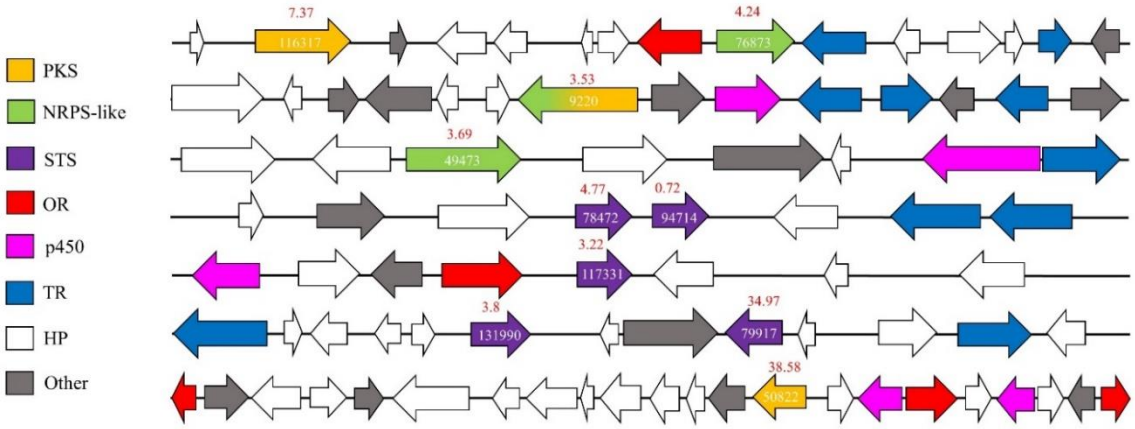

Figure 7.6: Secondary metabolite (SM) synthesis clusters in *Gloeophyllum trabeum* that contain at least one SM scaffold-synthesizing gene that is upregulated in interacting hyphae relative to 0-5 mm behind the leading hyphal front of single species cultures of *G. trabeum*. Arrows represent genes with JGI protein ID number on relevant genes. Fold changes in expression levels (IZ/Gt0-5) are shown in red over each SM synthesis-related gene. PKS, Polyketide synthases, OR, oxidoreductases, STS, sesquiterpene synthases, NRPS, Non-ribosomal peptide synthase, TR, Transporter

7.4 Discussion

Wood degrading basidiomycetes deploy several tactics to deal with competitors in wood, each characterized by specific morphological and/or biochemical alterations to fungal hyphae (BODDY and HISCOX 2016). This study identifies characteristic differences in protein secretion and gene expression in response to a fungal competitor in the two model brown-rot fungi *Gloeophyllum trabeum* and *Postia placenta*. Secretomes of interacting hyphae showed a general reduction in the prevalence of common decay-related genes such as glycoside hydrolases (GHs) and carbohydrate esterases (CEs)

compared to non-interacting hyphae and single species cultures (Figure 7.2) (Tables S7.1-S7.3). Most of the GHs and CEs previously shown to be secreted by these two fungi in single species cultures on aspen wafers were either downregulated or not significantly changed in the IZ (Tables S7.4-S7.7) compared to non-interacting hyphae or single species cultures. Likewise, the white-rot fungus *Pycnoporus coccineus*, did not upregulate plant cell wall-degrading enzymes when confronted with competitors (ARFI *et al.* 2013), indicating they were not important in mediating the interaction. The few GHs upregulated 4-fold or more in the IZ in this study, included one GH 16 in both *G. trabeum* and *P. placenta*, and two GH 18 proteins in *P. placenta*. *Phanerochaete chrysosporium* GH 18 chitinases were differentially expressed during contact with living and dead competitor hyphae (KARLSSON *et al.* 2016), and similar functional divergence in fungal cell wall-modifying enzymes may be responsible for differential expression patterns for GH 16 and 18 enzymes in this study. Laminarinase activity was also higher in the IZ than hyphal fronts of single species cultures (Figure 7.3), suggesting that fungal cell wall glucan metabolism, possibly mediated by upregulated GH 16s, is induced in the IZ.

Plant polysaccharide enzyme-degrading enzyme activities were not markedly reduced in the IZ compared to equivalent non-interacting hyphae (Figure 7.3), but these are known to be generally low at the leading hyphal edge of fungal cultures except for pectinase (ZHANG *et al.* 2016; PRESLEY and SCHILLING 2017). Pectinase activity was increased in the IZ compared to other samples, but no GH 28 pectinases were found or upregulated in IZ secretomes (Table S7.1, S7.4-7.7) (Data S7.1). Pectinolysis in the IZ

must then be facilitated by another enzyme class, possibly by one of the uncharacterized proteins found in the IZ (Table S7.1). One-way basidiomycetes compete in wood is by capturing greater resources than their competitors (BODDY 2000). Heightened IZ pectinase activity may be an attempt by fungi to "outmaneuver" competitors by overexpressing early stage colonization enzymes including pectinases (ZHANG *et al.* 2016) and oxidant-producing enzymes (HORI *et al.* 2014) to facilitate rapid resource capture (HISCOX *et al.* 2010; BODDY and HISCOX 2016).

Transcriptomics and proteomics of the IZ identified differing strategies for interaction in *G. trabeum* and *P. placenta*. *G. trabeum* appeared to rely more heavily on SM synthesis gene upregulation in the IZ than *P. placenta*, shown by the higher proportion of these genes among those upregulated in the IZ relative to Gt/Pp0-5 and Gt/Pp-5 (Figure 7.4A and 7.5A) and a highly upregulated PKS (Table 7.2). Interestingly, *G. trabeum* was previously shown to produce pore-forming endotoxin-like proteins in single species cultures (PRESLEY and SCHILLING 2017), but these were not found in IZ secretomes and were not among IZ-upregulated proteins in this study. This suggests these putative pore-forming enzymes are not involved in mediating fungal-fungal interactions, but instead may be part of a general anti-herbivory strategy in *G. trabeum* as is the function of homologs of this protein in bacteria and other basidiomycetes (JAQUET *et al.* 1987; WENG *et al.* 2004). Acid proteases were produced exclusively in the IZ by both fungi, suggesting these proteins may be induced by the presence of a competitor (Table 7.1). However, proteases were also a larger proportion of IZ-upregulated genes in *P. placenta* than *G. trabeum* (Figure 7.4A and 7.5A), indicating a more proteolytic strategy

in the former. Protease upregulation is common during basidiomycete interactions due to the degradation of competitor cell wall components (EYRE *et al.* 2010; ARFI *et al.* 2013), and this study suggests that is may be a preferred strategy by some fungi as opposed to another strategy such as SM-based antibiosis used by other fungi.

Basidiomycetes are rich sources of SMs and several studies have demonstrated the importance of SMs in mediating interspecific interactions in wood decay fungi (HYNES *et al.* 2007; EVANS *et al.* 2008; PEIRIS *et al.* 2008; EL ARIEBI *et al.* 2016). *Gloeophyllum* species are known to produce several classes of SMs, including terpenoids (RASSER *et al.* 2000; HAN *et al.* 2015) and polyketides (SONNENBICHLER *et al.* 1997), that have mild antibacterial and antifungal activity. *G. trabeum* upregulated several SM-synthesis genes in the IZ, implicating the products of these genes in mediating fungal-fungal interactions (Figure 7.4A). Nine upregulated SM-synthesis genes were identified on seven SM-synthesis clusters using AntiSMASH SM cluster analysis (Figure 7.6) (WEBER *et al.* 2015), some of which, such as the putative orsellinic acid synthase Gt116317, share high homology to characterized SM-synthesizing genes (LACKNER *et al.* 2012; LACKNER *et al.* 2013). These SM clusters also contain IZ-upregulated ORs and cytochrome p450s may perform oxidations necessary to produce orsellinic acid-derived metabolites and contribute to the overall greater proportion of ORs upregulated in the IZ compared to non-interacting hyphae (Figure 7.6). Our study suggests that antimicrobial orsellinic acid-derived SMs such as oosponols produced in relatives of *G. trabeum*, (SONNENBICHLER *et al.* 1997) may help mediate interspecific interactions in *G. trabeum*.

Increases in OR upregulation at the IZ were seen in both fungi in this study (Figure 7.4 and 7.5), and has also been shown in interacting hyphae of other wood-degrading basidiomycetes (ARFI *et al.* 2013). In *P. placenta,* OR upregulation may be a response to the SM-based strategy used by *G. trabeum* aimed at eliminating toxic metabolites (HISCOX *et al.* 2010; ARFI *et al.* 2013). Xenobiotic-metabolizing ORs are major secretome components in wood-degrading basidiomycete secretomes found among lignocellulose-degrading enzymes (MOODY *et al.* 2018) and IZ-upregulated ORs in this study may have similar functional roles. One OR, Pp105721, was both found in exclusively protein extracts of the IZ (Table 7.1) and was the 3rd most highly upregulated *P. placenta* gene in the IZ (Table 7.2), suggesting it may be important in SM breakdown.

Laccases are oxidoreductases that have been widely implicated in basidiomycetes interactions, where they may play a role in melanization (CORDERO and CASADEVALL 2017) or SM breakdown (HISCOX and BODDY 2017). Brown-rot fungal secretomes are generally characterized by a lack of phenol oxidase activity, but do contain these proteins in their genomes (RILEY *et al.* 2014) and produce them in low quantities (WEI *et al.* 2010). In this study, *G. trabeum* highly upregulated a laccase (Gt130426) in the IZ (Table 7.2), as is seen in protein extracts of the interacting hyphae of several white-rot fungi (BALDRIAN 2004; HISCOX *et al.* 2010). However, no laccase activity was found and no laccase peptides were identified in protein extracts from interaction microcosms in this study (data not shown), suggesting that upregulated laccases in *G. trabeum* were not secreted. Instead, Gt130426 may exist as a cell wall-associated protein, similar to some secretion signal-containing ascomycete laccases that localize to fungal cell walls (LIU and

FREE 2016). Cell wall-bound laccases are known to function in melanization of filamentous ascomycetes (LIU and FREE 2016; UPADHYAY *et al.* 2016b) and the basidiomycete yeast Cryptococcus (WATERMAN *et al.* 2007). Melanization protects cells from oxidative stress (CORDERO and CASADEVALL 2017) and serves as a recalcitrant barrier between interacting fungi (BODDY 2000). Therefore, Gt130426 may function outside of canonical laccase roles in lignin-degradation (BOURBONNAIS and PAICE 1990) or as a progenitor of Fenton's reagent (WEI *et al.* 2010) in *G. trabeum* and instead perform a protective function in interspecific interactions.

Basidiomycete interspecific interactions are ubiquitous processes necessary for the survival of these organisms. This study identifies general techniques utilized by wood degrading basidiomycetes during interspecific combat and identifies interspecific variation in combative mechanisms in two brown-rot species. Both species divert resources away from GH and CE production except for pectinase and laminarinase activity, the latter likely the result of fungal β-glucan-related metabolism. *G. trabeum* exhibited a SM-based interaction strategy during by upregulating several SM-synthesis genes, while *P. placenta* employed a proteolytic strategy. Several oxidoreductases, including those likely involved in SM synthesis, degradation, and cell wall melanization were upregulated in the IZ, indicating they are important in facilitating interactions. This work identifies several important fungal-fungal interaction mediators in wood-degrading basidiomycetes and begins to functionally categorize several uncharacterized basidiomycete proteins.

7.5 Supplemental information

Table S7.1: Proteins identified in protein extracts of interacting hyphae of *Gloeophyllum trabeum* and *Postia placenta*

Species	ID[1]	Name	Swiss prot[2]	Observations[3]
G. trabeum	101772	Hypothetical protein	no strong hits	1
G. trabeum	91843	Hypothetical protein	no strong hits	1
G. trabeum	128123	Hypothetical protein	no strong hits	1
G. trabeum	108762	Hypothetical protein	no strong hits	7
G. trabeum	81033	Metallophosphatase	Metallophosphatase	1
G. trabeum	136352	Protease, Acid	Acid protease	4
G. trabeum	112815	Ribosomal protein S15	Ribosomal S37	1
G. trabeum	116675	Formamidase	Formamidase	6
G. trabeum	121308	GH 115	no strong hits	8
G. trabeum	69843	GH 3	β-glucosidase	7
G. trabeum	130688	Hypothetical protein	no strong hits	11
G. trabeum	44870	Hypothetical protein	no strong hits	17
G. trabeum	112240	Hypothetical protein	no strong hits	2
G. trabeum	112664	Hypothetical protein	no strong hits	39
G. trabeum	92695	Hypothetical protein	no strong hits	4
G. trabeum	116097	Hypothetical protein	no strong hits	5
G. trabeum	93553	Hypothetical protein	no strong hits	1
G. trabeum	138715	Hypothetical protein	no strong hits	10
G. trabeum	129354	Hypothetical protein	no strong hits	2
G. trabeum	61365	Hypothetical protein	no strong hits	6
G. trabeum	104432	Nuclear transport factor	Nuclear transport factor	2
G. trabeum	62581	Protease, Acid	Aspergillopepsin	46
G. trabeum	48672	Protease, Tripeptidyl	Tripeptidyl Protease	5
G. trabeum	39789	Protease, Tripeptidyl	Tripeptidyl Protease	11
G. trabeum	134939	Thioredoxin	Thioredoxin	1
P. placenta	1183565	AB hydrolase	Lipase	2
P. placenta	105721	FAD-oxidoreductase	FAD binding protein	4
P. placenta	92184	Hypothetical protein	no strong hits	1
P. placenta	99255	Hypothetical protein	no strong hits	7
P. placenta	93455	Hypothetical protein	no strong hits	1
P. placenta	98779	Hypothetical protein	no strong hits	11
P. placenta	101552	Hypothetical protein	no strong hits	4
P. placenta	96562	Hypothetical protein	no strong hits	36
P. placenta	1127001	Protease, Acid	Polyporopepsin	3

[1]Protein ID numbers from the DOE JGI Mycocosm database (GRIGORIEV *et al.* 2014).

[2]Putative functions determined by BLAST searches of SWISS PROT database (BATEMAN *et al.* 2015).

[3]Number of observations in LC-MS/MS experiment (spectral counts)

Table S7.2: Proteins identified in protein extracts of *Gloeophyllum trabeum* hyphae 5 mm outside of the interaction zone. Proteins are listed with the total number of observations.

ID[1]	Name	Swiss prot[2]	Observations[3]
36245	Amidase	Amidase	2
46347	CE 15	Glucuronyl esterase	2
138785	GH 10	endo-β-1,4-xylanase	1
121308	GH 115	no strong hits	55
138821	GH 12	Xyloglucan-specific endoglucanase	2
69843	GH 3	β-glucosidase	34
122002	GH 3	endo-β-xylosidase	14
63180	GH 5	Endoglucanase	6
81248	Hypothetical protein	no strong hits	5
139330	Hypothetical protein	no strong hits	1
65283	Hypothetical protein	no strong hits	26
48343	Hypothetical protein	carboxylesterase	10
96567	Hypothetical protein	Carboxylesterase	8
131166	Hypothetical protein	no strong hits	4
122332	Hypothetical protein	no strong hits	1
131837	Hypothetical protein	Hercynyl cysteine sulfoxide lyase	1
122240	Hypothetical protein	no strong hits	1
96019	Hypothetical protein	no strong hits	1
48407	Hypothetical protein	no strong hits	1
112674	Hypothetical protein	Transcription factor	1
36877	Hypothetical protein	no strong hits	1
73954	Hypothetical protein	no strong hits	1
93128	Hypothetical protein	no strong hits	1
124440	Hypothetical protein	microtubule binding protein	1
138715	Hypothetical protein	no strong hits	1
24740	Lipase	Lipase	1
130556	Oxalate decarboxylase	Oxalate decarboxylase	1
81017	Profilin	Profilin	1
62581	Protease, Acid	Aspergillopepsin	50

57888	Protease, Acid	Polyporopepsin	6
48672	Protease, Tripeptidyl	Tripeptidyl Protease	29
48851	Protease, Tripeptidyl	Tripeptidyl Protease	4
39789	Protease, Tripeptidyl	Tripeptidyl Protease	2

[1]Protein ID numbers from the DOE JGI Mycocosm database (GRIGORIEV *et al.* 2014).

[2]Putative functions determined by BLAST searches of SWISS PROT database (BATEMAN *et al.* 2015).

[3]Number of observations in LC-MS/MS experiment (spectral counts)

Table S7.3: Proteins identified in protein extracts of *Postia placenta* hyphae 5 mm outside of the interaction zone.

Species	ID	Name	Swiss prot	Observations
P. placenta	127015	Cholinesterase	Fatty acyl CoA hydrolase	2
P. placenta	127015	Cholinesterase	Paranitro benzylesterase	19
P. placenta	96457	DNA ligase	DNA ligase	1
P. placenta	1076117	GH 115	no strong hits	1
P. placenta	57564	GH 2	β-mannosidase	12
P. placenta	134890	GH 3	exo-β-1,4-xylosidase	1
P. placenta	107557	GH 3	β-glucosidase	5
P. placenta	1073356	Glutamate synthase	Glutamate synthase	1
P. placenta	104279	Hypothetical protein	no strong hits	1
P. placenta	99255	Hypothetical protein	no strong hits	13
P. placenta	1064989	Hypothetical protein	Pumilio domain protein	2
P. placenta	100575	Hypothetical protein	no strong hits	1
P. placenta	101774	Hypothetical protein	no strong hits	2
P. placenta	90946	Hypothetical protein	no strong hits	5
P. placenta	1141136	Peptidase, Acid	Aspergillopepsin	3

[1]Protein ID numbers from the DOE JGI Mycocosm database (GRIGORIEV *et al.* 2014).

[2]Putative functions determined by BLAST searches of SWISS PROT database (BATEMAN *et al.* 2015).

[3]Number of observations in LC-MS/MS experiment (spectral counts)

Table S7.4: Glycoside hydrolases and carbohydrate esterases found in secretomes of *Gloeophyllum trabeum* on aspen wafers and their expression levels in the interaction zone (IZ) and at the actively growing hyphal front of *G. trabeum* cultures (Gt0-5).

ID[1]	Name[2]	Swiss prot[3]	RPKM IZ	RPKM Gt0-5	Log2 (IZ/Gt-5)	p value	q value
117128	CE 1	Acetyl xylan esterase	72.84	198.89	-1.45	0.09	0.16
46545	CE 15	4-O-methyl-glucuronyl methylesterase	10.75	43.71	-2.02	0.02	0.04
48624	CE 16	Uncharacterized CE 16	52.50	323.17	-2.62	0.03	0.05
56205	CE 16	Uncharacterized CE 16	214.59	374.05	-0.80	0.33	0.42
32318	CE 4	Chitin deacetylase	602.75	722.37	-0.26	0.75	0.80
112531	CE 8	Pectinesterase	289.92	543.26	-0.91	0.28	0.36
140289	GH 10	Endo-β-1,4-xylanase	53.10	98.73	-0.89	0.28	0.36
46499	GH 10	Endo-β-1,4-xylanase	286.22	697.95	-1.29	0.15	0.22
121307	GH 115	no strong hits	208.56	433.95	-1.06	0.19	0.26
121308	GH 115	no strong hits	145.84	286.65	-0.97	0.26	0.34
138821	GH 12	Xyloglucan specific endo-β-1,4-glucanase	38.60	630.53	-4.03	0.00	0.00
61700	GH 15- CBM 20	Glucoamylase, CBM20 domain	50.64	76.25	-0.59	0.49	0.57
52752	GH 16	β-glucan synthesis protein	64.22	104.35	-0.70	0.39	0.47
122074	GH 18	Chitinase	52.40	127.36	-1.28	0.14	0.20
115191	GH 2	β-Mannanase	112.82	282.05	-1.32	0.11	0.18
116582	GH 20	β-N-acetylglucosaminidase	179.72	454.79	-1.34	0.14	0.21
77583	GH 20	β-N-acetylglucosaminidase	36.15	92.35	-1.35	0.14	0.20
117566	GH 27	α-galactosidase	526.99	760.44	-0.53	0.53	0.60
110574	GH 28	Pectinase	268.53	784.22	-1.55	0.06	0.10
120615	GH 28	Pectinase	70.38	153.87	-1.13	0.21	0.28
138836	GH 28	Pectinase	121.24	291.71	-1.27	0.12	0.19
6650	GH 28	Pectinase	77.29	212.37	-1.46	0.08	0.14
69843	GH 3	β-glucosidase	34.34	151.98	-2.15	0.07	0.13
75899	GH 3	β-glucosidase	172.95	322.48	-0.90	0.30	0.39
122002	GH 3	Exo-β-1,4-xylosidase	174.11	362.08	-1.06	0.22	0.30
141329	GH 31	α-xylosidase	143.59	271.27	-0.92	0.27	0.35
111095	GH 35	β-galactosidase	100.18	188.55	-0.91	0.28	0.36
112205	GH 47	Mannosyl oligosaccharide α-1,2-mannosidase	323.39	696.63	-1.11	0.19	0.26
114574	GH 5	Endo-β-1,4-mannanase	144.44	107.21	0.43	0.63	0.70
110405	GH 5	Endo-β-1,4-mannanase	207.09	316.83	-0.61	0.51	0.59
135369	GH 5	Endo-β-1,4-mannanase	154.67	393.86	-1.35	0.21	0.29
63180	GH 5	Endo-β-1,4-glucanase	372.18	925.02	-1.31	0.22	0.30
134804	GH 51	α-arabinofuranosidase	27.16	73.57	-1.44	0.10	0.16
126879	GH 55	Exo-β-1,3-glucosidase	181.07	291.93	-0.69	0.52	0.60

113553	GH 72-CBM 43	β-1,3-glucanosyltransferase	195.01	338.41	-0.80	0.37	0.46
116837	GH 79	β-glucuronidase	49.42	116.63	-1.24	0.17	0.25
81814	GH 92	Glycosidase	40.51	68.76	-0.76	0.38	0.47

[1]Protein ID numbers from the DOE JGI Mycocosm database (GRIGORIEV *et al.* 2014), alleles are listed in red italics under its pair.

[2]Carbohydrate esterase (CE) and glycoside hydrolase (GH) families as defined in the CAZy database (LOMBARD *et al.* 2014).

[3]Putative functions determined by BLAST searches of SWISS PROT database (BATEMAN *et al.* 2015).

Table S7.5: Glycoside hydrolases and carbohydrate esterases found in secretomes of *Gloeophyllum trabeum* on aspen wafers and their expression levels in the interaction zone (IZ) and in *G. trabeum* hyphae 5 mm outside the interaction (Gt-5).

ID[1]	Name[2]	Swiss prot[3]	RPKM Gt-5	RPKM IZ	Log_2(IZ/Gt-5)	p value	q value
117128	CE 1	Acetyl xylan esterase	2269.23	72.84	-4.96	0.00	0.00
46545	CE 15	4-O-methyl-glucuronyl methylesterase	206.39	10.75	-4.26	0.00	0.00
48624	CE 16	Uncharacterized CE 16	1859.85	52.50	-5.15	0.00	0.00
56205	CE 16	Uncharacterized CE 16	2522.71	214.59	-3.56	0.00	0.00
32318	CE 4	Chitin deacetylase	1283.74	602.75	-1.09	0.25	0.33
112531	CE 8	Pectinesterase	954.52	289.92	-1.72	0.06	0.10
140289	GH 10	Endo-β-1,4-xylanase	201.13	53.10	-1.92	0.10	0.16
46499	GH 10	Endo-β-1,4-xylanase	3116.71	286.22	-3.44	0.00	0.00
121307	GH 115	no strong hits	189.00	208.56	0.14	0.87	0.90
121308	GH 115	no strong hits	1195.17	145.84	-3.03	0.00	0.00
138821	GH 12	Xyloglucan specific endo-β-1,4-glucanase	2681.53	38.60	-6.12	0.00	0.00
61700	GH 15-CBM 20	Glucoamylase, CBM20 domain	133.45	50.64	-1.40	0.15	0.22
52752	GH 16	β-glucan synthesis protein	154.04	64.22	-1.26	0.23	0.31
122074	GH 18	Chitinase	301.81	52.40	-2.53	0.01	0.01
115191	GH 2	β-Mannanase	671.19	112.82	-2.57	0.01	0.01
116582	GH 20	β-N-acetylglucosaminidase	1142.88	179.72	-2.67	0.01	0.02
77583	GH 20	β-N-acetylglucosaminidase	89.44	36.15	-1.31	0.19	0.27
117566	GH 27	α-galactosidase	2774.45	526.99	-2.40	0.01	0.02
110574	GH 28	Pectinase	985.55	268.53	-1.88	0.04	0.06

120615	GH 28	Pectinase	146.11	70.38	-1.05	0.47	0.55
138836	GH 28	Pectinase	867.03	121.24	-2.84	0.00	0.01
6650	GH 28	Pectinase	263.06	77.29	-1.77	0.07	0.12
69843	GH 3	β-glucosidase	1218.55	34.34	-5.15	0.00	0.01
75899	GH 3	β-glucosidase	1495.82	172.95	-3.11	0.02	0.04
122002	GH 3	Exo-β-1,4-xylosidase	1894.37	174.11	-3.44	0.00	0.00
141329	GH 31	α-xylosidase	552.41	143.59	-1.94	0.04	0.07
111095	GH 35	β-galactosidase	283.96	100.18	-1.50	0.12	0.19
112205	GH 47	α-1,2-mannosidase	1482.78	323.39	-2.20	0.02	0.04
114574	GH 5	Endo-β-1,4-mannanase	296.39	144.44	-1.04	0.30	0.38
110405	GH 5	Endo-β-1,4-mannanase	2361.21	207.09	-3.51	0.00	0.01
135369	GH 5	Endo-β-1,4-mannanase	2305.82	154.67	-3.90	0.01	0.02
63180	GH 5	Endo-β-1,4-glucanase	1111.49	372.18	-1.58	0.18	0.25
134804	GH 51	α-arabinofuranosidase	163.91	27.16	-2.59	0.01	0.02
126879	GH 55	Exo-β-1,3-glucosidase	728.58	181.07	-2.01	0.13	0.20
113553	GH 72-CBM43	β-1,3-glucanosyltransferase	925.82	195.01	-2.25	0.03	0.05
116837	GH 79	β-glucuronidase	453.76	49.42	-3.20	0.00	0.00
81814	GH 92	Glycosidase	197.26	40.51	-2.28	0.02	0.04

[1]Protein ID numbers from the DOE JGI Mycocosm database (GRIGORIEV *et al.* 2014), alleles are listed in red italics under its pair.

[2]Carbohydrate esterase (CE) and glycoside hydrolase (GH) families as defined in the CAZy database (LOMBARD *et al.* 2014).

[3]Putative functions determined by BLAST searches of SWISS PROT database (BATEMAN *et al.* 2015).

Table S7.6: Glycoside hydrolases and carbohydrate esterases found in secretomes of *Postia placenta* on aspen wafers and their expression levels in the interaction zone (IZ) and at the actively growing hyphal front of *P. placenta* cultures (Pp0-5).

Protein ID[1]	Name[2]	Swiss prot[3]	RPKM IZ	RPKM Pp0-5	Log_2(IZ/Pp0-5)	p value	q value
20448	CE 10	Lipase	3.06	7.54	-1.30	0.20	0.28
50078	CE 10	Lipase	3.64	5.91	-0.70	0.47	0.56
125801	CE 16	Carboxylesterase	197.41	636.49	-1.69	0.11	0.18
108959	CE 16	Carboxylesterase	53.32	252.08	-2.24	0.06	0.10
106710	CE 16	no strong hits	100.26	357.77	-1.84	0.09	0.15
113670	GH 10	Endo-β-1,4-xylanase	22.07	53.37	-1.27	0.21	0.29
112658	GH 12	Endo-β-1,4-glucanase	7.29	119.36	-4.03	0.00	0.00
121191	GH 12	Endo-β-1,4-glucanase	20.47	215.79	-3.40	0.01	0.03
113112	GH 15	Glucoamylase	32.63	43.73	-0.42	0.68	0.74

117345	GH 15	Glucoamylase	31.36	45.21	-0.53	0.59	0.67
116903	GH 16	Endo-β-1,3(4)-glucanase	114.92	103.07	0.16	0.88	0.91
128334	GH 16	Endo-β-1,3(4)-glucanase	118.65	114.80	0.05	0.96	0.97
112941	GH 16	Endo-β-1,3(4)-glucanase	173.55	193.81	-0.16	0.87	0.90
61809	GH 16	Endo-β-1,3(4)-glucanase	60.02	33.25	0.85	0.37	0.46
54949	GH 16	β-glucan synthesis protein	7.50	15.15	-1.01	0.34	0.42
44128	GH 18	Chitinase	13.21	12.84	0.04	0.96	0.97
53332	GH 18	Chitinase	17.78	15.64	0.18	0.88	0.90
128150	GH 27	α-galactosidase	54.98	165.15	-1.59	0.14	0.21
98662	GH 27	α-galactosidase	96.59	245.62	-1.35	0.20	0.28
111730	GH 28	Pectinase	10.46	293.31	-4.81	0.00	0.00
43189	GH 28	Pectinase	165.51	1311.10	-2.99	0.01	0.03
107557	GH 3	β-glucosidase	182.14	570.31	-1.65	0.21	0.29
115593	GH 47	α-1,2-mannosidase	75.87	284.80	-1.91	0.07	0.13
46679	GH 47	α-1,2-mannosidase	67.49	263.88	-1.97	0.07	0.12
103675	GH 5	Endoglucanase	54.26	237.64	-2.13	0.05	0.09
117690	GH 5	Endoglucanase	55.24	215.47	-1.96	0.07	0.13
95568	GH 5	Endo-β-1,4-mannosidase	68.71	259.93	-1.92	0.08	0.13
115648	GH 5	Endoglucanase	409.80	728.26	-0.83	0.40	0.48
108962	GH 5	Endoglucanase	17.79	63.00	-1.82	0.09	0.15
121831	GH 5	Endo-β-1,4-mannanase	172.17	393.80	-1.19	0.24	0.32
134772	GH 5	Endo-β-1,4-mannanase	#N/A	#N/A	#N/A	#N/A	#N/A
100251	GH 51	α-arabinofuranosidase	31.65	69.74	-1.14	0.28	0.36
108648	GH 55	Exo-β-1,3-glucanase	40.74	50.43	-0.31	0.81	0.85
105490	GH 55	Endo-β-1,3-glucanase	0.36	0.38	-0.09	1.00	1.00
119394	GH 55	Exo-β-1,3-glucanase	93.97	30.67	1.62	0.11	0.18
111332	GH 79	β-glucuronidase	27.56	95.77	-1.80	0.09	0.16

[1]Protein ID numbers from the DOE JGI Mycocosm database (GRIGORIEV *et al.* 2014), alleles are listed in red italics under its pair.

[2]Carbohydrate esterase (CE) and glycoside hydrolase (GH) families as defined in the CAZy database (LOMBARD *et al.* 2014).

[3]Putative functions determined by BLAST searches of SWISS PROT database (BATEMAN *et al.* 2015).

Table S7.7: Glycoside hydrolases and carbohydrate esterases found in secretomes of *Postia placenta* on aspen wafers and their expression levels in the interaction zone (IZ) and in *P. placenta* hyphae 5 mm outside the interaction (Pp-5).

Protein ID[1]	Name[2]	Swiss prot[3]	RPKM IZ	RPKM Pp-5	Log_2(IZ/Pp-5)	p_value	q_value
20448	CE 10	Lipase	3.06	58.29	-4.25	0.01	0.01
50078	CE 10	Lipase	3.64	71.78	-4.30	0.00	0.01
125801	CE 16	Carboxylesterase	197.41	5785.33	-4.87	0.00	0.01
108959	CE 16	Carboxylesterase	53.32	2245.00	-5.40	0.00	0.00
106710	CE 16	No strong hits	100.26	3209.47	-5.00	0.00	0.00
113670	GH 10	Endo-β-1,4-xylanase	22.07	764.04	-5.11	0.00	0.00
112658	GH 12	Endo-β-1,4-glucanase	7.29	645.32	-6.47	0.00	0.00
121191	GH 12	Endo-β-1,4-glucanase	20.47	1491.89	-6.19	0.00	0.00
113112	GH 15	Glucoamylase	32.63	255.57	-2.97	0.03	0.06
117345	GH 15	Glucoamylase	31.36	67.80	-1.11	0.40	0.48
116903	GH 16	Endo-β-1,3(4)-glucanase	114.92	287.28	-1.32	0.33	0.42
128334	GH 16	Endo-β-1,3(4)-glucanase	118.65	540.79	-2.19	0.11	0.18
112941	GH 16	Endo-β-1,3(4)-glucanase	173.55	915.19	-2.40	0.06	0.11
61809	GH 16	Endo-β-1,3(4)-glucanase	60.02	385.68	-2.68	0.04	0.08
54949	GH 16	β-glucan synthesis protein	7.50	124.87	-4.06	0.01	0.02
44128	GH 18	Chitinase	13.21	188.40	-3.83	0.01	0.02
53332	GH 18	Chitinase	17.78	222.48	-3.65	0.01	0.02
128150	GH 27	α-galactosidase	54.98	1032.60	-4.23	0.01	0.01
98662	GH 27	α-galactosidase	96.59	1921.19	-4.31	0.00	0.01
111730	GH 28	Pectinase	10.46	4.29	1.29	0.31	0.40
43189	GH 28	Pectinase	165.51	83.91	0.98	0.48	0.56
107557	GH 3	β-glucosidase	182.14	4240.92	-4.54	0.00	0.00
115593	GH 47	α-1,2-mannosidase	75.87	455.87	-2.59	0.05	0.09
46679	GH 47	α-1,2-mannosidase	67.49	360.79	-2.42	0.07	0.12
103675	GH 5	Endoglucanase	54.26	2550.33	-5.55	0.00	0.00
117690	GH 5	Endoglucanase	55.24	1781.16	-5.01	0.00	0.00
95568	GH 5	Endo-β-1,4-mannosidase	68.71	2024.03	-4.88	0.00	0.00
115648	GH 5	Endoglucanase	409.80	13777.20	-5.07	0.00	0.00
108962	GH 5	Endoglucanase	17.79	559.44	-4.97	0.00	0.00
121831	GH 5	Endo-β-1,4-mannanase	172.17	3451.12	-4.33	0.00	0.01
134772	GH 5	Endo-β-1,4-mannanase	#N/A	#N/A	#N/A	#N/A	#N/A

100251	GH 51	α-arabinofuranosidase	31.65	283.94	-3.17	0.03	0.05
108648	GH 55	Exo-β-1,3-glucanase	40.74	297.09	-2.87	0.03	0.06
105490	GH 55	Endo-β-1,3-glucanase	0.36	6.07	-4.07	0.01	0.02
119394	GH 55	Exo-β-1,3-glucanase	93.97	455.51	-2.28	0.08	0.13
111332	GH 79	β-glucuronidase	27.56	1184.16	-5.43	0.00	0.00

[1]Protein ID numbers from the DOE JGI Mycocosm database (GRIGORIEV *et al.* 2014), alleles are listed in red italics under its pair.

[2]Carbohydrate esterase (CE) and glycoside hydrolase (GH) families as defined in the CAZy database (LOMBARD *et al.* 2014).

[3]Putative functions determined by BLAST searches of SWISS PROT database (BATEMAN *et al.* 2015).

Bibliography

A'BEAR, A. D., T. H. JONES, E. KANDELER and L. BODDY, 2014 Interactive effects of temperature and soil moisture on fungal-mediated wood decomposition and extracellular enzyme activity. Soil Biology & Biochemistry **70:** 151-158.

ACEBES, S., F. J. RUIZ-DUENAS, M. TOUBES, V. SAEZ-JIMENEZ, M. PEREZ-BOADA *et al.*, 2017 Mapping the long-range electron transfer route in ligninolytic peroxidases. Journal of Physical Chemistry B **121:** 3946-3954.

ALFARO, M., J. A. OGUIZA, L. RAMIREZ and A. G. PISABARRO, 2014 Comparative analysis of secretomes in basidiomycete fungi. Journal of Proteomics **102:** 28-43.

AN, H. D., T. T. XIAO, H. FAN and D. S. WEI, 2015 Molecular characterization of a novel thermostable laccase PPLCC2 from the brown rot fungus *Postia placenta* MAD-698-R. Electronic Journal of Biotechnology **18:** 451-458.

ARANTES, V., Y. H. QIAN, A. M. F. MILAGRES, J. JELLISON and B. GOODELL, 2009 Effect of pH and oxalic acid on the reduction of Fe^{3+} by a biomimetic chelator and on Fe^{3+} desorption/adsorption onto wood: Implications for brown-rot decay. International Biodeterioration & Biodegradation **63:** 478-483.

ARFI, Y., A. LEVASSEUR and E. RECORD, 2013 Differential gene expression in *Pycnoporus coccineus* during interspecific mycelial interactions with different competitors. Applied and Environmental Microbiology **79:** 6626-6636.

ASPEBORG, H., P. M. COUTINHO, Y. WANG, H. BRUMER and B. HENRISSAT, 2012 Evolution, substrate specificity and subfamily classification of glycoside hydrolase family 5 (GH5). BMC Evolutionary Biology **12**.

ATANASOVA, L., S. LE CROM, S. GRUBER, F. COULPIER, V. SEIDL-SEIBOTH *et al.*, 2013 Comparative transcriptomics reveals different strategies of *Trichoderma* mycoparasitism. BMC Genomics **14**.

BAI, Z., Q. MA, Y. C. DAI, H. S. YUAN, J. YE *et al.*, 2017 Spatial heterogeneity of SOM concentrations associated with white-rot versus brown-rot wood decay. Scientific Reports **7**.

BALDRIAN, P., 2004 Increase of laccase activity during interspecific interactions of white-rot fungi. FEMS Microbiology Ecology **50:** 245-253.

BALDRIAN, P., 2006 Fungal laccases - occurrence and properties. FEMS Microbiology Reviews **30:** 215-242.

BALDRIAN, P., and V. VALASKOVA, 2008 Degradation of cellulose by basidiomycetous fungi. FEMS Microbiology Reviews **32:** 501-521.

BARDGETT, R. D., C. FREEMAN and N. J. OSTLE, 2008 Microbial contributions to climate change through carbon cycle feedbacks. ISME Journal **2:** 805-814.

BATEMAN, A., M. J. MARTIN, C. O'DONOVAN, M. MAGRANE, R. APWEILER *et al.*, 2015 UniProt: A hub for protein information. Nucleic Acids Research **43:** D204-D212.

BAYRY, J., V. AIMANIANDA, J. I. GUIJARRO, M. SUNDE and J. P. LATGE, 2012 Hydrophobins-Unique fungal proteins. Plos Pathogens **8**.

BEESON, W. T., C. M. PHILLIPS, J. H. D. CATE and M. A. MARLETTA, 2012 Oxidative cleavage of cellulose by fungal copper-dependent polysaccharide monooxygenases. Journal of the American Chemical Society **134:** 890-892.

BIELY, P., 2012 Microbial carbohydrate esterases deacetylating plant polysaccharides. Biotechnology Advances **30:** 1575-1588.

BIELY, P., S. SINGH and V. PUCHART, 2016 Towards enzymatic breakdown of complex plant xylan structures: State of the art. Biotechnology Advances **34:** 1260-1274.

BIELY, P., M. VRSANSKA, M. TENKANEN and D. KLUEPFEL, 1997 Endo-beta-1,4-xylanase families: Differences in catalytic properties. Journal of Biotechnology **57:** 151-166.

BLANCHETTE, R. A., 1980 Wood Decay - A Sub-Microscopic View. Journal of Forestry **78:** 734-737.

BLANCHETTE, R. A., 1991 Delignification by wood-decay fungi. Annual Review of Phytopathology **29:** 381-398.

BLANCHETTE, R. A., 1995 Degradation of the lignocellulose complex in wood. Canadian Journal of Botany-Revue Canadienne De Botanique **73:** S999-S1010.

BODDY, L., 2000 Interspecific combative interactions between wood-decaying basidiomycetes. FEMS Microbiology Ecology **31:** 185-194.

BODDY, L., and J. HEILMANN-CLAUSEN, 2008 Basidiomycete community development in temperate angiosperm wood, pp. 211-237 in *Ecology of Saprotrophic Basidiomycetes*, edited by L. BODDY, J. C. FRANKLAND and P. VANWEST.

BODDY, L., and J. HISCOX, 2016 Fungal ecology: Principles and mechanisms of colonization and competition by saprotrophic fungi. Microbiology Spectrum **4**.

BORNSCHEUER, U., K. BUCHHOLZ and J. SEIBEL, 2014 Enzymatic degradation of (ligno) cellulose. Angewandte Chemie-International Edition **53:** 10876-10893.

BOURBONNAIS, R., and M. G. PAICE, 1990 Oxidation of non-phenolic substrates - An expanded role for laccase in lignin biodegradation. FEBS Letters **267:** 99-102.

BOVI, M., L. CENCI, M. PERDUCA, S. CAPALDI, M. E. CARRIZO *et al.*, 2013 BEL beta-trefoil: A novel lectin with antineoplastic properties in king bolete (*Boletus edulis*) mushrooms. Glycobiology **23:** 578-592.

BRANDENBURGER, E., D. BRAGA, A. KOMBRINK, G. LACKNER, J. GRESSLER *et al.*, 2016 Multi-genome analysis identifies functional and phylogenetic diversity of basidiomycete adenylate-forming reductases. Fungal Genetics and Biology **ePub ahead of print**.

BRUNOW, G., I. KILPELAINEN, J. SIPILA, K. SYRJANEN, P. KARHUNEN *et al.*, 1998 Oxidative coupling of phenols and the biosynthesis of lignin in *Lignin and Lignin Biosynthesis* edited by N. G. LEWIS and S. SARKANEN. Oxford University Press, Oxford.

BUGG, T. D. H., M. AHMAD, E. M. HARDIMAN and R. RAHMANPOUR, 2011 Pathways for degradation of lignin in bacteria and fungi. Natural Product Reports **28:** 1883-1896.

CAI, H., J. B. DUNN, Z. C. WANG, J. HAN and M. Q. WANG, 2013 Life-cycle energy use and greenhouse gas emissions of production of bioethanol from sorghum in the United States. Biotechnology for Biofuels **6**.

CAMARERO, S., S. SARKAR, F. J. RUIZ-DUENAS, M. J. MARTINEZ and A. T. MARTINEZ, 1999 Description of a versatile peroxidase involved in the natural degradation of

lignin that has both manganese peroxidase and lignin peroxidase substrate interaction sites. Journal of Biological Chemistry **274:** 10324-10330.

CHAPELA, I. H., and L. BODDY, 1988 The fate of early fungal colonizers in beech branches decomposing on the forest floor. FEMS Microbiology Ecology **53:** 273-283.

CHOAT, B., A. R. COBB and S. JANSEN, 2008 Structure and function of bordered pits: New discoveries and impacts on whole-plant hydraulic function. New Phytologist **177:** 608-625.

COHEN, R., M. R. SUZUKI and K. E. HAMMEL, 2004 Differential stress-induced regulation of two quinone reductases in the brown rot basidiomycete *Gloeophyllum trabeum*. Applied and Environmental Microbiology **70:** 324-331.

CORDERO, R. J. B., and A. CASADEVALL, 2017 Functions of fungal melanin beyond virulence. Fungal Biology Reviews **31:** 99-112.

COWLING, E. B., 1961 Comparative biochemistry of the decay of sweetgum sapwood by white-rot and brown-rot fungi, pp. in *United States Forest Service Technical Bulletin*.

CREPIN, V. F., C. B. FAULDS and I. F. CONNERTON, 2003 A non-modular type B feruloyl esterase from *Neurospora crassa* exhibits concentration-dependent substrate inhibition. Biochemical Journal **370:** 417-427.

CROWTHER, T. W., L. BODDY and D. S. MAYNARD, 2017 The use of aritificial media in fungal ecology. Fungal Ecology **In Press:** 1-5.

DANIEL, G., J. VOLC, L. FILONOVA, O. PLIHAL, E. KUBATOVA *et al.*, 2007 Characteristics of *Gloeophyllum trabeum* alcohol oxidase, an extracellular source of H_2O_2 in brown rot decay of wood. Applied and Environmental Microbiology **73:** 6241-6253.

DANIEL, G., J. VOLC and E. KUBATOVA, 1994 Pyranose oxidase, A major source of H2O2 during wood degradation by *Phanerochaete-chrysosporium*, *Trametes-versicolor*, and *Oudemansiella-mucida*. Applied and Environmental Microbiology **60:** 2524-2532.

DIAZ-CHAVEZ, R., and C. JAMIESON, 2010 Biofuels possibilities in the southern Africa context. Journal of Biobased Materials and Bioenergy **4:** 256-266.

DICK-PEREZ, M., Y. A. ZHANG, J. HAYES, A. SALAZAR, O. A. ZABOTINA *et al.*, 2011 Structure and interactions of plant cell-wall polysaccharides by two- and three-dimensional magic-angle-spinning solid-state NMR. Biochemistry **50:** 989-1000.

DIXON, R. K., S. BROWN, R. A. HOUGHTON, A. M. SOLOMON, M. C. TREXLER *et al.*, 1994 Carbon pools and flux of global forest ecosystems. Science **263:** 185-190.

DUTTON, M. V., M. KATHIARA, I. M. GALLAGHER and C. S. EVANS, 1994 Purification and characterization of oxalate decarboxylase from *Coriolus versicolor*. FEMS Microbiology Letters **116:** 321-325.

EASTWOOD, D. C., D. FLOUDAS, M. BINDER, A. MAJCHERCZYK, P. SCHNEIDER *et al.*, 2011 The plant cell wall-decomposing machinery underlies the functional diversity of forest fungi. Science **333:** 762-765.

EL ARIEBI, N., J. HISCOX, S. A. SCRIVEN, C. T. MULLER and L. BODDY, 2016 Production and effects of volatile organic compounds during interspecific interactions. Fungal Ecology **20:** 144-154.

ELLSTROM, M., F. SHAH, T. JOHANSSON, D. AHREN, P. PERSSON *et al.*, 2015 The carbon starvation response of the ectomycorrhizal fungus *Paxillus involutus*. FEMS Microbiology Ecology **91**.

ERIKSSON, K. E., R. A. BLANCHETTE and P. ANDER, 1990 *Microbial and enzymatic degradation of wood and wood components*. Springer-Verlag, Berlin.

EVANS, J. A., C. A. EYRE, H. J. ROGERS, L. BODDY and C. T. MULLER, 2008 Changes in volatile production during interspecific interactions between four wood rotting fungi growing in artificial media. Fungal Ecology **1:** 57-68.

EYRE, C., W. MUFTAH, J. HISCOX, J. HUNT, P. KILLE *et al.*, 2010 Microarray analysis of differential gene expression elicited in *Trametes versicolor* during interspecific mycelial interactions. Fungal Biology **114:** 646-660.

FERNANDES, A. N., L. H. THOMAS, C. M. ALTANER, P. CALLOW, V. T. FORSYTH *et al.*, 2011 Nanostructure of cellulose microfibrils in spruce wood. Proceedings of the

National Academy of Sciences of the United States of America **108:** E1195-E1203.

FERNANDEZ-FUEYO, E., F. J. RUIZ-DUENAS, M. F. LOPEZ-LUCENDO, M. PEREZ-BOADA, J. RENCORET *et al.*, 2016 A secretomic view of woody and nonwoody lignocellulose degradation by *Pleurotus ostreatus*. Biotechnology for Biofuels **9**.

FILLEY, T. R., G. D. CODY, B. GOODELL, J. JELLISON, C. NOSER *et al.*, 2002 Lignin demethylation and polysaccharide decomposition in spruce sapwood degraded by brown rot fungi. Organic Geochemistry **33:** 111-124.

FLOUDAS, D., M. BINDER, R. RILEY, K. BARRY, R. A. BLANCHETTE *et al.*, 2012 The paleozoic origin of enzymatic lignin decomposition reconstructed from 31 fungal genomes. Science **336:** 1715-1719.

FLOURNOY, D. S., T. K. KIRK and T. L. HIGHLEY, 1991 Wood decay by brown-rot fungi - Changes in pore structure and cell-wall volume. Holzforschung **45:** 383-388.

FROMMHAGEN, M., S. K. MUTTE, A. H. WESTPHAL, M. J. KOETSIER, S. W. A. HINZ *et al.*, 2017 Boosting LPMO-driven lignocellulose degradation by polyphenol oxidase-activated lignin building blocks. Biotechnology for Biofuels **10**.

FUKAZAWA, K., J. F. REVOL, L. JURASEK and D. A. I. GORING, 1982 Relationship between ball milling and the susceptibility of wood to digestion by cellulase. Wood Science and Technology **16:** 279-285.

GARRON, M. L., and M. CYGLER, 2010 Structural and mechanistic classification of uronic acid-containing polysaccharide lyases. Glycobiology **20:** 1547-1573.

GASKELL, J., R. A. BLANCHETTE, P. E. STEWART, S. S. BONDURANT, M. ADAMS *et al.*, 2016 Transcriptome and secretome analyses of the wood decay fungus *Wolfiporia cocos* support alternative mechanisms of lignocellulose conversion. Applied and Environmental Microbiology **82:** 3979-3987.

GASPARATOS, A., G. P. VON MALTITZ, F. X. JOHNSON, L. LEE, M. MATHAI *et al.*, 2015 Biofuels in sub-Saharan Africa: Drivers, impacts and priority policy areas. Renewable & Sustainable Energy Reviews **45:** 879-901.

GHOSE, T. K., 1987 Measurement of cellulase activities. Pure and Applied Chemistry **59:** 257-268.

GILBERTSON, R. L., and L. RYVARDEN, 1986 *North American Polypores* Fungiflora, Oslo, Norway.

GOODELL, B., Y. ZHU, S. KIM, K. KAFLE, D. EASTWOOD *et al.*, 2017 Modification of the nanostructure of lignocellulose cell walls via a non-enzymatic lignocellulose deconstruction system in brown rot wood-decay fungi. Biotechnology for Biofuels **10**.

GREEN, F., M. J. LARSEN, J. E. WINANDY and T. L. HIGHLEY, 1991 Role of oxalic-acid in incipient brown-rot decay. Material Und Organismen **26:** 191-213.

GRIGORIEV, I. V., R. NIKITIN, S. HARIDAS, A. KUO, R. OHM *et al.*, 2014 MycoCosm portal: Gearing up for 1000 fungal genomes. Nucleic Acids Research **42:** D699-D704.

GUILLEN, F., and C. S. EVANS, 1994 Anisaldehyde and Veratraldehyde Acting as Redox Cycling Agents for H_2O_2 Production by *Pleurotus eryngii*. Applied and Environmental Microbiology **60:** 2811-2817.

GUILLEN, F., A. T. MARTINEZ and M. J. MARTINEZ, 1990 Production of hydrogen-peroxide by aryl alcohol oxidase from the ligninolytic fungus *Pleurotus eryngii*. Applied Microbiology and Biotechnology **32:** 465-469.

GUPTA, A., and J. P. VERMA, 2015 Sustainable bio-ethanol production from agro-residues: A review. Renewable & Sustainable Energy Reviews **41:** 550-567.

GUTIERREZ, A., L. CARAMELO, A. PRIETO, M. J. MARTINEZ and A. T. MARTINEZ, 1994 Anisaldehyde production and aryl alcohol oxidase and dehydrogenase-activities in ligninolytic fungi of the genus *Pleurotus*. Applied and Environmental Microbiology **60:** 1783-1788.

HALTRICH, D., B. NIDETZKY, K. D. KULBE, W. STEINER and S. ZUPANCIC, 1996 Production of fungal xylanases. Bioresource Technology **58:** 137-161.

HAMMEL, K. E., and D. CULLEN, 2008 Role of fungal peroxidases in biological ligninolysis. Current Opinion in Plant Biology **11:** 349-355.

HAN, J. J., L. BAO, Q. Q. TAO, Y. J. YAO, X. Z. LIU *et al.*, 2015 Gloeophyllins A-J, Cytotoxic ergosteroids with various skeletons from a chinese tibet fungus *Gloeophyllum abietinum*. Organic Letters **17:** 2538-2541.

HARMAN, G. E., C. R. HOWELL, A. VITERBO, I. CHET and M. LORITO, 2004 *Trichoderma* species - Opportunistic, avirulent plant symbionts. Nature Reviews Microbiology **2:** 43-56.

HATAKKA, A., and K. E. HAMMEL, 2010 Fungal biodegradation of lignocelluloses, pp. 319-340 in *Mycota: Industrial Applications, Vol 10, Second Edition*, edited by M. HOFRICHTER.

HEILMANN-CLAUSEN, J., and L. BODDY, 2005 Inhibition and stimulation effects in communities of wood decay fungi: Exudates from colonized wood influence growth by other species. Microbial Ecology **49:** 399-406.

HENRIKSSON, G., G. JOHANSSON and G. PETTERSSON, 2000 A critical review of cellobiose dehydrogenases. Journal of Biotechnology **78:** 93-113.

HERNANDEZ-ORTEGA, A., P. FERREIRA and A. T. MARTINEZ, 2012 Fungal aryl alcohol oxidase: A peroxide-producing flavoenzyme involved in lignin degradation. Applied Microbiology and Biotechnology **93:** 1395-1410.

HIBBETT, D. S., and M. J. DONOGHUE, 2001 Analysis of character correlations among wood decay mechanisms, mating systems, and substrate ranges in homobasidiomycetes. Systematic Biology **50:** 215-242.

HIGHLEY, T. L., 1973a Influence of carbon source on cellulase acitvity of white-rot and brown-rot fungi. Wood and Fiber **5**.

HIGHLEY, T. L., 1973b Influence of carbon source on cellulase activity of white-rot and brown-rot fungi. Wood Fiber **5:** 50-58.

HIGHLEY, T. L., 1987 Changes in Chemical-Components of Hardwood and Softwood by Brown Rot Fungi. Material Und Organismen **22:** 39-45.

HILDEN, K., M. R. MAKELA, K. T. STEFFEN, M. HOFRICHTER, A. HATAKKA *et al.*, 2014 Biochemical and molecular characterization of an atypical manganese peroxidase of the litter-decomposing fungus *Agrocybe praecox*. Fungal Genetics and Biology **72:** 131-136.

HIMMEL, M. E., 2008 *Biomass recalcitrance*. Blackwell Publishing Oxford, UK.

HISCOX, J., P. BALDRIAN, H. J. ROGERS and L. BODDY, 2010 Changes in oxidative enzyme activity during interspecific mycelial interactions involving the white-rot fungus *Trametes versicolor*. Fungal Genetics and Biology **47:** 562-571.

HISCOX, J., and L. BODDY, 2017 Armed and dangerous - Chemical warfare in wood decay communities. Fungal Biology Reviews **31:** 169-184.

HISCOX, J., M. SAVOURY, C. T. MULLER, B. D. LINDAHL, H. J. ROGERS *et al.*, 2015a Priority effects during fungal community establishment in beech wood. ISME Journal **9:** 2246-2260.

HISCOX, J., M. SAVOURY, I. P. VAUGHAN, C. T. MULLER and L. BODDY, 2015b Antagonistic fungal interactions influence carbon dioxide evolution from decomposing wood. Fungal Ecology **14:** 24-32.

HOFRICHTER, M., R. ULLRICH, M. J. PECYNA, C. LIERS and T. LUNDELL, 2010 New and classic families of secreted fungal heme peroxidases. Applied Microbiology and Biotechnology **87:** 871-897.

HOLMER, L., and J. STENLID, 1997 Competitive hierarchies of wood decomposing basidiomycetes in artificial systems based on variable inoculum sizes. Oikos **79:** 77-84.

HORI, C., J. GASKELL, K. IGARASHI, P. KERSTEN, M. MOZUCH *et al.*, 2014 Temporal alterations in the secretome of the selective ligninolytic fungus *Ceriporiopsis subvermispora* during growth on aspen wood reveal this organism's strategy for degrading lignocellulose. Applied and Environmental Microbiology **80:** 2062-2070.

HRYCAY, E. G., and S. M. BANDIERA, 2015 Monooxygenase, peroxidase and peroxygenase properties and reaction mechanisms of cytochrome P450 enzymes, pp. 1-61 in *Monooxygenase, Peroxidase and Peroxygenase Properties and Mechanisms of Cytochrome P450*, edited by E. G. HRYCAY and S. M. BANDIERA.

HUNT, C., W. KENEALY, E. HORN and C. HOUTMAN, 2004 A biopulping mechanism: Creation of acid groups on fiber. Holzforschung **58:** 434-439.

HUNT, C. G., C. J. HOUTMAN, D. C. JONES, P. KITIN, P. KORRIPALLY *et al.*, 2013 Spatial mapping of extracellular oxidant production by a white rot basidiomycete on

wood reveals details of ligninolytic mechanism. Environmental Microbiology **15:** 956-966.

HYDE, S. M., and P. M. WOOD, 1997 A mechanism for production of hydroxyl radicals by the brown-rot fungus *Coniophora puteana*: Fe(III) reduction by cellobiose dehydrogenase and Fe(II) oxidation at a distance from the hyphae. Microbiology-Uk **143:** 259-266.

HYNES, J., C. T. MULLER, T. H. JONES and L. BODDY, 2007 Changes in volatile production during the course of fungal mycelial interactions between *Hypholoma fasciculare* and *Resinicium bicolor*. Journal of Chemical Ecology **33:** 43-57.

IAKOVLEV, A., and J. STENLID, 2000 Spatiotemporal patterns of laccase activity in interacting mycelia of wood-decaying basidiomycete fungi. Microbial Ecology **39:** 236-245.

IMANAKA, H., S. TANAKA, B. FENG, K. IMAMURA and K. NAKANISHI, 2010 Cultivation characteristics and gene expression profiles of *Aspergillus oryzae* by membrane-surface liquid culture, shaking-flask culture, and agar-plate culture. Journal of Bioscience and Bioengineering **109:** 267-273.

INBAR, J., A. MENENDEZ and I. CHET, 1996 Hyphal interaction between *Trichoderma harzianum* and *Sclerotinia sclerotiorum* and its role in biological control. Soil Biology & Biochemistry **28:** 757-763.

JAQUET, F., R. HUTTER and P. LUTHY, 1987 Specificity of *Bacillus thuringiensis* Delta-Endotoxin. Applied and Environmental Microbiology **53:** 500-504.

JENNINGS, D. H., and A. F. BRAVERY, 1991 *Serpula Lacrymans: Fundamental Biology and Control Strategies*. Wiley.

JENSEN, K. A., C. J. HOUTMAN, Z. C. RYAN and K. E. HAMMEL, 2001 Pathways for extracellular fenton chemistry in the brown rot basidiomycete *Gloeophyllum trabeum*. Applied and Environmental Microbiology **67:** 2705-2711.

JONSSON, L. J., and C. MARTIN, 2016 Pretreatment of lignocellulose: Formation of inhibitory by-products and strategies for minimizing their effects. Bioresource Technology **199:** 103-112.

JORDAN, C. R., W. V. DASHEK and T. L. HIGHLEY, 1996 Detection and quantification of oxalic acid from the brown-rot decay fungus, *Postia placenta*. Holzforschung **50:** 312-318.

JORGENSEN, E., and K. VEJLBY, 1953 A new polyphenol oxidase test. Physiologia Plantarum **6**.

KAFFENBERGER, J. T., and J. S. SCHILLING, 2013 Using a grass substrate to compare decay among two clades of brown rot fungi. Applied Microbiology and Biotechnology **97:** 8831-8840.

KAFFENBERGER, J. T., and J. S. SCHILLING, 2015 Comparing lignocellulose physiochemistry after decomposition by brown rot fungi with distinct evolutionary origins. Environmental Microbiology **17:** 4885-4897.

KALB, D., G. LACKNER and D. HOFFMEISTER, 2013 Fungal peptide synthetases: An update on functions and specificity signatures. Fungal Biology Reviews **27:** 43-50.

KAPICH, A. N., K. A. JENSEN and K. E. HAMMEL, 1999 Peroxyl radicals are potential agents of lignin biodegradation. FEBS Letters **461:** 115-119.

KARLSSON, M., J. STENLID and B. LINDAHL, 2016 Functional differentiation of chitinases in the white-rot fungus *Phanerochaete chrysosporium*. Fungal Ecology **22:** 52-60.

KEREM, Z., K. A. JENSEN and K. E. HAMMEL, 1999 Biodegradative mechanism of the brown rot basidiomycete *Gloeophyllum trabeum*: Evidence for an extracellular hydroquinone-driven fenton reaction. FEBS Letters **446:** 49-54.

KERSTEN, P., and D. CULLEN, 2014 Copper radical oxidases and related extracellular oxidoreductases of wood-decay Agaricomycetes. Fungal Genetics and Biology **72:** 124-130.

KERSTEN, P. J., 1990 Glyoxal oxidase of *Phanerochaete chrysosporium* - Its characterization and activation by lignin peroxidase. Proceedings of the National Academy of Sciences of the United States of America **87:** 2936-2940.

KHAZRAJI, A. C., and S. ROBERT, 2013 Interaction effects between cellulose and water in nanocrystalline and amorphous regions: A novel approach using molecular modeling. Journal of Nanomaterials.

KIM, S., and B. E. DALE, 2004 Global potential bioethanol production from wasted crops and crop residues. Biomass & Bioenergy **26:** 361-375.

KIM, S., and P. A. PEVZNER, 2014 MS-GF plus makes progress towards a universal database search tool for proteomics. Nature Communications **5**.

KIM, S. H., C. M. LEE and K. KAFLE, 2013 Characterization of crystalline cellulose in biomass: Basic principles, applications, and limitations of XRD, NMR, IR, Raman, and SFG. Korean Journal of Chemical Engineering **30:** 2127-2141.

KOENIGS, J., 1974 Hydrogen peroxide and iron: A proposed system for decomposition of wood by brown rot basidiomycetes. Wood and Fiber **6:** 66-79.

KOJIMA, Y., A. VARNAI, T. ISHIDA, N. SUNGAWA, D. M. PETROVIC *et al.*, 2016 A lytic polysaccharide monooxygenase with broad xyloglucan specificity from the brown rot fungus *Gloeophyllum trabeum* and its action on cellulose-xyloglucan complexes. Applied and Environmental Microbiology **82:** 6557-6572.

KORRIPALLY, P., V. I. TIMOKHIN, C. J. HOUTMAN, M. D. MOZUCH and K. E. HAMMEL, 2013 Evidence from *Serpula lacrymans* that 2,5-dimethoxyhydroquinone is a lignocellulolytic agent of divergent brown rot basidiomycetes. Applied and Environmental Microbiology **79:** 2377-2383.

KUES, U., and M. RUHL, 2011 Multiple multi-copper oxidase gene families in basidiomycetes - What for? Current Genomics **12:** 72-94.

KUMAR, R., G. MAGO, V. BALAN and C. E. WYMAN, 2009 Physical and chemical characterizations of corn stover and poplar solids resulting from leading pretreatment technologies. Bioresource Technology **100:** 3948-3962.

KUUSKERI, J., M. HAKKINEN, P. LAINE, O. P. SMOLANDER, F. TAMENE *et al.*, 2016 Time-scale dynamics of proteome and transcriptome of the white-rot fungus *Phlebia radiata*: Growth on spruce wood and decay effect on lignocellulose. Biotechnology for Biofuels **9**.

LACKNER, G., M. BOHNERT, J. WICK and D. HOFFMEISTER, 2013 Assembly of melleolide antibiotics involves a polyketide synthase with cross-coupling activity. Chemistry & Biology **20:** 1101-1106.

LACKNER, G., M. MISIEK, J. BRAESEL and D. HOFFMEISTER, 2012 Genome mining reveals the evolutionary origin and biosynthetic potential of basidiomycete polyketide synthases. Fungal Genetics and Biology **49:** 996-1003.

LAFOND, M., D. NAVARRO, M. HAON, M. COUTURIER and J. G. BERRIN, 2012 Characterization of a broad-specificity beta-glucanase acting on beta-(1,3)-, beta-(1,4)-, and beta-(1,6)-glucans that defines a new glycoside hydrolase family. Applied and Environmental Microbiology **78:** 8540-8546.

LAKSHMANAN, D., and C. SADASIVAN, 2016 *Trichoderma viride* laccase plays a crucial role in defense mechanism against antagonistic organisms. Frontiers in Microbiology **7**.

LANGNER, T., and V. GOHRE, 2016 Fungal chitinases: Function, regulation, and potential roles in plant/pathogen interactions. Current Genetics **62:** 243-254.

LANGSTON, J. A., T. SHAGHASI, E. ABBATE, F. XU, E. VLASENKO *et al.*, 2011 Oxidoreductive cellulose depolymerization by the enzymes cellobiose dehydrogenase and glycoside hydrolase 61. Applied and Environmental Microbiology **77:** 7007-7015.

LEWIS, N. G., and E. YAMAMOTO, 1990 Lignin - Occurrence, biogenesis and biodegradation. Annual Review of Plant Physiology and Plant Molecular Biology **41:** 455-496.

LIERS, C., C. BOBETH, M. PECYNA, R. ULLRICH and M. HOFRICHTER, 2010 DyP-like peroxidases of the jelly fungus *Auricularia auricula-judae* oxidize nonphenolic lignin model compounds and high-redox potential dyes. Applied Microbiology and Biotechnology **85:** 1869-1879.

LIN, S. C., Y. C. LO, J. Y. LIN and Y. C. LIAW, 2004 Crystal structures and electron micrographs of fungal volvatoxin A2. Journal of Molecular Biology **343:** 477-491.

LINDE, D., F. J. RUIZ-DUENAS, E. FERNANDEZ-FUEYO, V. GUALLAR, K. E. HAMMEL *et al.*, 2015 Basidiomycete DyPs: Genomic diversity, structural-functional aspects, reaction mechanism and environmental significance. Archives of Biochemistry and Biophysics **574:** 66-74.

LINDER, M. B., G. R. SZILVAY, T. NAKARI-SETALA and M. E. PENTTILA, 2005 Hydrophobins: The protein-amphiphiles of filamentous fungi. FEMS Microbiology Reviews **29:** 877-896.

LIU, L. Z., and S. J. FREE, 2016 Characterization of the *Sclerotinia sclerotiorum* cell wall proteome. Molecular Plant Pathology **17:** 985-995.

LOMBARD, V., H. G. RAMULU, E. DRULA, P. M. COUTINHO and B. HENRISSAT, 2014 The carbohydrate-active enzymes database (CAZy) in 2013. Nucleic Acids Research **42:** D490-D495.

LUNDELL, T. K., M. R. MAKELA, R. P. DE VRIES and K. S. HILDEN, 2014 Genomics, lifestyles and future prospects of wood-decay and litter-decomposing basidiomycota, pp. 329-370 in *Fungi*, edited by F. M. MARTIN.

LUO, F., Z. X. ZHONG, L. LIU, Y. IGARASHI, D. T. XIE *et al.*, 2017 Metabolomic differential analysis of interspecific interactions among white rot fungi *Trametes versicolor*, *Dichomitus squalens* and *Pleurotus ostreatus*. Scientific Reports **7**.

MACDONALD, J., M. DOERING, T. CANAM, Y. C. GONG, D. S. GUTTMAN *et al.*, 2011 Transcriptomic responses of the softwood-degrading white-rot fungus *Phanerochaete carnosa* during growth on coniferous and deciduous wood. Applied and Environmental Microbiology **77:** 3211-3218.

MACDONALD, J., H. SUZUKI and E. R. MASTER, 2012 Expression and regulation of genes encoding lignocellulose-degrading activity in the genus *Phanerochaete*. Applied Microbiology and Biotechnology **94:** 339-351.

MAHAJAN, S., and E. R. MASTER, 2010 Proteomic characterization of lignocellulose-degrading enzymes secreted by *Phanerochaete carnosa* grown on spruce and microcrystalline cellulose. Applied Microbiology and Biotechnology **86:** 1903-1914.

MAKELA, M. R., O. M. SIETIO, R. P. DE VRIES, S. TIMONEN and K. HILDEN, 2014 Oxalate-metabolising genes of the white-rot fungus *Dichomitus squalens* are differentially induced on wood and at high proton concentration. Plos One **9**.

MALI, T., J. KUUSKERI, F. SHAH and T. K. LUNDELL, 2017 Interactions affect hyphal growth and enzyme profiles in combinations of coniferous wood-decaying fungi of Agaricomycetes. Plos One **12**.

MARTIN, K., B. M. MCDOUGALL, S. MCILROY, JAYUS, J. Z. CHEN *et al.*, 2007 Biochemistry and molecular biology of exocellular fungal beta-(1,3)- and beta-(1,6)-glucanases. FEMS Microbiology Reviews **31:** 168-192.

MARTINEZ, D., J. CHALLACOMBE, I. MORGENSTERN, D. HIBBETT, M. SCHMOLL *et al.*, 2009 Genome, transcriptome, and secretome analysis of wood decay fungus *Postia placenta* supports unique mechanisms of lignocellulose conversion. Proceedings of the National Academy of Sciences of the United States of America **106:** 1954-1959.

MARTINEZ, D., L. F. LARRONDO, N. PUTNAM, M. D. S. GELPKE, K. HUANG *et al.*, 2004 Genome sequence of the lignocellulose degrading fungus *Phanerochaete chrysosporium* strain RP78. Nature Biotechnology **22:** 695-700.

MAYAMPURATH, A. M., N. JAITLY, S. O. PURVINE, M. E. MONROE, K. J. AUBERRY *et al.*, 2008 DeconMSn: A software tool for accurate parent ion monoisotopic mass determination for tandem mass spectra. Bioinformatics **24:** 1021-1023.

MICALES, J. A., 1997 Localization and induction of oxalate decarboxylase in the brown-rot wood decay fungus *Postia placenta*. International Biodeterioration & Biodegradation **39:** 125-132.

MOHNEN, D., 2008 Pectin structure and biosynthesis. Current Opinion in Plant Biology **11:** 266-277.

MOODY, S. C., E. DUDLEY, J. HISCOX, L. BODDY and D. C. EASTWOOD, 2018 Interdependence of primary metabolism and xenobiotic mitigation characterizes the proteome of *Bjerkandera adusta* during wood decomposition. Applied and Environmental Microbiology **84**.

MUNIR, E., T. HATTORI and M. SHIMADA, 2002 Purification and characterization of isocitrate lyase from the wood-destroying basidiomycete *Fomitopsis palustris* grown on glucose. Archives of Biochemistry and Biophysics **399:** 225-231.

MUNIR, E., J. J. YOON, T. TOKIMATSU, T. HATTORI and M. SHIMADA, 2001a New role for glyoxylate cycle enzymes in wood-rotting basidiomycetes in relation to biosynthesis of oxalic acid. Journal of Wood Science **47:** 368-373.

MUNIR, E., J. J. YOON, T. TOKIMATSU, T. HATTORI and M. SHIMADA, 2001b A physiological role for oxalic acid biosynthesis in the wood-rotting basidiomycete

Fomitopsis palustris. Proceedings of the National Academy of Sciences of the United States of America **98:** 11126-11130.

NEWELL, S. Y., T. L. ARSUFFI and R. D. FALLON, 1988 Fundamental procedures for determining ergosterol content of decaying plant material by liquid chromatography. Applied and Environmental Microbiology **54:** 1876-1879.

NIEMINEN, S., J. HEIKKINEN and J. RATY, 2013 Laser transillumination imaging for determining wood defects and grain angle. Measurement Science and Technology **24**.

NITSCHE, B. M., T. R. JORGENSEN, M. AKEROYD, V. MEYER and A. F. J. RAM, 2012 The carbon starvation response of *Aspergillus niger* during submerged cultivation: Insights from the transcriptome and secretome. BMC Genomics **13**.

OLSON, D. G., J. E. MCBRIDE, A. J. SHAW and L. R. LYND, 2012 Recent progress in consolidated bioprocessing. Current Opinion in Biotechnology **23:** 396-405.

OSULLIVAN, A. C., 1997 Cellulose: The structure slowly unravels. Cellulose **4:** 173-207.

PALFREYMAN, J. W., J. S. GARTLAND, C. J. STURROCK, D. LESTER, N. A. WHITE *et al.*, 2003 The relationship between 'wild' and 'building' isolates of the dry rot fungus *Serpula lacrymans*. FEMS Microbiology Letters **228:** 281-286.

PARFITT, D., J. HUNT, D. DOCKRELL, H. J. ROGERS and L. BODDY, 2010 Do all trees carry the seeds of their own destruction? PCR reveals numerous wood decay fungi latently present in sapwood of a wide range of angiosperm trees. Fungal Ecology **3:** 338-346.

PASTORELLI, R., A. E. AGNELLI, I. DE MEO, A. GRAZIANI, A. PALETTO *et al.*, 2017 Analysis of microbial diversity and greenhouse gas production of decaying pine logs. Forests **8**.

PAYNE, C. M., B. C. KNOTT, H. B. MAYES, H. HANSSON, M. E. HIMMEL *et al.*, 2015 Fungal cellulases. Chemical Reviews **115:** 1308-1448.

PEIRIS, D., W. B. DUNN, M. BROWN, D. B. KELL, I. ROY *et al.*, 2008 Metabolite profiles of interacting mycelial fronts differ for pairings of the wood decay basidiomycete fungus, *Stereum hirsutum* with its competitors *Coprinus micaceus* and *Coprinus disseminatus*. Metabolomics **4:** 52-62.

PEREZ-BOADA, M., F. J. RUIZ-DUENAS, R. POGNI, R. BASOSI, T. CHOINOWSKI *et al.*, 2005 Versatile peroxidase oxidation of high redox potential aromatic compounds: Site-directed mutagenesis, spectroscopic and crystallographic investigation of three long-range electron transfer pathways. Journal of Molecular Biology **354:** 385-402.

PETERSEN, T. N., S. BRUNAK, G. VON HEIJNE and H. NIELSEN, 2011 SignalP 4.0: Discriminating signal peptides from transmembrane regions. Nature Methods **8:** 785-786.

PHILLIPS, C. M., W. T. BEESON, J. H. CATE and M. A. MARLETTA, 2011 Cellobiose dehydrogenase and a copper-dependent polysaccharide monooxygenase potentiate cellulose degradation by *Neurospora crassa*. ACS Chemical Biology **6:** 1399-1406.

PIONTEK, K., A. T. SMITH and W. BLODIG, 2001 Lignin peroxidase structure and function. Biochemical Society Transactions **29:** 111-116.

POLLEGIONI, L., F. TONIN and E. ROSINI, 2015 Lignin-degrading enzymes. FEBS Journal **282:** 1190-1213.

PRESLEY, G. N., and J. S. SCHILLING, 2017 Distinct Growth and Secretome Strategies for Two Taxonomically Divergent Brown Rot Fungi. Applied and Environmental Microbiology **83**.

PRESLEY, G. N., J. ZHANG and J. S. SCHILLING, 2016 A genomics-informed study of oxalate and cellulase regulation by brown rot wood-degrading fungi. Fungal Genetics and Biology **Online first**.

PULS, J., 1997 Chemistry and biochemistry of hemicelluloses: Relationship between hemicellulose structure and enzymes required for hydrolysis. Macromolecular Symposia **120:** 183-196.

QUINLAN, R. J., M. D. SWEENEY, L. LO LEGGIO, H. OTTEN, J. C. N. POULSEN *et al.*, 2011 Insights into the oxidative degradation of cellulose by a copper metalloenzyme that exploits biomass components. Proceedings of the National Academy of Sciences of the United States of America **108:** 15079-15084.

RABEMANOLONTSOA, H., and S. SAKA, 2016 Various pretreatments of lignocellulosics. Bioresource Technology **199:** 83-91.

RAJALA, T., M. PELTONIEMI, J. HANTULA, R. MAKIPAA and T. PENNANEN, 2011 RNA reveals a succession of active fungi during the decay of Norway spruce logs. Fungal Ecology **4:** 437-448.

RAJALA, T., M. PELTONIEMI, T. PENNANEN and R. MAKIPAA, 2012 Fungal community dynamics in relation to substrate quality of decaying Norway spruce (*Picea abies* L. Karst.) logs in boreal forests. FEMS Microbiology Ecology **81:** 494-505.

RASSER, F., T. ANKE and O. STERNER, 2000 Secondary metabolites from a *Gloeophyllum* species. Phytochemistry **54:** 511-516.

RAYNER, A. D. M., and L. BODDY, 1988 *Fungal decomposition of wood: Its biology and ecology*. John Wiley and Sons, Chichester, UK.

RAYNER, A. D. M., L. BODDY and C. G. DOWSON, 1987 Temporary parasitism of *Coriolus spp* by *Lenzites betulina* : A strategy for domain capture in wood decay fungi. FEMS Microbiology Ecology **45:** 53-58.

REGASSA, T. H., and C. S. WORTMANN, 2014 Sweet sorghum as a bioenergy crop: Literature review. Biomass & Bioenergy **64:** 348-355.

RILEY, R., A. A. SALAMOV, D. W. BROWN, L. G. NAGY, D. FLOUDAS *et al.*, 2014 Extensive sampling of basidiomycete genomes demonstrates inadequacy of the white-rot/brown-rot paradigm for wood decay fungi. Proceedings of the National Academy of Sciences of the United States of America **111:** 9923-9928.

ROBERTS, J. N., R. SINGH, J. C. GRIGG, M. E. P. MURPHY, T. D. H. BUGG *et al.*, 2011 Characterization of dye-decolorizing peroxidases from *Rhodococcus jostii* RHA1. Biochemistry **50:** 5108-5119.

ROWELL, R. M., 2005 *Handbook of wood Chemistry and Wood Composites*. CRC press, Boca Raton.

RUIZ-DUENAS, F. J., T. LUNDELL, D. FLOUDAS, L. G. NAGY, J. M. BARRASA *et al.*, 2013 Lignin-degrading peroxidases in Polyporales: An evolutionary survey based on 10 sequenced genomes. Mycologia **105:** 1428-1444.

RUIZ-DUENAS, F. J., and A. T. MARTINEZ, 2009 Microbial degradation of lignin: How a bulky recalcitrant polymer is efficiently recycled in nature and how we can take advantage of this. Microbial Biotechnology **2:** 164-177.

RYTIOJA, J., K. HILDEN, M. DI FALCO, M. M. ZHOU, M. V. AGUILAR-PONTES *et al.*, 2017 The molecular response of the white-rot fungus *Dichomitus squalens* to wood and non-woody biomass as examined by transcriptome and exoproteome analyses. Environmental Microbiology **19:** 1237-1250.

RYTIOJA, J., K. HILDEN, J. YUZON, A. HATAKKA, R. P. DE VRIES *et al.*, 2014 Plant polysaccharide-degrading enzymes from Basidiomycetes. Microbiology and Molecular Biology Reviews **78:** 614-649.

RYU, J. S., S. SHARY, C. J. HOUTMAN, E. A. PANISKO, P. KORRIPALLY *et al.*, 2011 Proteomic and functional analysis of the cellulase system expressed by *Postia placenta* during brown rot of solid wood. Applied and Environmental Microbiology **77:** 7933-7941.

SAKAI, S., T. NISHIDE, E. MUNIR, K. BABA, H. INUI *et al.*, 2006 Subcellular localization of glyoxylate cycle key enzymes involved in oxalate biosynthesis of wood-destroying basidiomycete *Fomitopsis palustris* grown on glucose. Microbiology-SGM **152:** 1857-1866.

SALVACHUA, D., A. T. MARTINEZ, M. TIEN, M. F. LOPEZ-LUCENDO, F. GARCIA *et al.*, 2013 Differential proteomic analysis of the secretome of *Irpex lacteus* and other white-rot fungi during wheat straw pretreatment. Biotechnology for Biofuels **6**.

SANTOS, A., S. MENDES, V. BRISSOS and L. O. MARTINS, 2014 New dye-decolorizing peroxidases from *Bacillus subtilis* and *Pseudomonas putida* MET94: towards biotechnological applications. Applied Microbiology and Biotechnology **98:** 2053-2065.

SCHADEL, C., A. BOCHL, A. RICHTER and G. HOCH, 2010 Quantification and monosaccharide composition of hemicelluloses from different plant functional types. Plant Physiology and Biochemistry **48:** 1-8.

SCHILLING, J. S., J. AI, R. A. BLANCHETTE, S. M. DUNCAN, T. R. FILLEY *et al.*, 2012 Lignocellulose modifications by brown rot fungi and their effects, as pretreatments, on cellulolysis. Bioresource Technology **116:** 147-154.

SCHILLING, J. S., S. M. DUNCAN, G. N. PRESLEY, T. R. FILLEY, J. A. JURGENS *et al.*, 2013 Localizing incipient reactions in wood degraded by the brown rot fungus *Postia placenta*. International Biodeterioration & Biodegradation **83:** 56-62.

SCHILLING, J. S., and J. JELLISON, 2005 Oxalate regulation by two brown rot fungi decaying oxalate-amended and non-amended wood. Holzforschung **59:** 681-688.

SCHILLING, J. S., and J. JELLISON, 2006 Metal accumulation without enhanced oxalate secretion in wood degraded by brown rot fungi. Applied and Environmental Microbiology **72:** 5662-5665.

SCHILLING, J. S., J. T. KAFFENBERGER, F. J. LIEW and Z. W. SONG, 2015 Signature Wood Modifications Reveal Decomposer Community History. Plos One **10**.

SCHIRMBOCK, M., M. LORITO, Y. L. WANG, C. K. HAYES, I. ARISANATAC *et al.*, 1994 Parallel formation and synergism of hydrolytic enzymes and peptaibol antibiotics: Molecular mechanisms involved in the antagonistic action of *Trichoderma-harzianum* against phytopathogenic fungi. Applied and Environmental Microbiology **60:** 4364-4370.

SCHMIDHALTER, D. R., and G. CANEVASCINI, 1993a Isolation and characterization of the cellobiose dehydrogenase from the brown-rot fungus *Coniophora puteana* (SCHUM EX-FR) KARST. Archives of Biochemistry and Biophysics **300:** 559-563.

SCHMIDHALTER, D. R., and G. CANEVASCINI, 1993b Purification and characterization of 2 exocellobiohydrolases from the brown-rot fungus *Coniophora-puteana* (SCHUM EX-FR) Karst. Archives of Biochemistry and Biophysics **300:** 551-558.

SCHMITTGEN, T. D., and K. J. LIVAK, 2008 Analyzing real-time PCR data by the comparative C-T method. Nature Protocols **3:** 1101-1108.

SCHNEPF, H. E., 1995 *Bacillus thuringiensis* toxins : Regulation, activities and structural diversity. Current Opinion in Biotechnology **6:** 305-312.

SERDECZNY, O., S. ADAMS, F. BAARSCH, D. COUMOU, A. ROBINSON *et al.*, 2016 Climate change impacts in Sub-Saharan Africa: From physical chances to their social repercussions. Regional Environmental Change **Online First**.

SHIMADA, M., Y. AKAMTSU, T. TOKIMATSU, K. MII and T. HATTORI, 1997 Possible biochemical roles of oxalic acid as a low molecular weight compound involved in brown-rot and white-rot wood decays. Journal of Biotechnology **53:** 103-113.

SHIN, K. S., H. D. YOUN, Y. H. HAN, S. O. KANG and Y. C. HAH, 1993 Purification and characterization of d-glucose oxidase from white-rot fungus *Pleurotus ostreatus*. European Journal of Biochemistry **215:** 747-752.

SHORTLE, W. C., K. R. DUDZIK and K. T. SMITH, 2010 Development of wood decay in wound-initiated discolored wood of eastern red cedar. Holzforschung **64:** 529-536.

SILAR, P., 2005 Peroxide accumulation and cell death in filamentous fungi induced by contact with a contestant. Mycological Research **109:** 137-149.

SINNOTT, M. L., 1990 Catalytic mechanisms of enzymatic glycosyl transfer. Chemical Reviews **90:** 1171-1202.

SJORSTROM, E., 1981 *Wood Chemistry: Fundamentals and Applications*. Academic Press, New York.

SLUITER, A., B. HAMES, R. RUIZ, C. SCARLATA, J. SLUITER *et al.*, 2008 Determination of structural carbohydrates and lignin in biomass. NREL Laboratory and Analytical Procedures **https://**www.nrel.gov/bioenergy/biomass-compositional-analysis.html.

SMITH, G. R., R. D. FINLAY, J. STENLID, R. VASAITIS and A. MENKIS, 2017 Growing evidence for facultative biotrophy in saprotrophic fungi: Data from microcosm tests with 201 species of wood-decay basidiomycetes. New Phytologist **215:** 747-755.

SMITH, P. K., R. I. KROHN, G. T. HERMANSON, A. K. MALLIA, F. H. GARTNER *et al.*, 1985 Measurement of protein using bicinchoninic acid. Analytical Biochemistry **150:** 76-85.

SNAJDR, J., P. DOBIASOVA, T. VETROVSKY, V. VALASKOVA, A. ALAWI *et al.*, 2011 Saprotrophic basidiomycete mycelia and their interspecific interactions affect the spatial distribution of extracellular enzymes in soil. FEMS Microbiology Ecology **78:** 80-90.

SONG, Z. W., A. VAIL, M. J. SADOWSKY and J. S. SCHILLING, 2012 Competition between two wood-degrading fungi with distinct influences on residues. FEMS Microbiology Ecology **79:** 109-117.

SONNENBICHLER, J., J. DIETRICH and H. PEIPP, 1994 Secondary fungal metabolites and their biological-activities, .5. Investigations concerning the induction of the biosynthesis of toxic secondary metabolites in basidiomycetes. Biological Chemistry Hoppe-Seyler **375:** 71-79.

SONNENBICHLER, J., H. PEIPP and J. DIETRICH, 1993 Secondary fungal metabolites and their biological-activities .3. Further metabolites from dual cultures of the antagonistic basidiomycetes *Heterobasidion annosum* and *Gloeophyllum abietinum*. Biological Chemistry Hoppe-Seyler **374:** 467-473.

SONNENBICHLER, J., I. SONNENBICHLER and D. SCHWARZ, 1997 Biosynthesis of oosponol and oospoglycol elucidated by C-13 NMR. Phytochemistry **44:** 267-269.

STEIGER, M. G., R. L. MACH and A. R. MACH-AIGNER, 2010 An accurate normalization strategy for RT-qPCR in *Hypocrea jecorina* (*Trichoderma reesei*). Journal of Biotechnology **145:** 30-37.

STEPHEN, J. D., W. E. MABEE and J. N. SADDLER, 2012 Will second-generation ethanol be able to compete with first-generation ethanol? Opportunities for cost reduction. Biofuels Bioproducts & Biorefining-Biofpr **6:** 159-176.

SUNDARAMOORTHY, M., K. KISHI, M. H. GOLD and T. L. POULOS, 1994 The crystal-structure of manganese peroxidase from *Phanerochaete chrysosporium* at 2.06-angstrom resolution. Journal of Biological Chemistry **269:** 32759-32767.

SUZUKI, M. R., C. G. HUNT, C. J. HOUTMAN, Z. D. DALEBROUX and K. E. HAMMEL, 2006 Fungal hydroquinones contribute to brown rot of wood. Environmental Microbiology **8:** 2214-2223.

TANAKA, N., YASUMI, A., HATTORI, T., AND SHIMADA, M., 1994 Effect of oxalic acid on the oxidative breakdown or cellulose by the fenton reaction. Wood Research: Bulletin of the Wood Research Institute Kyoto University **81:** 8-10.

TANG, J. D., L. A. PARKER, A. D. PERKINS, T. S. SONSTEGARD, S. G. SCHROEDER *et al.*, 2013 Gene expression analysis of copper tolerance and wood decay in the brown rot fungus *Fibroporia radiculosa*. Applied and Environmental Microbiology **79:** 1523-1533.

TATENO, H., and I. J. GOLDSTEIN, 2003 Molecular cloning, expression, and characterization of novel hemolytic lectins from the mushroom *Laetiporus*

sulphureus, which show homology to bacterial toxins. Journal of Biological Chemistry **278:** 40455-40463.

TIEN, M., and T. K. KIRK, 1983 Lignin degrading enzyme from the hymenomycete *Phanerochaete chrysosporium* Burds. Science **221:** 661-662.

TRAPNELL, C., A. ROBERTS, L. GOFF, G. PERTEA, D. KIM *et al.*, 2012 Differential gene and transcript expression analysis of RNA-seq experiments with TopHat and Cufflinks. Nature Protocols **7:** 562-578.

UJOR, V. C., D. G. PEIRIS, M. MONTI, A. S. KANG, M. O. CLEMENTS *et al.*, 2012 Quantitative proteomic analysis of the response of the wood-rot fungus, *Schizophyllum commune*, to the biocontrol fungus, *Trichoderma viride*. Letters in Applied Microbiology **54:** 336-343.

UPADHYAY, S., X. P. XU and X. R. LIN, 2016a Interactions between melanin enzymes and their atypical recruitment to the secretory pathway by palmitoylation. Mbio **7**.

UPADHYAY, S., X. P. XU, D. LOWRY, J. C. JACKSON, R. W. ROBERSON *et al.*, 2016b Subcellular compartmentalization and trafficking of the biosynthetic machinery for fungal melanin. Cell Reports **14:** 2511-2518.

VALASKOVA, V., and P. BALDRIAN, 2006 Degradation of cellulose and hemicelluloses by the brown rot fungus *Piptoporus betulinus* - Production of extracellular enzymes and characterization of the major cellulases. Microbiology-SGM **152:** 3613-3622.

VAN DEN BRINK, J., and R. P. DE VRIES, 2011 Fungal enzyme sets for plant polysaccharide degradation. Applied Microbiology and Biotechnology **91:** 1477-1492.

VANDEN WYMELENBERG, A., G. SABAT, M. MOZUCH, P. J. KERSTEN, D. CULLEN *et al.*, 2006 Structure, organization, and transcriptional regulation of a family of copper radical oxidase genes in the lignin-degrading basidiomycete *Phanerochaete chrysosporium*. Applied and Environmental Microbiology **72:** 4871-4877.

VARELA, E., and M. TIEN, 2003 Effect of pH and oxalate on hydroquinone-derived hydroxyl radical formation during brown rot wood degradation. Applied and Environmental Microbiology **69:** 6025-6031.

VARROT, A., S. M. BASHEER and A. IMBERTY, 2013 Fungal lectins: Structure, function and potential applications. Current Opinion in Structural Biology **23:** 678-685.

VOGEL, J., 2008 Unique aspects of the grass cell wall. Current Opinion in Plant Biology **11:** 301-307.

WALZ, A., THEISEN, S., AND BUCHENAUER, H., 2003 Oxalate decarboxylase from *Trametes versicolor:* Molecular cloning and overexpression in plants. EMBL Sequence Database Entry **AY370675**.

WATERMAN, S. R., M. HACHAM, J. PANEPINTO, G. W. HU, S. SHIN *et al.*, 2007 Cell wall targeting of laccase of *Cryptococcus neoformans* during infection of mice. Infection and Immunity **75:** 714-722.

WAWRZYN, G. T., M. B. QUIN, S. CHOUDHARY, F. LOPEZ-GALLEGO and C. SCHMIDT-DANNERT, 2012 Draft genome of *Omphalotus olearius* provides a predictive framework for sesquiterpenoid natural product biosynthesis in Basidiomycota. Chemistry & Biology **19:** 772-783.

WEBER, T., K. BLIN, S. DUDDELA, D. KRUG, H. U. KIM *et al.*, 2015 antiSMASH 3.0: A comprehensive resource for the genome mining of biosynthetic gene clusters. Nucleic Acids Research **43:** W237-W243.

WEED, A. S., M. P. AYRES and J. A. HICKE, 2013 Consequences of climate change for biotic disturbances in North American forests. Ecological Monographs **83:** 441-470.

WEI, D. S., C. J. HOUTMAN, A. N. KAPICH, C. G. HUNT, D. CULLEN *et al.*, 2010 Laccase and its role in production of extracellular reactive oxygen species during wood decay by the brown rot basidiomycete *Postia placenta*. Applied and Environmental Microbiology **76:** 2091-2097.

WENG, Y. P., Y. P. LIN, C. I. HSU and J. Y. LIN, 2004 Functional domains of a pore-forming cardiotoxic protein, volvatoxin A2. Journal of Biological Chemistry **279:** 6805-6814.

WHITE, N. A., G. A. LOW, J. SINGH, H. STAINES and J. W. PALFREYMAN, 1997 Isolation and environmental study of 'wild' *Serpula lacrymans* and *Serpula himantioides* from the Himalayan Forests. Mycological Research **101:** 580-584.

WHITTAKER, J. W., 2005 The radical chemistry of galactose oxidase. Archives of Biochemistry and Biophysics **433:** 227-239.

WHITTAKER, M. M., P. J. KERSTEN, N. NAKAMURA, J. SANDERSLOEHR, E. S. SCHWEIZER *et al.*, 1996 Glyoxal oxidase from *Phanerochaete chrysosporium* is a new radical-copper oxidase. Journal of Biological Chemistry **271:** 681-687.

WILLFOR, S., A. PRANOVICH, T. TAMMINEN, J. PULS, C. LAINE *et al.*, 2009 Carbohydrate analysis of plant materials with uronic acid-containing polysaccharides: A comparison between different hydrolysis and subsequent chromatographic analytical techniques. Industrial Crops and Products **29:** 571-580.

WONGNATE, T., and P. CHAIYEN, 2013 The substrate oxidation mechanism of pyranose 2-oxidase and other related enzymes in the glucose-methanol-choline superfamily. FEBS Journal **280:** 3009-3027.

WYMELENBERG, A. V., J. GASKELL, M. MOZUCH, S. S. BONDURANT, G. SABAT *et al.*, 2011 Significant alteration of gene expression in wood decay fungi *Postia placenta* and *Phanerochaete chrysosporium* by plant species. Applied and Environmental Microbiology **77:** 4499-4507.

WYMELENBERG, A. V., J. GASKELL, M. MOZUCH, G. SABAT, J. RALPH *et al.*, 2010 Comparative transcriptome and secretome analysis of wood decay fungi *Postia placenta* and *Phanerochaete chrysosporium*. Applied and Environmental Microbiology **76:** 3599-3610.

XIAO, C. W., and C. T. ANDERSON, 2013 Roles of pectin in biomass yield and processing for biofuels. Frontiers in Plant Science **4**.

YANG, Y., J. BAE, J. KIM and S. SUH, 2012 Replacing gasoline with corn ethanol results in significant environmental problem-shifting. Environmental Science & Technology **46:** 3671-3678.

YAO, L., L. P. ZHU, X. Y. XU, L. L. TAN, M. SADILEK *et al.*, 2016 Discovery of novel xylosides in co-culture of basidiomycetes *Trametes versicolor* and *Ganoderma applanatum* by integrated metabolomics and bioinformatics. Scientific Reports **6**.

YELLE, D. J., J. RALPH, F. C. LU and K. E. HAMMEL, 2008 Evidence for cleavage of lignin by a brown rot basidiomycete. Environmental Microbiology **10:** 1844-1849.

YELLE, D. J., D. S. WEI, J. RALPH and K. E. HAMMEL, 2011 Multidimensional NMR analysis reveals truncated lignin structures in wood decayed by the brown rot basidiomycete *Postia placenta*. Environmental Microbiology **13:** 1091-1100.

YOON, J. J., T. HATTORI and M. SHIMADA, 2002 A metabolic role of the glyoxylate and tricarboxylic acid cycles for development of the copper-tolerant brown-rot fungus *Fomitopsis palustris*. FEMS Microbiology Letters **217:** 9-14.

ZEGADA-LIZARAZU, W., and A. MONTI, 2012 Are we ready to cultivate sweet sorghum as a bioenergy feedstock? A review on field management practices. Biomass & Bioenergy **40:** 1-12.

ZHANG, J., and J. S. SCHILLING, 2017 Role of carbon source in the shift from oxidative to hydrolytic wood decomposition by *Postia placenta*. Fungal Genetics and Biology **106:** 1-8.

ZHANG, J. W., G. N. PRESLEY, K. E. HAMMEL, J. S. RYU, J. R. MENKE *et al.*, 2016 Localizing gene regulation reveals a staggered wood decay mechanism for the brown rot fungus *Postia placenta*. Proceedings of the National Academy of Sciences of the United States of America **113:** 10968-10973.

ZHAO, X. B., L. H. ZHANG and D. H. LIU, 2012 Biomass recalcitrance. Part I: The chemical compositions and physical structures affecting the enzymatic hydrolysis of lignocellulose. Biofuels Bioproducts & Biorefining-Biofpr **6:** 465-482.

ZHU, N., J. W. LIU, J. S. YANG, Y. J. LIN, Y. YANG *et al.*, 2016 Comparative analysis of the secretomes of *Schizophyllum commune* and other wood-decay basidiomycetes during solid-state fermentation reveals its unique lignocellulose-degrading enzyme system. Biotechnology for Biofuels **9**.

ZHUANG, L. P., W. H. GUO, M. YOSHIDA, X. Y. FENG and B. GOODELL, 2015 Investigating oxalate biosynthesis in the wood-decaying fungus *Gloeophyllum trabeum* using C-13 metabolic flux analysis. RSC Advances **5:** 104043-104047.